

AMMONIA SYNTHESIS REACTION UNDER TIME INTERRUPTED  
CONDITIONS

A THESIS SUBMITTED TO  
THE GRADUATE SCHOOL OF NATURAL AND APPLIED SCIENCES  
OF  
MIDDLE EAST TECHNICAL UNIVERSITY

BY

MUSTAFA YASIN ASLAN

IN PARTIAL FULFILLMENT OF THE REQUIREMENTS  
FOR  
THE DEGREE OF DOCTOR OF PHILOSOPHY  
IN  
CHEMICAL ENGINEERING

SEPTEMBER 2019



Approval of the thesis:

**AMMONIA SYNTHESIS REACTION UNDER TIME INTERRUPTED  
CONDITIONS**

submitted by **MUSTAFA YASIN ASLAN** in partial fulfillment of the requirements  
for the degree of **Doctor of Philosophy in Chemical Engineering Department,**  
**Middle East Technical University** by,

Prof. Dr. Halil Kalıpçılar  
Dean, Graduate School of **Natural and Applied Sciences**

\_\_\_\_\_

Prof. Dr. Pınar Çalık  
Head of Department, **Chemical Engineering**

\_\_\_\_\_

Prof. Dr. Deniz Üner  
Supervisor, **Chemical Engineering, METU**

\_\_\_\_\_

**Examining Committee Members:**

Assist. Prof. Dr. Harun Koku  
Chemical Engineering, METU

\_\_\_\_\_

Prof. Dr. Deniz Üner  
Chemical Engineering, METU

\_\_\_\_\_

Prof. Dr. Saim Özkar  
Department of Chemistry, METU

\_\_\_\_\_

Prof. Dr. Justin Stephen James Hargreaves  
School of Chemistry, University of Glasgow

\_\_\_\_\_

Assoc. Prof. Dr. Dilek Varışlı  
Chemical Engineering, Gazi University

\_\_\_\_\_

Date: 07.09.2019

**I hereby declare that all information in this document has been obtained and presented in accordance with academic rules and ethical conduct. I also declare that, as required by these rules and conduct, I have fully cited and referenced all material and results that are not original to this work.**

Name, Surname: Mustafa Yasin Aslan

Signature:

## ABSTRACT

### AMMONIA SYNTHESIS REACTION UNDER TIME INTERRUPTED CONDITIONS

Aslan, Mustafa Yasin  
Doctor of Philosophy, Chemical Engineering  
Supervisor: Prof. Dr. Deniz Üner

September 2019, 140 pages

The objective of this thesis study is to demonstrate a solution for a sustainable ammonia production process based on the unsteady state operating conditions under milder temperatures and atmospheric pressure. In this framework, the elimination of the ammonia synthesis catalyst deactivation was investigated to improve the rates under milder operating conditions.

The hydrogen adsorption /desorption characteristics over SiO<sub>2</sub> and Vulcan supported Ru catalysts with different Ru metal loadings were investigated. It was shown that Ru metal dispersion decreased with increasing Ru metal loading. In addition, It was observed that Vulcan support Ru catalysts accommodated higher amounts of hydrogen compared to SiO<sub>2</sub> supported Ru catalysts. It was demonstrated that dissociated hydrogen over Ru metal migrated from Ru metal surface to support surface and higher temperatures were needed to desorb the spilled over hydrogen from the support surface.

The inhibition effect of ammonia was conducted in the context of the study. Ammonia synthesis reaction experiments were performed with zeolite-Y, hydroxyapatite (HAp), and Vulcan supported Ru catalysts at 300 – 400 °C and atmospheric pressure. It was observed that ammonia synthesis catalyst was poisoned and deactivated by synthesized ammonia within 1 h., regardless of surface acidities of the supports. N<sub>2</sub> pulses were used to diminish the poisoning effect of ammonia. It was demonstrated that under pulsed flow conditions, the inhibition effect of ammonia was eliminated.

In the final part of the study, Co<sub>3</sub>Mo<sub>3</sub>N as a next generation ammonia synthesis catalyst was investigated. This catalyst operates through a different mechanism, by involving lattice nitrogen in the process. Ammonia synthesis reaction experiments were performed with different H<sub>2</sub>:N<sub>2</sub> ratios between 0.05 and 3.0. It was observed that ammonia synthesis rate did not change between H<sub>2</sub>:N<sub>2</sub> ratio of 3.0 and 0.5. Besides, ammonia synthesis rate decreased with decreasing H<sub>2</sub>:N<sub>2</sub> ratio below 0.5. On the other hand, N<sub>2</sub> pulses was also applied to the ammonia synthesis reaction over Co<sub>3</sub>Mo<sub>3</sub>N, but no improvement was obtained. As a result, it was demonstrated that ammonia synthesis reaction over Co<sub>3</sub>Mo<sub>3</sub>N catalysts can be carried out with similar rates using lower hydrogen amount (H<sub>2</sub>:N<sub>2</sub>=0.5:1) compared to stoichiometric H<sub>2</sub>:N<sub>2</sub> ratio of 3:1 under steady flow conditions.

Keywords: Ammonia Synthesis, Hydrogen Spillover, Ru Catalysts, Cobalt Molybdenum Nitride, Forced Unsteady State

## ÖZ

### ZAMAN KESİNTİLİ ŞARTLAR ALTINDA AMONYAK SENTEZ REAKSİYONU

Aslan, Mustafa Yasin  
Doktora, Kimya Mühendisliği  
Tez Danışmanı: Prof. Dr. Deniz Üner

Eylül 2019, 140 sayfa

Bu tez çalışmasının amacı, düşük sıcaklıklarda ve atmosferik basınç altında yatışkın olmayan operasyon koşullarında sürdürülebilir bir amonyak üretim prosesi için bir çözüm sunmaktır. Bu çerçevede, daha ılımlı operasyon şartlarında amonyak sentez hızını iyileştirmek için, amonyak sentez katalizörünü deaktive eden (zehirleyen) faktörlerin ortadan kaldırılması araştırılmıştır.

Farklı miktarlarda Ru metali yüklenmiş  $\text{SiO}_2$  ve Vulcan destekli Ru katalizörler üzerinde hidrojenin adsorpsiyon/desorpsiyon karakteristikleri incelenmiştir. Ru metal yükleme oranı arttıkça, Ru metal dağılımının azaldığı gösterilmiştir. Buna ek olarak, Vulcan destekli Ru katalizörlerin,  $\text{SiO}_2$  destekli Ru katalizörlere göre daha fazla hidrojene ev sahipliği yaptığı gözlemlenmiştir. Ru metali üzerinde parçalanmış hidrojenin Ru metalinden destek madde üzerine göç ettiği ve destek madde üzerine göç eden hidrojenin desorplanması için yüksek sıcaklık gerektirdiği ortaya konulmuştur.

Amonyakın destekli Ru katalizörleri üzerinde zehirlenme etkisi bu çalışmanın kapsamında incelenmiştir. Amonyak sentez reaksiyon deneyleri 300 – 400 °C ve atmosferik basınçta zeolite-Y, hidroksiapatit (HAp) ve Vulcan ile desteklenmiş Ru katalizörleri varlığında yapılmıştır. Destek maddenin yüzey asitliğine bakılmaksızın, amonyak sentez katalizörünü, bir saat içerisinde, üretilen amonyak tarafından zehirlendiği ve deaktive edildiği gözlemlenmiştir. N<sub>2</sub> vuruları amonyağın zehirlenme etkisini yok etmek için kullanılmıştır. Vuru akış koşullarında, amonyağın zehirlenme etkisinin ortadan kaldırıldığı gösterilmiştir.

Bu çalışmanın son kısmında, gelecek nesil Co<sub>3</sub>Mo<sub>3</sub>N amonyak sentez katalizörleri araştırılmıştır. Bu katalizör, kristal yapısındaki azot atomunu kullanan farklı bir mekanizma ile çalışmaktadır. Amonyak sentez reaksiyon deneyleri farklı H<sub>2</sub>:N<sub>2</sub> oranlarında 0.05 ve 3.0 aralığında gerçekleştirilmiştir. Amonyak sentez hızının 3.0 ve 0.5 H<sub>2</sub>:N<sub>2</sub> oranları arasında değişmediği gözlemlenmiştir. Diğer taraftan, N<sub>2</sub> vuruları Co<sub>3</sub>Mo<sub>3</sub>N katalizörü varlığında amonyak sentez reaksiyonuna uygulanmış, fakat bir gelişme elde edilememiştir. Sonuç olarak, amonyak sentez reaksiyon, Co<sub>3</sub>Mo<sub>3</sub>N varlığında, yatışkın akış koşullarında, H<sub>2</sub>:N<sub>2</sub> (3:1) oranına göre daha düşük H<sub>2</sub>:N<sub>2</sub> (0.5:1) oranlarında, benzer amonyak sentez hızlarında yürütülebileceği gösterilmiştir.

Anahtar Kelimeler: Amonyak Sentezi, Hidrojen Taşması, Ru Katalizörleri, Kobalt Molibdenum Nitrür, Zorlanmış Yatışkın Olmayan Hal

To my beloved wife

## ACKNOWLEDGEMENTS

I would like to thank my thesis supervisor Prof. Dr. Deniz Üner for her support, advice and guidance throughout the study as an advisor, personally as well as professionally.

I would be hard to finish this thesis study without her intellectual guidance, forward-thinking, patience and concreteness.

I would like to present my thanks to Prof. Dr. Saim Özkar and Dr. Serdar Akbayrak for collaborating my PhD thesis studies with Ru catalysts that synthesized in their laboratories.

My brief visit to Prof. Dr. Justin Hargreaves's laboratory at University of Glasgow broadened my perspective both academically and personally. I am thankful to Prof. Dr. Justin Hargreaves for giving me the opportunity to work in his laboratory.

I would like to thank the former and current Uner Research Group members who helped me through all this work. I particularly thank to Atalay Çalışan, Güvenç Oğulgönen, Hale Ay, Arzu Kanca, Mehmet Mert Oymak, Deniz Kaya, Veysi Helvacı, Ezgi Yavuzyılmaz and Begüm Yılmaz.

I want also thank to my childhood friends Oytun Üstün and Ömer Faruk Kuru who always support me during my PhD.

I would like to thank my friends Zeynep Karakaş, İlker Tezsevin, Berrak Erkmen, Fatma Şahin, Berkan Atman, Merve Özkutlu, Seda Sivri, Bilal Bayram, and Özgen Yalçın.

I would like to present my thanks to the technical staff, especially Gülten Orakçı for BET measurements and İsa Çağlar for his talented hands for glass processing, of Chemical Engineering Department.

I would like to express my endless thanks to my beloved mother and father, who was passed away during my MSc Thesis studies, for their continuous love, encouragement and support through my life.

Last but not the least, I would like to express by deepest thanks to my beloved wife, Semra Aslan. She walked together this difficult and grueling PhD way with me. I will never forget your enthusiasm and patience for me to finish my PhD in this journey.

The PhD scholarship grant of TUBITAK 2211 program are gratefully acknowledged. The author also thanks YOK-OYP program for financial support and leave of absence from Uşak University for graduate studies at the Middle East Technical University.

## TABLE OF CONTENTS

ABSTRACT .....	v
ÖZ .....	vii
ACKNOWLEDGEMENTS.....	x
TABLE OF CONTENTS .....	xii
LIST OF TABLES.....	xvi
LIST OF FIGURES .....	xviii
LIST OF ABBREVIATIONS.....	xxi
LIST OF SYMBOLS.....	xxii
CHAPTERS	
1 INTRODUCTION AND SCOPE.....	1
1.1 Ammonia Production vs. Energy .....	1
1.2 Haber-Bosch Process .....	2
1.3 Sustainable Ammonia Production.....	4
1.4 Objective of the Thesis .....	5
1.5 Scope of Thesis .....	6
2 AMMONIA SYNTHESIS .....	9
2.1 Catalytic Ammonia Synthesis Rates .....	10
2.2 Proposed Rate Equations .....	11
2.3 Literature on Catalytic/Enzymatic Ammonia Synthesis.....	12
2.3.1 Supported Ruthenium Catalysts .....	13
2.3.1.1 Effect of Particle Size.....	13
2.3.1.2 Hydrogen Poisoning and Suggested Solutions.....	16
2.3.1.3 Ammonia Poisoning and Suggested Solutions.....	23
2.3.2 Molybdenum Nitride Catalysts.....	24
2.3.3 Enzymatic (Biological) Ammonia Synthesis Route .....	26
2.4 Process Intensifications and Energy Improvements .....	29
3 MATERIALS AND METHODS .....	31

3.1	Catalyst Preparation .....	31
3.1.1	Incipient Wetness Impregnation Method .....	31
3.1.1.1	Synthesis of SBA-15 .....	31
3.1.2	Ion-Exchange Method .....	32
3.1.3	Synthesis of $\text{Co}_3\text{Mo}_3\text{N}$ Catalyst .....	32
3.2	Catalyst Characterization .....	33
3.2.1	BET Surface Area Measurements .....	33
3.2.2	X-Ray Diffraction .....	33
3.2.3	CHN Analysis .....	33
3.2.4	ATR-IR Spectroscopy .....	33
3.2.5	$\text{H}_2$ -Chemisorption .....	34
3.2.6	Microcalorimetry .....	35
3.2.6.1	Measurement of Heat of Adsorption of Ammonia over HAp .....	36
3.2.6.2	Measurement of Acidity of HAp, Zeolite-Y and Carbon Vulcan .....	36
3.2.7	High Resolution Transmission Electron Microscopy (HR-TEM) .....	37
3.2.8	Temperature Programmed Analysis .....	37
3.2.8.1	$\text{O}_2$ -Titration .....	38
3.3	Ammonia Synthesis Reaction Studies .....	39
3.3.1	In-situ DRIFTS Measurements .....	39
3.3.2	Steady State Ammonia Synthesis Reaction .....	40
3.3.3	Unsteady State Ammonia Synthesis Reaction .....	40
4	FUNDAMENTALS OF HYDROGEN ADSORPTION & STORAGE PROCESSES OVER $\text{Ru}/\text{SiO}_2$ AND $\text{Ru}/\text{Vulcan}$ .....	43
4.1	Introduction .....	43
4.2	Results and Discussion .....	48
4.2.1	Dispersion of Ru Particles over $\text{Ru}/\text{SiO}_2$ and $\text{Ru}/\text{Vulcan}$ catalysts .....	48
4.2.2	Temperature Programmed Analysis .....	52
4.2.2.1	Temperature Programmed Reduction .....	52
4.2.2.2	Temperature Programmed Desorption and $\text{O}_2$ -Titration .....	56
4.3	Chapter Summary .....	61

5	SUPPORT EFFECTS IN AMMONIA SYNTHESIS .....	63
5.1	Introduction.....	63
5.2	Results and Discussion.....	66
5.2.1	Support Characterization .....	67
5.2.1.1	Support Acidity .....	67
5.2.1.2	Surface Area of Support .....	68
5.2.2	Characterization of Ru Nanoparticles.....	69
5.2.3	Ammonia Formation Rates.....	71
5.2.4	Degree of Ammonia Retention.....	72
5.2.5	N <sub>2</sub> Pulse Experiments .....	74
5.3	Chapter Summary .....	77
6	NH <sub>3</sub> SYNTHESIS over CO <sub>3</sub> MO <sub>3</sub> N UNDER TIME INTERRUPTED CONDITIONS.....	79
6.1	Introduction.....	79
6.2	Results and Discussion.....	81
6.2.1	Characterization.....	81
6.2.1.1	XRD and Elemental Analysis.....	81
6.2.1.2	Temperature Programmed Reduction .....	82
6.2.1.3	H <sub>2</sub> Adsorption Isotherm.....	84
6.2.2	Kinetic Studies.....	85
6.2.2.1	NH <sub>3</sub> Synthesis Experiments under Steady State Flow .....	85
6.2.2.2	NH <sub>3</sub> Synthesis Experiments at Different H <sub>2</sub> :N <sub>2</sub> Ratio.....	85
6.2.2.3	Pulse Flow Experiments.....	87
6.3	Chapter Summary .....	90
7	CONCLUSIONS.....	91
8	RECOMMENDATIONS .....	93
	REFERENCES .....	95
9	APPENDICES.....	117
A.	Supplementary Information – Fundamentals of Hydrogen Storage Properties over Ru/SiO <sub>2</sub> and Ru/Vulcan.....	117

A.1. H <sub>2</sub> -Chemisorption Experiment .....	117
A.2. Average Particle Size Distribution of Ru/SiO <sub>2</sub> and Ru/Vulcan.....	119
A.3. Cooling in H <sub>2</sub> Flow .....	119
B. Supplementary Information – Support Effects in Ammonia Synthesis .....	121
B.1. Heat of Adsorption of H <sub>2</sub> and CO Measurement.....	121
B.2. Ru metal dispersions of Ru/HAp catalysts .....	121
B.3. Details of Single Point Ammonia Adsorption Calorimetry.....	122
B.4. Effect of reactant pressure on NH <sub>3</sub> synthesis reaction rate.....	123
B.5. Ammonia synthesis rate with quartz dilution .....	124
B.6. Ammonia desorption over Ru catalysts diluted with quartz.....	125
B.7. Conversion vs. Space Time Graph .....	125
C. H <sub>2</sub> -Chemisorption Experiment .....	128
C.1. Reduction Procedure .....	128
D.2. Measurement of H <sub>2</sub> Adsorption Isotherms.....	128
D. Heat and Mass Transfer Limitations .....	130
D.1. External Mass Transfer Resistance .....	130
E.2. Heat Transfer Resistance .....	133
F. Calculation for Conductivity Measurements .....	136
G. Calculation of H <sub>2</sub> Consumption in Temperature Programmed Analysis.....	137
CURRICULUM VITAE .....	139

## LIST OF TABLES

### TABLES

Table 2.1. Experimental NH <sub>3</sub> Synthesis Reaction Rates at Steady State Operating Conditions.....	11
Table 2.2. Rate expressions for the ammonia synthesis reaction. ....	12
Table 4.1. Hydrogen storage materials and reported adsorption/desorption characteristics data.....	45
Table 4.2. H <sub>2</sub> consumption amounts of fresh Ru/SiO <sub>2</sub> catalysts during H <sub>2</sub> -TPR.....	53
Table 4.3. H <sub>2</sub> consumption amounts of fresh Ru/Vulcan catalysts during H <sub>2</sub> -TPR..	54
Table 4.4. Ru metal dispersions of Ru/SiO <sub>2</sub> catalysts obtained from different methods. ....	57
Table 4.5. Ru metal dispersions of Ru/Vulcan materials obtained from different methods.....	58
Table 5.1. Ammonia synthesis reaction rates, TOF values and the related operating conditions reported in the literature over supported Ru based catalysts .....	65
Table 5.2. The reported apparent activation energies of Ru based catalysts used for ammonia synthesis reaction.....	65
Table 5.3. Comparison of surface area of supports using BET and amounts of adsorbed ammonia .....	69
Table 5.4. Loading, dispersion and average particle diameter of supported Ru <sup>0</sup> nanoparticles .....	69
Table 5.5. Initial NH <sub>3</sub> formation rates over supported Ru catalysts (H <sub>2</sub> :N <sub>2</sub> :Ar=3:1:2) .....	71
Table 5.6. Total amount of NH <sub>3</sub> production during one hour of the synthesis and desorbed amounts after the reaction over supported Ru catalysts.....	73
Table 6.1. Elemental analysis results (nitrogen content) of Co <sub>3</sub> Mo <sub>3</sub> N.....	82
Table 6.2. Comparison of required amount of H <sub>2</sub> to reduce the possible oxides on passivated Co <sub>3</sub> Mo <sub>3</sub> N surface .....	84

Table 6.3. Measured ammonia formation rates and calculated apparent activation energy over $\text{Co}_3\text{Mo}_3\text{N}$ catalyst.....	85
Table 6.4. Summary of amount of formed and desorbed $\text{NH}_3$ during/after reactor operation.....	90

## LIST OF FIGURES

### FIGURES

Figure 1.1. Trends in human population with and without synthetic nitrogen fertilizers throughout the 20 <sup>th</sup> Century [2], [3].....	1
Figure 1.2. Energy consumption vs. production volume diagram of the most produced chemicals all over the world [4] .....	2
Figure 1.3. Flow diagram of ammonia synthesis process with different hydrocarbon raw materials: a) Steam reforming route, b) Partial oxidation route .....	3
Figure 1.4. Energy consumption for ammonia production through the years and comparison with biological ammonia production [9].....	4
Figure 2.1. Equilibrium conversion vs. temperature diagram of ammonia synthesis reaction at different feed ratios (H <sub>2</sub> :N <sub>2</sub> ) and operation pressure.....	10
Figure 2.2. Two possible types of B <sub>5</sub> -type active sites.....	14
Figure 2.3. Crystal structure of nitrogenase enzyme [98] (reproduced by the permission of Springer Nature. Permission to reuse must be obtained from the rightsholder).....	26
Figure 2.4. Lowe-Thorneley nitrogen reduction reaction mechanism [100].....	28
Figure 2.5. Proposed reaction mechanism by Yandulov and Schrock and intermediates in the reduction of dinitrogen at a hypothetical Mo center through the stepwise addition of protons and electrons [106] .....	29
Figure 3.1. Temperature program scheme of ammonolysis process .....	33
Figure 3.2. Schematic Representation of Chemisorption Manifold .....	34
Figure 3.3. Schematic Representation of Chemisorption Manifold and Microcalorimeter .....	36
Figure 3.4. Schematic representation of experimental setup for ammonia synthesis using DRIFTS spectrometry .....	39
Figure 3.5. Experimental Setup for Ammonia Synthesis Reaction under Steady Flow Conditions.....	40

Figure 3.6. Experimental Setup for Ammonia Synthesis Reaction under Unsteady State Flow Conditions .....	41
Figure 4.1. HR-TEM images of a) 1 wt% Ru/SiO <sub>2</sub> , b) 3 wt% Ru/SiO <sub>2</sub> , c) 5 wt% Ru/SiO <sub>2</sub> .....	49
Figure 4.2. Ru metal particle size distributions of Ru/SiO <sub>2</sub> catalysts .....	50
Figure 4.3. HR-TEM images of a) 1 wt% Ru/Vulcan b) 3 wt% Ru/Vulcan, c) 5 wt% Ru/Vulcan .....	51
Figure 4.4. Ru metal particle size distributions of Ru/Vulcan catalysts .....	52
Figure 4.5. Temperature Programmed Reduction of 1,3 and 5 wt% Ru/SiO <sub>2</sub> catalysts. ....	53
Figure 4.6. Temperature Programmed Reduction of 1,3 and 5 wt% Ru/Vulcan catalysts. ....	54
Figure 4.7. ATR-IR spectra of a) pure Vulcan, b) fresh 1, 3, and 5 wt% Ru/Vulcan catalysts, c) 1, 3, 5 wt% Ru/Vulcan catalysts after H <sub>2</sub> -TPR, TPD and O <sub>2</sub> -titration experiments .....	55
Figure 4.8. Temperature Programmed Desorption profiles of Ru/SiO <sub>2</sub> materials. ....	56
Figure 4.9. Temperature Programmed Desorption profiles of Ru/Vulcan materials. ....	58
Figure 4.10. Differential heats of adsorption of hydrogen on 1 wt% Ru/Vulcan at 50 °C.....	59
Figure 4.11. Hydrogen release at lower hydrogen coverages is diffusion limited, requiring higher temperatures. ....	60
Figure 5.1. Heat of adsorption of ammonia over HAp at 323 K; • belongs to differential heat of adsorption of ammonia, ■ belongs to single point heat of ammonia adsorption at 515 Torr.....	68
Figure 5.2. HR-TEM images of a) 1.37 wt% Ru/Zeolite-Y, b) 4.0 wt% Ru/HAp, c) 1.0 wt% Ru/Vulcan and corresponding particle size distribution histograms of d) 1.37 wt% Ru/Zeolite-Y, e) 4.0 wt% Ru/HAp, f) 1.0 wt% Ru/Vulcan.....	70
Figure 5.3. Conversion vs. temperature graph of ammonia synthesis reaction over supported Ru catalysts.....	72

Figure 5.4. Comparison of desorbed amount of ammonia and total amount of synthesized ammonia during reaction tests a) 2 wt% HAp and 4 wt% HAp; b) 1.37 wt% Ru/Zeolite-Y and 1 wt% Ru/Vulcan (Reaction tests were carried out app. for 1 hr.).....	73
Figure 5.5. Cumulative ammonia synthesis with time under pulse flow ( $H_2:N_2=3:1 - 10 \text{ min} \ \& \ N_2 - 10 \text{ min}$ , 100 mL/min) and steady state flow ( $H_2:N_2=3:1$ , 100 mL/min) conditions over 2.0 wt% Ru/HAp at 400 °C. The dashed-vertical lines correspond to end of $H_2:N_2=3:1$ flow, the straight-vertical lines correspond to end of pure $N_2$ flow under pulse flow .....	75
Figure 5.6. IR spectra of fresh and consumed 4 wt% Ru/HAp catalysts.....	75
Figure 5.7. Ammonia synthesis reaction over 2.0 wt% Ru/HAp operated under firstly at steady state flow conditions, followed by pulse flow conditions at 400 °C and atmospheric pressure. ....	76
Figure 6.1. XRD Pattern of $Co_3Mo_3N$ (the peaks marked with a diamond belong to $Co_3Mo_3N$ ) .....	82
Figure 6.2. $H_2$ -TPR pattern of $Co_3Mo_3N$ .....	83
Figure 6.3. $H_2$ adsorption isotherms of $Co_3Mo_3N$ at 25 °C, 50 °C, and 100 °C .....	84
Figure 6.4. Effect of $H_2:N_2$ ratio on the ammonia formation rate over $Co_3Mo_3N$ catalyst at 400 °C .....	86
Figure 6.5. Cumulative ammonia synthesis with time under pulse flow of $H_2:N_2=3:1 \ \& \ N_2$ and $H_2:N_2=0.5:1 \ \& \ N_2$ under 100 mL/min at 400 °C. The valve switching time was 10 min.....	87
Figure 6.6. Cumulative $NH_3$ synthesis under 100 mL/min $H_2:N_2=3:1$ and pure $N_2$ flows over $Co_3Mo_3N$ at 400 °C and atmospheric pressure .....	88
Figure 6.7. Cumulative ammonia synthesis with time under pulse flow ( $H_2:N_2=3:1 - 10 \text{ min} \ \& \ N_2 - 10 \text{ min}$ , 100 mL/min) and steady state flow ( $H_2:N_2=3:1$ , 100 mL/min) conditions over $Co_3Mo_3N$ at 400 °C.....	88
Figure 6.8. Cumulative ammonia synthesis for long period of times under pulse flow ( $H_2:N_2=3:1 - 10 \text{ min} \ \& \ N_2 - 10 \text{ min}$ , 100 mL/min) and steady state flow ( $H_2:N_2=3:1$ , 100 mL/min) conditions over $Co_3Mo_3N$ at 400 °C. ....	89

## LIST OF ABBREVIATIONS

### ABBREVIATIONS

ATR-IR	Attenuated Total Reflectance-Infrared Spectroscopy
BET Method	Brunauer-Emmett-Teller Method
CNF	Carbon Nanofiber
DFT	Density Functional Theory
DRIFTS	Diffuse Reflectance Infrared Fourier Transform Spectroscopy
EXAFS	Extended X-Ray Absorption Fine Structure
HAp	Hydroxyapatite
HR-TEM	High Resolution Transmission Electron Microscopy
ICP-OES	Inductively Coupled Plasma – Optical Emission Spectroscopy
NMR	Nuclear Magnetic Resonance
SBA-15	Santa Barbara Amorphous-15
SWCNT	Single Wall Carbon Nanotube
TOF	Turnover Frequency, $\frac{[\# \text{ of molecules}]}{[\# \text{ of active sites}][\text{time}]}$
TPD	Temperature Programmed Desorption
TPO	Temperature Programmed Oxidation
TPR	Temperature Programmed Reduction
XPS	X-Ray Photoelectron Spectroscopy
XRD	X-Ray Diffraction

## LIST OF SYMBOLS

### SYMBOLS

$a_i$	Activity coefficient of species i
$C_{i,b}, \text{ kmol m}^{-3}$	Bulk concentration of i
$C_{i,s}, \text{ kmol m}^{-3}$	Surface concentration of i
$D_{AB}, \text{ m}^2 \text{ s}^{-1}$	Diffusion coefficient
$D_e, \text{ m}^2 \text{ s}^{-1}$	Effective diffusion coefficient
$d_p, \text{ m}$	Particle diameter
$E_A, \text{ kJ mol}^{-1}$	Apparent activation energy
$h, \text{ kW m}^{-2} \text{ K}^{-1}$	Heat transfer coefficient
$k, \text{ s}^{-1} \text{ or Pa.s}^{-1}$	Rate constant
$K_i$	Equilibrium constant of species i
$k_m, \text{ m s}^{-1}$	External mass transfer coefficient
$P_i, \text{ bar}$	Partial pressure of species i
$R, \text{ J/mol}\cdot\text{K}$	Ideal gas constant
$Re$	Reynolds number
$R_i, \text{ kmol kg}^{-1} \text{ s}^{-1}$	Reaction rate of species i
$\rho_b, \text{ kg m}^{-3}$	Bulk density of catalyst
$\sigma_c$	Constriction factor
$\tau$	Tortuosity
$\Phi_p$	Porosity

# CHAPTER 1

## INTRODUCTION AND SCOPE

### 1.1 Ammonia Production vs. Energy

In a recent publication, ammonia production was defined as “Never Ending Story” [1]. The core meaning of this statement mainly originated from ammonia molecule itself because of its fixed nitrogen content. Ammonia is one of the main sources of nitrogen that has been used in nature. The significant effect of the invention of ammonia production process from its elements, called the Haber-Bosch process, at the beginning of the 20<sup>th</sup> Century on the rapid increase of the world population is given in Figure 1.1. [2]. The production of nitrogen based fertilizers and the increase in the world population have supported each other through the years. In the scope of sustainable manufacturing, technology of ammonia production requiring lower temperatures and pressures is needed.

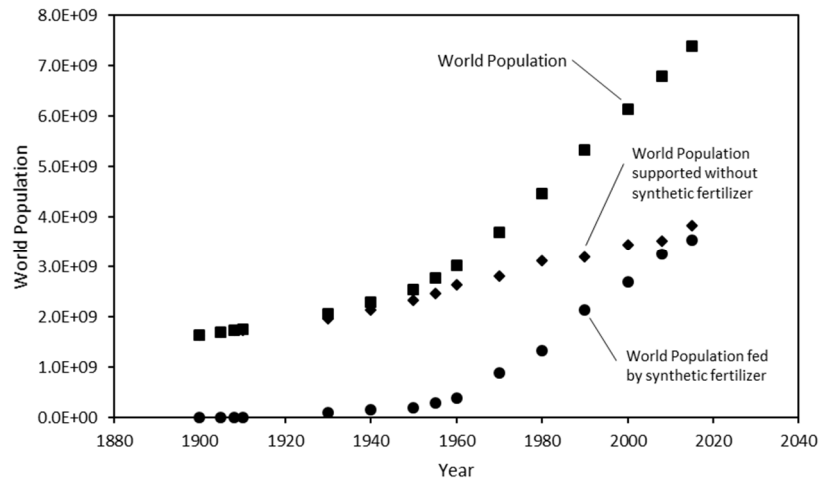


Figure 1.1. Trends in human population with and without synthetic nitrogen fertilizers throughout the 20<sup>th</sup> Century [2], [3]

Figure 1.2. shows that ammonia is the most produced commodity chemical and at the same time it is the one of the most energy-intensive processes among petroleum based industry [4]. The Haber-Bosch process consumes annually 2% of world energy production and 4 % of the total natural gas output [5]. The ammonia production process operates under high temperature and high pressure operating conditions due to its mildly exothermic thermodynamics. High temperatures is needed to obtain significant reaction rates, and high pressure is needed to shift the reaction in the forward direction. R&D efforts have focused on inventing a more sustainable and energy efficient ammonia production process. Moreover, the U.S. National Academy of Engineering have set the management of the nitrogen cycle problem as one of the 14 Grand Challenges of Engineering that need to be overcome in the 21<sup>st</sup> Century[6].

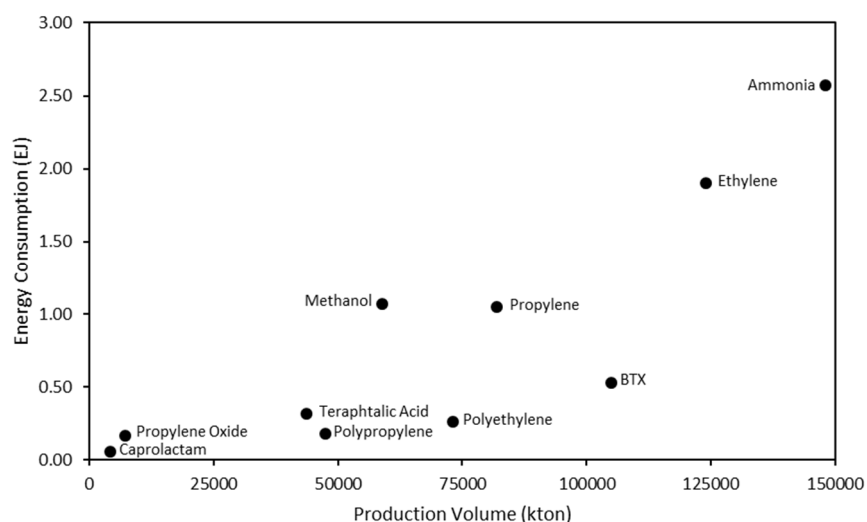


Figure 1.2. Energy consumption vs. production volume diagram of the most produced chemicals all over the world [4]

## 1.2 Haber-Bosch Process

In 1909, Fritz Haber and his assistant, Robert Le Rossignol, synthesized ammonia from its elements at a rate of ~2 ml/min in an experimental setup that had the capability of operation at high temperatures and high pressures [7]. Later, the BASF company purchased all the rights of the experimental demonstration of ammonia synthesis to develop an industrial high pressure ammonia synthesis process. One of the process

engineers working for the BASF company, Carl Bosch, was tasked with the industrialization of ammonia synthesis. In 1910, BASF company announced the first industrial high pressure ammonia production process. The process was termed the Haber-Bosch process. The general operating conditions of the Haber-Bosch process are 150-250 bar and 400 – 500 °C in the presence of a magnetite derived catalyst.

In Figure 1.3., the general flow diagram of the Haber-Bosch process is given [8]. Hydrogen can be obtained through two different methods: steam reforming or partial oxidation. After the completion of the required steps to obtain stoichiometric  $H_2:N_2$  ratio, the gas mixture is compressed and sent into the ammonia synthesis reactor. Compressors, the ammonia synthesis reactor and separation of ammonia units are operated in a cycle, which means the unreacted gas recycles to the ammonia synthesis reactor.

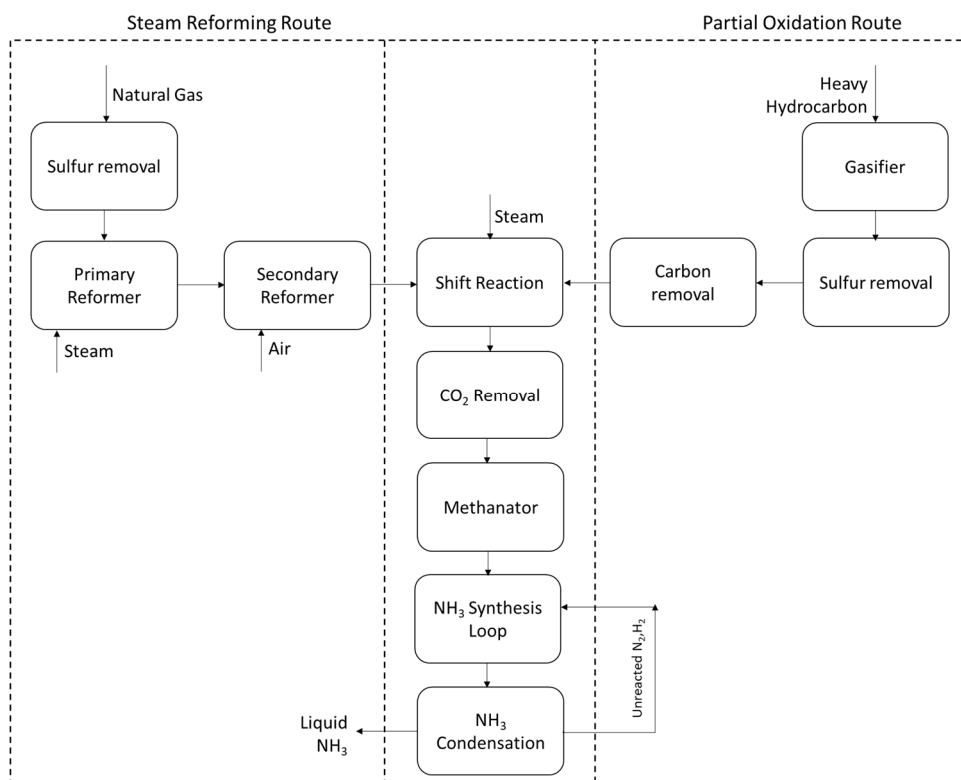


Figure 1.3. Flow diagram of ammonia synthesis process with different hydrocarbon raw materials: a) Steam reforming route, b) Partial oxidation route

### 1.3 Sustainable Ammonia Production

Figure 1.4. shows the decrease in energy requirement for production of ammonia over a number of years [9]. It can be easily seen that discovery of the Haber-Bosch process is a milestone for ammonia production. Although there has been a great improvement within 100 years in terms of energy efficiency and even low energy need with respect to the biological systems (500 kJ/mole NH<sub>3</sub>) [10], today's technology is insufficient for sustainable ammonia production. High-energy intensive characteristics, CO<sub>2</sub> emissions, extra energy requirement for hydrogen production and recycling of unreacted synthesis gas in ammonia synthesis loop were the main drawbacks of the Haber-Bosch process [5]. Large investment costs and the lack of a sustainable catalyst make the process more inefficient.

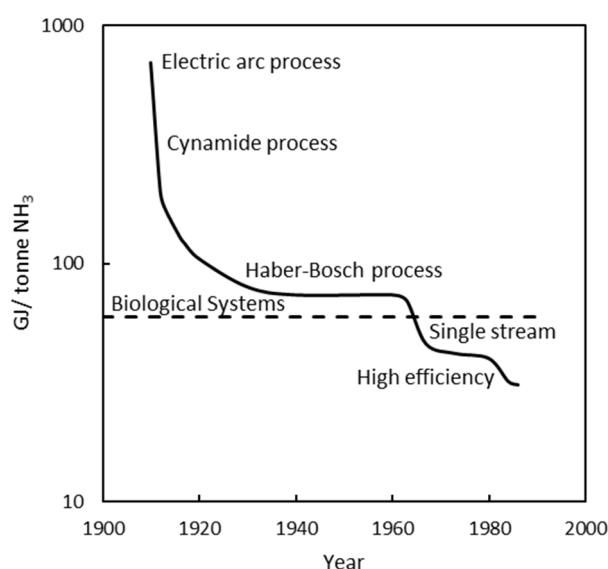


Figure 1.4. Energy consumption for ammonia production through the years and comparison with biological ammonia production [9]

Recent research studies showed that an agent is required to reduce the molecular nitrogen, which has the stable triple bond, to atomic nitrogen for the ammonia synthesis. Norskov et al. stated that a sustainable and active catalyst (agent) should

synthesize ammonia at a rate of  $1 \frac{\text{NH}_3 \text{ molecule}}{(\text{active site})(\text{sec.})}$  [11]. Biological ammonia synthesis is a catalytic route utilizing nitrogenase enzyme, which does not need any renovation throughout the years [7]. There are many efforts attempting to invent a new ammonia synthesis route that can replace Haber-Bosch technology and that can be operated at room temperature and atmospheric pressure such as electrochemical routes [12], photocatalytic routes [13], (solar) chemical looping [14] and biochemical routes [15]. Although these new routes are promising, they still cannot be efficient as a conventional method for production.

Ammonia and ammonia derivatives also can be good candidates as hydrogen carriers due to their high gravimetric hydrogen content, non-hazardous by-products. Furthermore, ammonia and derivatives satisfy the DOE targets, in terms of hydrogen amount in their structure, in principle [16], [17]. One of the main advantages of ammonia as an energy carrier is that transportation of ammonia is well established compared to hydrogen. Ammonia can be one of the carbon free fuels due to easiness of its shipment and storage although the production of ammonia with industrial Haber-Bosch process releases significant amount of CO<sub>2</sub>.

#### **1.4 Objective of the Thesis**

The aim of this thesis is to demonstrate a solution for a sustainable ammonia production process based on surface reaction characteristics of ammonia synthesis using unsteady state operating conditions under milder temperatures and atmospheric pressure.

Ammonia synthesis is a thermodynamically limited reaction. Therefore, steady state production of ammonia eventually reaches equilibrium, and per pass conversion is about 30% under industrial operating conditions (400-500 °C and 100-300 bar). In order to sustain ammonia production in a more efficient way, one should either increase the conversion, which require operating at lower temperatures, hence sacrificing rates, or decrease the cost of the process at similar conversion.

In order to achieve higher ammonia synthesis rate under milder temperature and pressure conditions over supported Ru catalysts, the effects that deactivate the supported Ru catalysts should be eliminated. Ammonia synthesis reaction is inhibited by hydrogen and ammonia in the presence of Ru based catalysts. In the framework of this study, the ways of elimination of inhibition effects of hydrogen and ammonia are investigated.

Another way of improving the efficiency of ammonia production is to decrease the cost of the process. One of the main cost items of ammonia production is production of hydrogen. In this circumstance, the efficient use of hydrogen in the process is investigated over  $\text{Co}_3\text{Mo}_3\text{N}$  catalyst using unsteady flow conditions.

## **1.5 Scope of Thesis**

In the scope of this thesis, the following studies are carried out in order to propose a potential unsteady state ammonia synthesis production method to achieve reasonable rates under milder temperature and pressure conditions:

In chapter two, a general literature survey on ammonia synthesis reaction over supported Ru and  $\text{Co}_3\text{Mo}_3\text{N}$  catalysts were given. The parameters that influence the ammonia synthesis rate over supported Ru catalysts and related studies are explained such as effect of Ru particle size, support type, addition of alkaline/earth alkaline promoters. In addition, the inhibition effects of hydrogen and ammonia and related solution strategies were mentioned.

From an experimental point of view, hydrogen poisoning was monitored by adsorption and desorption characteristics as well as spillover on Ru based catalysts in chapter four. The effect of Ru metal loading and support type on the amount of hydrogen adsorption and the energetics of hydrogen adsorption/desorption over supported Ru catalysts were investigated.

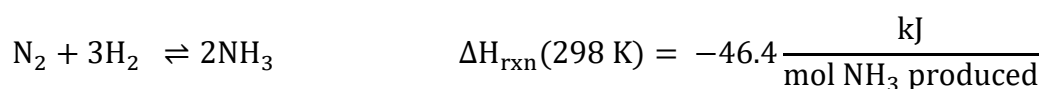
In chapter five, the effect of ammonia retention on the ammonia synthesis rate was studied over Ru/zeolite-Y, Ru/HAp and Ru/Vulcan catalysts. It was observed during steady state ammonia synthesis reaction experiments that ammonia eventually inhibited and stopped the reaction regardless of surface acidity of the support material. In order to revive the deactivated supported Ru catalyst under steady state flow due to the poisoning effect of synthesized ammonia, N<sub>2</sub> pulses were fed to the reactor in a specified time period of 10 min. As a result, supported Ru catalysts were re-activated. Finally, unsteady state ammonia synthesis reactions experiments were performed over Co<sub>3</sub>Mo<sub>3</sub>N catalyst. It was shown that there was no effect of H<sub>2</sub>:N<sub>2</sub> feeding ratio on the ammonia synthesis rate over Co<sub>3</sub>Mo<sub>3</sub>N for H<sub>2</sub> partial pressures greater than 100 Torr. This pressure was determined as the pressure the catalyst surface saturated with adsorbed hydrogen by static chemisorption experiments. Similar ammonia synthesis rates were obtained under steady and pulse flow conditions.



## CHAPTER 2

### AMMONIA SYNTHESIS

In the 19<sup>th</sup> Century, ammonia was produced with different methods such as the electric arc process and cyanamide process [18]. The main disadvantage of traditional ammonia production processes at that time was to use of energy; for example, cyanamide process consumed approximately 190 GJ per ton of ammonia [18]. The trials to synthesize ammonia from its elements started in the beginning of the 19<sup>th</sup> Century. A strong basis of knowledge on the equilibrium thermodynamics was needed before the attempts were successful [18]. Fritz Haber developed first process that could be scaled up where ammonia could be produced from nitrogen and hydrogen molecules. The reaction stoichiometry of ammonia production is given below:



The thermodynamics of the ammonia synthesis reaction give important details relating to the production strategy. Figure 2.1 represents that decreasing the feed ratio of H<sub>2</sub>:N<sub>2</sub> from 3.0, which is the stoichiometric ratio, to 1.5 improves the equilibrium conversion value at the same operating conditions. At low pressure conditions, equilibrium conversion line of ammonia synthesis reaction shifts to the left. In addition, while ammonia synthesis reaction is a spontaneous reaction ( $\Delta G = -16.6 \text{ kJ/mol}$  at 300 K), ammonia synthesis reaction at higher temperatures become a non-spontaneous reaction ( $\Delta G = 15.8 \text{ kJ/mol}$ , at 600 K). Although it seems to be an advantage to carry out production process at milder conditions (in terms of temperature and pressure), ammonia synthesis rates are extremely low at milder temperature and pressure conditions. In addition, Le-Chatelier's principle dictates higher operating pressures to shift the reaction in forward direction.

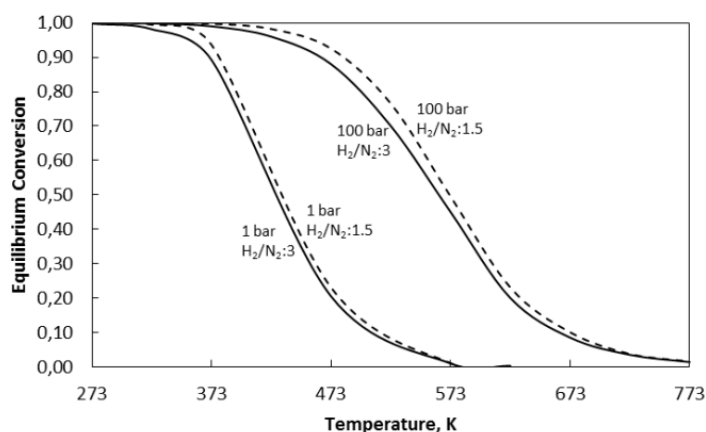


Figure 2.1. Equilibrium conversion vs. temperature diagram of ammonia synthesis reaction at different feed ratios ( $H_2:N_2$ ) and operation pressure.

## 2.1 Catalytic Ammonia Synthesis Rates

There are several type of catalysts used for ammonia synthesis reaction. Traditional magnetite catalyst, supported Ru based catalysts and molybdenum nitride based catalysts are the well-known catalysts. For a sustainable ammonia production, Norskov and his coworkers stated that a catalyst having ammonia synthesis activity of 1 turnover frequency (TOF,  $\frac{\text{molecule}}{(\text{active site})(\text{sec.})}$ ) at 373 K and 1 bar pressure can be said as to be an ideal catalyst [11]. Activities of different type of ammonia synthesis catalysts are given in Table 2.1. Although supported Ru based catalysts have higher activity with respect to magnetite catalysts at same operating conditions, most of the industrial process use magnetite as ammonia synthesis catalyst due to that magnetite is three orders of magnitude cheaper than ruthenium.

Table 2.1. Experimental NH<sub>3</sub> Synthesis Reaction Rates at Steady State Operating Conditions

Reference	Catalyst	Metal Loading, %wt	Temperature, K	Pressure, bar	Flow Rate, ml min <sup>-1</sup>	Rate, μmol g <sup>-1</sup> s <sup>-1</sup>
[19]	Cs-Ru/MgO	5.0	588	1	120	0.40
[20]	Cs-Ru/MgO	5.0	673	63	---	11.40
[21]	Ru/BHA	8.0	588	1	60	0.23
[21]	Ru/BHA	8.0	588	11	60	0.33
[22]	Ru/C <sub>12</sub> A <sub>7</sub> :e-	1.2	633	1	60	0.76
[23]	Co <sub>3</sub> Mo <sub>3</sub> N	---	673	1	60	0.05
[24]	Co <sub>3</sub> Mo <sub>3</sub> N	---	673	31	60	2.78
[24]	Cs-Co <sub>3</sub> Mo <sub>3</sub> N	---	673	31	60	5.83
[25]	Ru/Al <sub>2</sub> O <sub>3</sub>	7.0	373	4	40	1.10
[26]	Fe <sub>3</sub> O <sub>4</sub>	---	673	86	---	2.72
[27]	Ba-Ru/Graphite	5.4	673	50	40	32.80

## 2.2 Proposed Rate Equations

The reported semi-empirical ammonia synthesis reaction rate expressions throughout the years are given in Table 2.2. Ammonia synthesis rate expression derived based on Langmuir-Hinshelwood model assuming that N<sub>2</sub> adsorption and dissociation is the rate limiting step is also given. When ammonia synthesis rate expressions are examined, it is seen that the activity coefficients (or partial pressures) of both hydrogen and ammonia are in the denominator which mean that they inhibit the reaction. In some of the expressions,  $\alpha$  appears. “ $\alpha$ ” is the ratio of linear variation of change of activation of nitrogen adsorption with respect to nitrogen coverage to linear variation of heat of adsorption of nitrogen with respect to nitrogen coverage. The value of  $\alpha$  changes between 0.4-0.5 [28].

Table 2.2. Rate expressions for the ammonia synthesis reaction.

	Rate Expressions		
Temkin and Pzyhev [28]	$r = k'_1 P_{N_2} \left( \frac{P_{H_2}^3}{P_{NH_3}^2} \right)^\alpha - k'_2 \left( \frac{P_{NH_3}^2}{P_{H_2}^3} \right)^{1-\alpha}$		
Ozaki et al. [29]	Langmuir Adsorption Model	Temkin Adsorption Model	
	$r = k P_{N_2} \frac{1}{\left( 1 + K \frac{P_{NH_3}}{P_{H_2}^{1.5}} \right)^2}$	$r = k P_{N_2} \frac{1}{\left( 1 + K \frac{P_{NH_3}}{P_{H_2}^{1.5}} \right)^{2\alpha}}$	
Cappelli and Collina [30]	$r = \frac{k_2^0 \left[ a_{N_2} K_a^2 - \left( \frac{a_{NH_3}^2}{a_{H_2}^3} \right) \right]}{\left[ 1 + K_3 \left( \frac{a_{NH_3}}{a_{H_2}^{\omega}} \right) \right]^{2\alpha}}$		
Rossetti et al. [31]	$r = k_r \lambda(q) \frac{(a_{N_2})^{0.5} \left[ \frac{(a_{H_2})^{0.375}}{(a_{NH_3})^{0.25}} - \frac{1}{K_a} \left[ \frac{(a_{NH_3})^{0.75}}{(a_{H_2})^{1.125}} \right] \right]}{1 + K_{H_2} (a_{H_2})^{0.3} + K_{NH_3} (a_{NH_3})^{0.2}}$		
Rambeau et al. [32]–[34]	Iron surface	Ruthenium Surface	Osmium Surface
	$r = \frac{k_s P_{N_2}}{(1 + K P_{NH_3})^2}$	$r = \frac{k_s P_{N_2}}{P_{H_2}}$	$r = \frac{k_s P_{N_2}}{P_{H_2} (1 + K P_{NH_3})^2}$
Reaction Rate derived from a microkinetic model	$r = k P_{N_2} \theta_v^2$ $\theta_v = \frac{1}{1 + (K_6 P_{H_2})^{1/2} + \left( \frac{1}{K_2 K_3 K_4 K_5 K_6^{1.5} P_{H_2}^{1.5}} + \frac{1}{K_3 K_4 K_5 K_6 P_{H_2}} + \frac{1}{K_4 K_5 K_6^{0.5} P_{H_2}^{0.5}} + \frac{1}{K_5} \right) P_{NH_3}}$		

### 2.3 Literature on Catalytic/Enzymatic Ammonia Synthesis

The research studies to find the best catalyst for ammonia synthesis reaction are focused on supported ruthenium catalysts and cobalt molybdenum catalysts in recent years. The parameters that affect the ammonia synthesis reaction over ruthenium based catalysts are explained. In addition, the problems and suggested solutions related to ammonia synthesis reaction in the presence of supported Ru catalysts are mentioned.

Cobalt molybdenum nitride ( $Co_3Mo_3N$ ) catalysts are getting attention due to its nitrogen transfer characteristics and long-term stability for the ammonia synthesis reaction. A general literature survey on ammonia synthesis reaction over  $Co_3Mo_3N$  catalysts are given in the literature survey part of the thesis.

Ammonia synthesis reaction in the nature are carried out in the presence of nitrogenase enzyme at ambient temperature and atmospheric pressure conditions. Therefore, the studies in the literature to enlighten the mechanism of ammonia synthesis over nitrogenase enzyme is one of the subjects of the researchers. Discovery of the details of the ammonia synthesis mechanism over nitrogenase enzyme can be a very important milestone for producing of ammonia at milder temperature and pressure conditions.

### **2.3.1 Supported Ruthenium Catalysts**

Supported Ru based catalysts are termed as the second-generation ammonia synthesis catalysts [35]–[37]. The reason is to show the higher activity at same operating conditions with respect to traditional magnetite derived catalysts. Since there are many studies in the literature for Ru based ammonia synthesis catalysts, the effective parameters and related literature will be discussed in this section. A brief literature survey is given below for the parameters that affect ammonia synthesis rate:

#### **2.3.1.1 Effect of Particle Size**

Studies in the literature showed that ammonia synthesis is a highly structure sensitive reaction in the presence of supported Ru catalysts [27], [38]. B<sub>5</sub>-type active sites (shown in Figure 2.2) were proposed as the responsible sites for the nitrogen molecule adsorption and dissociation, which is known to be the rate determining step for ammonia synthesis [27], [38], [39]. van Hardeveld and van Monfoort described the B<sub>5</sub>-type sites, which are three atoms located in a triangular coordination with two adjacent atoms located in one layer above, using the marble models of a Ni face centered cubic (fcc) crystal with basic orthorhombic surface morphology [40]. Their modelling calculations showed that B<sub>5</sub>-type active sites could be present when the metal particle size change between 1.8-2.5 nm.

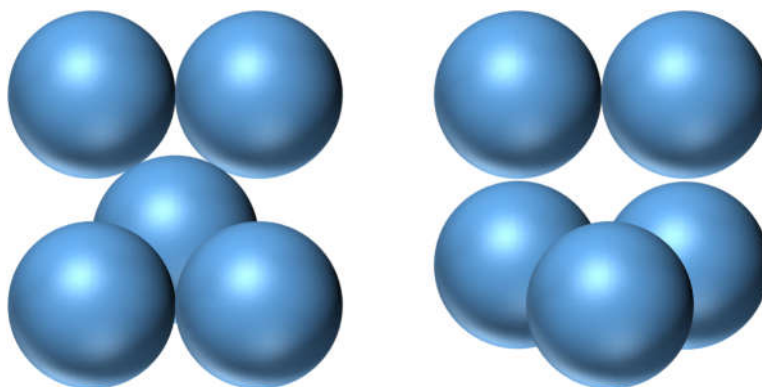


Figure 2.2. Two possible types of B<sub>5</sub>-type active sites

There are several studies in the literature on the effect of Ru particle size on the ammonia synthesis reaction. Experimental studies showed that Ru metal particle size is an important parameter for catalytic activity. Most of the experimental studies showed that highly active supported Ru catalysts have an average particle diameter app. 1.5 – 3.0 nm [38], [41]–[44].

Jacobsen et al. performed both an experimental and theoretical study on the effect of Ru metal particle size upon the ammonia synthesis reaction rate [38]. Single crystal and electronic DFT calculations showed that the ammonia synthesis reaction is a very structure sensitive reaction due to the possibility of the existence of B<sub>5</sub>-type active sites on Ru particles. They also presented a correlation between the ratio of B<sub>5</sub>-type active sites to the total number of surface atoms and particle diameter. According to calculation, the density of B<sub>5</sub>-type active sites is maximum when the particle diameter is 1.8-2.0 nm. They also explained the activity loss of Ru/MgAl<sub>2</sub>O<sub>4</sub>, which showed the highest catalytic activity, with time as the increasing particle diameter of Ru due to sintering under reaction conditions.

Rarog-Pilecka et al. carried out a similar research study on the presence of B<sub>5</sub>-type active sites and the relationship between the Ru particle diameter and ammonia synthesis rate [44]. According to theoretical calculations, it was found that the density of B<sub>5</sub>-type sites in 3-4 nm particles were higher than for 1-2 nm particles. Experimental studies showed for all promoted (Ba+Cs, Cs, Ba) Ru/C catalysts that the ammonia

synthesis reaction rate was optimum in the presence of 1.5-2.0 nm diameter Ru metal particle. TOF values increased with increasing Ru metal particle size. They also extrapolated the TOF vs particle diameter graph and commented that there should not be any activity observed below 0.7-0.8 nm particle diameter.

Lin et al. investigated the effect of Ru particle size on the ammonia synthesis rate [42]. They also examined factors, such as metal loading and pre-treatment conditions that influence the Ru metal particle diameter. They showed that the Ru metal particle diameter increased with increasing the temperature in either hydrogen reduction treatment or air calcination treatment. It was also shown that metal loading increased the metal particle diameter. According to the results of experimental study, they could not find a direct relationship between Ru particle size and TOF values. They reported that increasing the metal loading increased the ammonia synthesis rate but decreased the TOF values due to the fact that increasing the metal loading decreased the number of B<sub>5</sub>-type sites because of the particle size increase. They obtained the maximum TOF value in the presence of 2.2 nm Ru particle diameter catalyst.

By contrast to the observation there is an optimum Ru particle diameter for ammonia synthesis reaction, there are several studies which report that there is a synergistic effect when supported Ru catalyst have a broad Ru metal particle size [25], [45]–[48]. Fernandez et al. synthesized broad particle size distributed Ru/Al<sub>2</sub>O<sub>3</sub> catalysts with Ru metal loading in the range 3 – 7 wt% [45]–[48]. According to catalytic activity experiments, the catalyst having a broad Ru particle size distribution showed the highest catalytic activity. The authors argued that while large particles were responsible for dissociative hydrogen adsorption and diffusion to small particles via surface hydroxyl groups over support surface, small particles were responsible for ammonia synthesis. Therefore, the cooperation of small and large particles showed a synergy in both reaction rate promotion and hydrogen mobility. They concluded that for high activity in ammonia synthesis in the presence of Ru based catalysts, a broad particle size distribution was needed.

A similar experimental study was carried out by Karim et al. [48] for the ammonia decomposition reaction over Ru/Al<sub>2</sub>O<sub>3</sub> catalysts. On the contrary to the literature values, for optimum Ru particle diameter which was determined via both theoretically and experimentally, they observed the highest activity with the catalyst having approximately 7 nm Ru particle size. They explained this observation with the structural shape of the metal particles. They showed that the number of B<sub>5</sub> type sites for elongated shape Ru metal particles was observed when the particle diameter was about 7 nm. In addition, for hemispherical Ru metal particles, the number of B<sub>5</sub>-type sites were maximum when the particle diameters were between 1.8 and 3.3 nm. They proposed that broad Ru metal particle size distribution was responsible for high catalytic activity.

There are also DFT studies on the influence of Ru particle size on the ammonia synthesis reaction [49], [50]. Dooling et al. investigated the effect of particle size and surface structure of Ru on the catalytic activity [50]. They determined that the adsorption energy of nitrogen molecule on the Ru particles closely related with the surface Ru atom coordination. Ishikawa et al. carried out a DFT study with Ru, Os, and Rh based catalysts. In this study, they correlated the number of step sites with metal particle size. It was shown that the ratio between step sites and total number of particle sites was maximum when the Ru particle size is equal to 2.5 nm. This relation (between the ratio of number of step sites to total number of sites) was also coupled with experimental reaction rate values.

### **2.3.1.2 Hydrogen Poisoning and Suggested Solutions**

The inhibition effect of hydrogen as a reactant for ammonia synthesis reaction over supported Ru catalysts is already acknowledged. The results of experimental studies of both Siporin and Davis [51], and Muhler et al. [52] showed that hydrogen poisons the reaction with an order of ca. -1 over Ru/MgO catalyst. The reported solutions for the removal of inhibition effect of hydrogen in the literature are addition of alkaline/earth alkaline/lanthanide promoters, use of a feed ratio of H<sub>2</sub>:N<sub>2</sub> = 1.5:1

instead of using stoichiometric ( $H_2:N_2=3:1$ ) ratio and operate the reactor under forced unsteady state conditions.

#### *Alkaline/Earth Alkaline/Lanthanide Promotion*

Alwin Mittasch had shown that alkali addition to the iron based ammonia synthesis catalysts increased the catalytic activity [53]. In the same manner, Aika et al. reported that addition of alkali promoter to Ru/carbon catalysts increased the catalytic activity remarkably [54]. Besides they showed that the activity increase was a function of alkali promoter type which is in order of  $Cs > K > Na$ . They proposed the reason of activity increase to be related to the charge transfer from the alkali promoter to the Ru metal to easily reduce the molecular nitrogen.

Later, Aika et al. investigated the effect of alkali addition to Ru/ $Al_2O_3$  catalysts using XPS and TPR [55]. They reported that alkali promotion both increased Ru metal dispersion and TOF values of the catalysts. In addition, XPS and TPR results showed that hydrogen reduction at 400 °C caused the chemical conversion of the alkali nitrate phase to alkali hydroxide. Therefore, the authors concluded that electron donating properties of the alkali hydroxide determine the promotion in catalytic activity.

Murata and Aika studied the effect of lanthanide ( $La(NO_3)_3$ ,  $Ce(NO_3)_3$ ,  $Sm(NO_3)_3$ ) based promoters over Ru based catalysts in the ammonia synthesis reaction [56]. They observed that lanthanide promoters were more effective than alkali promoters. They also proposed that while alkali promoter ( $CsNO_3$ ) located on the support surface ( $Al_2O_3$ ), lanthanide promoters covered Ru metal particles. Therefore, even the electron donation tendency of the lanthanide oxides were low compared to alkali oxides, the close interaction of lanthanide oxide with Ru metal facilitated the high catalytic activity. In a follow-up study, Niwa and Aika investigated the effect of reduction temperature on the catalytic activity of Ru/MgO catalyst promoted with lanthanide oxide promoters [57]. When they reduced the catalysts at high temperature (873 K), the catalytic activity increased five times and they attributed such catalytic

improvement to the partial reduction of lanthanide oxides and easy electron donation to Ru metal.

Kadowaki and Aika investigated the effect of  $\text{Sm}_2\text{O}_3$  promoter over a  $\text{Ru}/\text{Al}_2\text{O}_3$  catalyst in terms of dependence of the rate equation to the hydrogen partial pressure [58]. The kinetic study showed that in the presence of  $\text{Sm}_2\text{O}_3$  promoter, hydrogen poisoning on  $\text{Ru}/\text{Al}_2\text{O}_3$  catalyst diminished. Moreover, the ammonia synthesis rate increased with increasing operating pressure in the presence of  $\text{Sm}_2\text{O}_3\text{-Ru}/\text{Al}_2\text{O}_3$  catalysts while the opposite effect was seen in the presence of  $\text{CsOH-Ru}/\text{Al}_2\text{O}_3$  catalysts.

Becue et al. studied the effect of alkali/earth alkaline promoters and their loading scheme over  $\text{Ru}/\text{Zeolite-X}$  catalyst on the kinetics of the ammonia synthesis reaction [59]. Successive impregnations of Ba precursor on  $\text{Ru}/\text{Zeolite-X}$  resulted in a  $\text{Ru}/\text{BaX}$  catalyst with an earth-alkaline-metal loading beyond the ion-exchange capacity of Zeolite-X. Their experimental studies showed that alkaline earth promoted Ru catalysts exhibited higher performance with respect to alkali promoted ones. The  $\text{Ba-Ru}/\text{BaX}$  catalyst especially had similar catalytic activity to  $\text{Cs-Ru}/\text{MgO}$ , which had shown the highest catalytic activity up to that time.

Rossetti et al. investigated the effect of promoters on singly (Ba), doubly (Ba+Cs, Ba+K) and triply (Ba+Cs+K) promoted  $\text{Ru}/\text{C}$  catalysts upon catalytic activity and stability [60]. It was shown that the maximum catalytic activity was obtained in the presence of the triply promoted  $\text{Ru}/\text{C}$  catalyst. Besides, they explained the improvement of promoters on the catalyst as Ba increasing the catalytic activity, Cs increasing the resistance to metal sintering and K improving the catalytic activity further. Furthermore, they supported their arguments with activity measurements, XRD and XPS results. Kowalczyk et al. carried out a similar study [61].  $\text{O}_2$  chemisorption experiments indicated that Cs containing  $\text{Ru}/\text{C}$  catalysts had a higher  $\text{O}_2$  uptake amongst the other catalysts. They suggested that Cs was highly reduced under ammonia synthesis operating conditions. They also observed that doubly

promoted (Ba+Cs) Ru/C catalysts showed the highest activity. They proposed a structural scheme of the location of Ba and Cs promoters, -very similar to Murata and Aika's approach-, that while Cs promoter covered mainly carbon support surface and acted as an electronic promoter due to that Cs atoms encircled the Ru atoms/particles as a ring, Ba was located on the Ru metal surface and acted as either a structural or an electronic promoter.

Several studies were performed in order to find out the state of promoters on supported Ru catalysts using XPS [62]–[64]. Guraya et al. studied the effect of alkali/earth alkaline promoters upon Ru/C catalysts in terms of changing their electronic structure [62]. They reported that addition of Ba promoter to Ru/C did not change the electronic structure of the catalyst. XPS of K promoter addition to Ru/C catalyst indicated that the density of occupied sites at the Fermi level increased. This caused a shift of Fermi level to the conduction band due to the charge transfer from K promoter to support material. Shitova et al. investigated the effect of nature of alkali promoters (Cs, K) over Ru/Sibunit catalyst using XPS, EXAFS and electron microscopy [63]. XPS results showed that a portion of Cs and Ru were in the metallic phase during the reaction conditions. Larichev et al. reported that while Cs were both in a close interaction with Ru and the support, Rb did not show any interaction with the support material [64]. The authors also investigated the effect of addition sequence of promoters to catalytic activity. They observed that when the Cs promoter was added before Ru metal precursor, the synthesized catalysts did not show any activity.

According to the studies examined up to now, the reason of increase of ammonia synthesis activity with the addition of alkaline, earth alkaline and lanthanides was explained as the electron donation from promoter to Ru metal particle surface to be used for breaking the triple bond of nitrogen. However, the researchers have not been able to put forth a real proof about the transfer of electron from promoter to Ru metal particle.

The studies on the ammonia synthesis reaction kinetics showed that the ruthenium catalyst is poisoned by hydrogen [31], [51], [65], [66]. Siporin and Davis studied the intrinsic reaction kinetics of ammonia synthesis over Ru and alkali promoted Ru catalysts [51]. It was observed that in the presence of alkali promoted Ru catalyst the reaction order for hydrogen was - 0.37, but for Ru, it was -1.

The effect of alkali promoters on Ru catalysts on the mechanism and kinetics of adsorption of H<sub>2</sub> were investigated by Uner et al. via solid state <sup>1</sup>H NMR and H<sub>2</sub> chemisorption techniques [67]. Solid-state NMR spectroscopy allowed them to identify two different adsorbed states of hydrogen,  $\alpha$  and  $\beta$ , over a Ru/SiO<sub>2</sub> surface. The  $\alpha$  state was revealed to hydrogen in close proximity to the surface, with a chemical shift equal to the chemisorbed hydrogen. The  $\beta$  state, on the other hand, was weakly bound adsorbed hydrogen that is in rapid exchange with the gas phase. <sup>1</sup>H-NMR measurements revealed that in the presence of Na promoter, the  $\beta$  state peak could not be observed.

Uner [68] later demonstrated through a reaction modelling study that weakly bound hydrogen has an important role for the Fischer-Tropsch reaction in terms of product distribution. In the presence of weakly bound hydrogen, products of the Fischer-Tropsch reaction shifted to paraffinic materials. In the absence of the  $\beta$  state hydrogen, the products shifted to olefin based products, which are desired due to their high reactivity compared to paraffinic products.

In addition, Uner et al. [69] further demonstrated that alkali promoter interacts with silanol groups, the hydroxyl groups on the SiO<sub>2</sub> support, decreasing the number of protons on the support surface. They demonstrated that alkali promoters on the support surface inhibited hydrogen spillover. This study was further used in the literature to design a highly selective catalyst for selective CO oxidation reaction. Pedrero et al. [70] have demonstrated that by the elimination of spilled over hydrogen, using alkali promoters, it was possible to increase the CO conversions in selective CO oxidation reaction.

The other hypothesis about the effect of alkali promoters on Ru based ammonia synthesis catalysts is that alkali promoters blocks the sites over Ru metal particles therefore the adsorption of hydrogen is restricted. This hypothesis has direct experimental proofs such as the results of  $^1\text{H}$  NMR and  $\text{H}_2$ -chemisorption experiments. Moreover, the kinetic studies with different reactions verify the idea. In the light of experimental findings, it seems that alkaline promoters act as a structural promoter (site blocking) instead of electronic promoter ( $e^-$  donation). Future studies may prove the influence of electron donation properties of alkaline promoters for dissociation of  $\text{N}_2$  over Ru based catalysts.

### Feed Ratio

Another solution to overcome the inhibition effect of hydrogen over supported Ru catalyst is to operate the reactor at substoichiometric  $\text{H}_2:\text{N}_2$  ratios. Rosowski et al. have investigated the ammonia synthesis under substoichiometric  $\text{H}_2:\text{N}_2$  mixtures in the range 5:95 - 75:25 (by volume) over  $\text{Cs}_2\text{CO}_3\text{-Ru/MgO}$  catalyst [65]. Tennison has also published industrial kinetic data over a Ru/C catalyst [26]. Both of these studies have reported higher rates up to five times depending on the experimental conditions for ammonia synthesis reaction under substoichiometric  $\text{H}_2:\text{N}_2$  flows.

### Forced Unsteady State Ammonia Synthesis Reactor Operation

Unsteady state (periodic, forced) reactor operation is generally used to increase conversion, selectivity of desired product and to reduce catalyst deactivation[71]. The main advantage(improvement) of changing the operation conditions of a heterogeneous catalytic reaction from steady state to unsteady state can be explained with the possibility of modification of the surface of the catalyst such that the productivity of the process is significantly increased [72]. Matros stated that an optimized unsteady state operation cannot be less efficient compared to an optimized steady state operation [73]. Matros emphasized that the most important bottleneck for the commercialization of unsteady state catalytic reactor operations was the absence of sufficient information on the catalyst surface dynamics.

Rambeau and Amariglio have performed cyclic ammonia synthesis experiments with pre-adsorbed hydrogen and/or nitrogen on powder ruthenium to demonstrate that cycling the reactants decreased the inhibition by hydrogen [74]. Their results show that the reaction rate is increased up to three orders of magnitude with pre-adsorbed hydrogen and gas phase nitrogen.

The only study was performed unsteady state ammonia synthesis reaction over ruthenium catalyst by Rambeau and Amariglio [33], [74]. The other studies related on the unsteady state reactor operation were carried out over the magnetite derived catalysts. Therefore, in the upcoming paragraphs, ammonia synthesis reactor under unsteady state conditions will be explained.

Ammonia synthesis under time interrupted conditions has also been considered as an alternative to overcome the thermodynamic equilibrium barrier of the reaction [75]. Under cyclic conditions, the rate of reaction is anticipated to increase with respect to its steady state rate value. Along these lines, Jain et al. have reported a 30% improvement in reaction rate for ammonia synthesis over Fe catalysts under cyclic conditions (from pure hydrogen to pure nitrogen) in comparison to steady state rate [76].

Cussler group presented a different approach to forced unsteady state. Cussler group has published two consecutive papers for obtaining 95% ammonia synthesis conversion by placing an ammonia adsorbent inside the same reactor [77], [78]. The adsorbent would hold up ammonia and shift the reaction equilibrium to right. When the adsorbent is saturated the reactor conditions are set to desorb ammonia. The same research group has also studied a small-scale plant for the following three resistances: ammonia synthesis rate, condensation and separation. They reported that the resistance of catalytic reaction is at least three orders of magnitude higher than that of condensation and separation processes [79].

### 2.3.1.3 Ammonia Poisoning and Suggested Solutions

The inhibition effect of ammonia over supported Ru based catalyst is due to the partial pressure of ammonia in the denominator in all of the suggested/proposed ammonia synthesis rate expressions [28]–[31]. Researchers proposed that support type is an effective parameter on the ammonia synthesis rate due to its surface acidity characteristics [19], [35], [51], [80]–[82]. While Siporin and Davis carried out a kinetic study over Ru/MgO and estimated that the effect of ammonia on the reaction rate is almost negligible [51], Rosowski et al. found out that the order of partial pressure of ammonia vary between -0.3 and -0.5. over Ru/MgO and Ru/Al<sub>2</sub>O<sub>3</sub> catalysts [65].

Most of the investigators concluded that support materials having basic surface characteristics showed higher activity compared to acidic supports [19], [35], [51], [80]. They attributed the reason of the high activity to an electron donation of basic support materials to Ru metal surface to facilitate dissociation of the molecular nitrogen.

On the other hand, Larichev et al. investigated the effect of support material on the reaction rate via X-ray photoelectron spectroscopy (XPS) [81], [82]. In XPS studies, the binding energy of Ru 3d<sub>5/2</sub>, which is 280.5 eV, was measured in a Ru/MgO catalyst as 1 eV decreased compared to Ru/Al<sub>2</sub>O<sub>3</sub> and Ru/SiO<sub>2</sub> catalysts. Although the results are in agreement with the literature, Larichev et al. commented on that the decrease in binding energy of Ru 3d<sub>5/2</sub> was not caused by the donated electrons by the MgO support but the local differences in the electronic states of Ru metal. Therefore, they could not find any direct relationship between the surface acidity of support material and reaction rate. A similar study was performed by Muhler et al. and observed a 1 eV decrease in the binding energy of Ru 3d<sub>5/2</sub> from 280 eV to 279 eV after addition of Cs promoter due to electron transfer from Cs to Ru [52].

You et al. compared the activity of Ru/MgO and Ru/BHA (barium hexaaluminate) to investigate the effect of support material on the reaction rate [21]. According to

experimental results, since the BHA support material showed a similar surface basicity with BaO, the electron donation tendency is higher. Besides, they also found that the surface layers of BHA are very similar to those of activated carbon. Therefore, they explained the superior catalytic activity of Ru/BHA with these arguments. Wang et al. carried out a similar study [83]. They prepared and examined Ru/BaTiO<sub>3</sub> and compared with Ru/TiO<sub>2</sub> in terms of catalytic activity for ammonia synthesis. They determined a strong relationship between Ru metal particles and the BaTiO<sub>3</sub> support material using CO<sub>2</sub>-TPD, H<sub>2</sub>-TPR and HR-TEM. They commented that there is a high probability that electron transfer from BaTiO<sub>3</sub> to Ru metal particles can take place at reaction conditions with respect to the TiO<sub>2</sub> support material. The high activity of Ru/BaTiO<sub>3</sub> can be explained with this argument.

### **2.3.2 Molybdenum Nitride Catalysts**

Nitride based materials (especially molybdenum nitrides) have attracted great attention in recent years due to catalytic activity for ammonia synthesis at high temperature (400 °C) and atmospheric pressure [84]–[86]. In molybdenum nitride materials, nitrogen is doped to the material as atomic nitrogen. In other words, molybdenum nitride catalysts are a potential source of activated nitrogen which is very important for ammonia synthesis.

Volpe and Boudart reported that molybdenum nitride catalysts are active materials for ammonia synthesis reaction [84]. Mittasch found that molybdenum nitride materials are active when they combined with iron, cobalt or nickel [53]. Aika and coworkers studied the Co<sub>3</sub>Mo<sub>3</sub>N catalyst at high temperatures and atmospheric pressure [24], [85], [87], [88]. They reported that the activity of Co<sub>3</sub>Mo<sub>3</sub>N catalyst is similar to magnetite derived catalyst. Further, they promoted Co<sub>3</sub>Mo<sub>3</sub>N catalyst with Cs. The activity of Cs-Co<sub>3</sub>Mo<sub>3</sub>N catalyst was reportedly became higher than magnetite derived catalyst.

Hargreaves and co-workers have been recently studying the structure, morphology and activity of the molybdenum nitride materials for the ammonia synthesis reaction

[23], [86], [89]–[93]. In their lab, many molybdenum nitride materials have been synthesized up to now such as  $\text{Ni}_2\text{Mo}_3\text{N}$ ,  $\text{Co}_3\text{Mo}_3\text{N}$ ,  $\beta\text{-Mo}_2\text{N}_{0.78}$ ,  $\gamma\text{-Mo}_2\text{N}$  etc. Hargreaves and McKay investigated the reactivity of the lattice nitrogen of  $\text{Co}_3\text{Mo}_3\text{N}$  and  $\text{Ni}_2\text{Mo}_3\text{N}$  catalysts [23]. They found that ammonolysis is a better option for nitriding the CoMo and/or NiMo like species compared to  $\text{H}_2/\text{N}_2$  pretreatment. In addition, XRD analysis showed that the  $\text{Ni}_2\text{Mo}_3\text{N}$  catalyst derived from  $\text{NiMoO}_4$  consists of some metallic Ni after each nitriding process. Reactivity of lattice nitrogen was proved by reaction of both catalysts with  $\text{C}_6\text{H}_6$  and  $\text{H}_2$ . As a result of treatment of catalysts with  $\text{C}_6\text{H}_6$ , carbide structures were formed. In the same manner, as a result of treatment of catalysts with  $\text{H}_2$ ,  $\text{Co}_6\text{Mo}_6\text{N}$  and  $\text{Ni}_2\text{Mo}_3\text{N}_{1-x}$  were obtained.

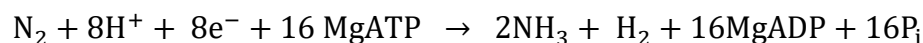
Furthermore, Hargreaves' group studied the regeneration ability of  $\text{Co}_3\text{Mo}_3\text{N}$  catalyst during ammonia synthesis reaction [90], [91], [93]. They showed that when they carried out ammonia synthesis reaction at  $700\text{ }^\circ\text{C}$  with  $\text{Ar}/\text{H}_2$  feed and ambient pressure,  $\text{Co}_3\text{Mo}_3\text{N}$  catalyst structure is changed to  $\text{Co}_6\text{Mo}_6\text{N}$  structure. The formation of  $\text{Co}_6\text{Mo}_6\text{N}$  structure is proved via powder neutron diffraction analysis. In order to regenerate the catalyst, catalyst was further treated with  $\text{N}_2$  at  $700\text{ }^\circ\text{C}$  for 6 hours. At the end of the pretreatment,  $\text{Co}_3\text{Mo}_3\text{N}$  structure is obtained with the same theoretical nitrogen content inside the catalyst.

Mckay et al. investigated the reactivity of lattice nitrogen of the  $\text{Co}_3\text{Mo}_3\text{N}$  catalyst at different operational conditions for ammonia synthesis [89]. When they treated catalyst at  $400\text{ }^\circ\text{C}$  with  $\text{H}_2/\text{N}_2$  flow, there was not observed significant nitrogen content change in the catalyst. When they used  $\text{Ar}/\text{H}_2$  flow at  $400\text{ }^\circ\text{C}$ , a small amount of nitrogen was lost from the catalyst. In the presence of these data, they treated catalyst with same streams given above at  $700\text{ }^\circ\text{C}$ . At the end of the study, they show that the nitrogen content was the half of the initial amount ( $\text{Co}_6\text{Mo}_6\text{N}$ ) in the presence of  $\text{Ar}/\text{H}_2$  flow. Furthermore, they sent  $\text{H}_2/\text{N}_2$  flow at  $700\text{ }^\circ\text{C}$  and regenerated the  $\text{Co}_3\text{Mo}_3\text{N}$  structure. These results suggested that lattice nitrogen was used in each stream condition. Besides catalyst could regenerate itself when stream contained  $\text{N}_2$ . In other

words, the catalyst potentially operates through Mars-van Krevelen mechanism for nitrogen reactivity.

### 2.3.3 Enzymatic (Biological) Ammonia Synthesis Route

Biological ammonia synthesis is carried out by the nitrogenase enzyme (shown in Figure 2.3) in nature. The atomic/molecular structure of the nitrogenase enzyme was determined via XRD at a 2.7 Å resolution by Kim and Rees [94], [95]. XRD studies on the nitrogenase enzyme revealed that it consisted of MoFe and Fe proteins. Spatzal defined the nitrogenase as the largest and the most complex metal-containing enzyme known in biological systems [96]. The stoichiometry of the biological ammonia synthesis reaction is given below:



It is important to note that for 1 mole of nitrogen reduction, 2 mole of ammonia and 1 mol hydrogen are produced. The energy requirement of the reaction is provided by the hydrolysis of 16 mole of MgATP to MgADP, which corresponds to approximately 500 kJ/mol [97].

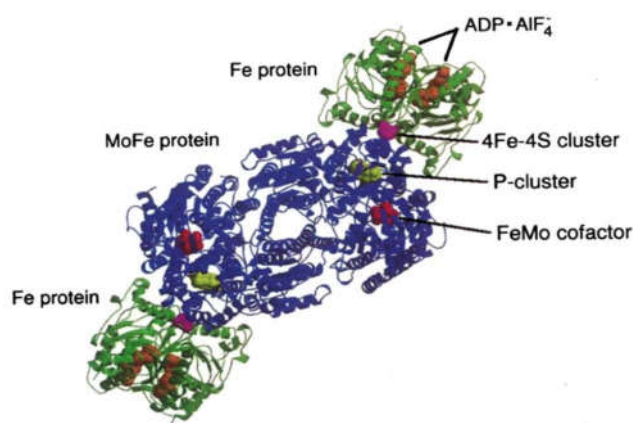


Figure 2.3. Crystal structure of nitrogenase enzyme [98] (reproduced by the permission of Springer Nature. Permission to reuse must be obtained from the rights holder)

Fe-protein has been defined as a dimer of two identical subunits coordinating with a [4Fe-4S]-cluster [94]. Fe protein is mainly responsible for electron transfer to MoFe protein. According to the literature, Fe protein, first, is reduced by either ferredoxin or flavodoxin then electrons are transferred to MoFe protein. At the same time, hydrolysis of MgATP to MgADP has occurred. The details of oxidation of Fe protein, binding of MgATP to Fe protein and hydrolysis mechanism to MgADP, and electron transfer to MoFe protein steps occurred during the nitrogen reduction to ammonia have not yet been clarified in the absence of isolation of any intermediate [94].

The main duty of the MoFe protein is reported to be to produce ammonia and hydrogen [95]. The MoFe protein is a tetramer that has two identical subunits named as  $\alpha$  and  $\beta$ . The MoFe protein has two metallic centers inside its structure which are the FeMo cofactor and P-cluster ([8Fe:7S]-cluster) pair. Although most studies have assumed that the FeMo cofactor (or MoFe protein) is responsible for the nitrogen reduction, there is not any evidence to prove this assumption [10], [99].

Thorneley and Lowe studied the ammonia synthesis reaction mechanism over the nitrogenase enzyme and proposed the Thorneley-Lowe mechanism (given in Figure 2.4) [100]. Besides, they reported kinetic parameters for each step. In their mechanistic model, they proposed the oxidation of Fe protein, hydrolysis of MgATP to MgADP, electron transfer from Fe protein to MoFe protein, reduction of nitrogen molecule, and the corresponding production of the hydrogen molecule. They also found out that hydrogen synthesis is inhibited over MoFe protein by Fe protein due to the Fe protein being bound to the MoFe protein which is a required condition for nitrogen reduction according to their mechanism.

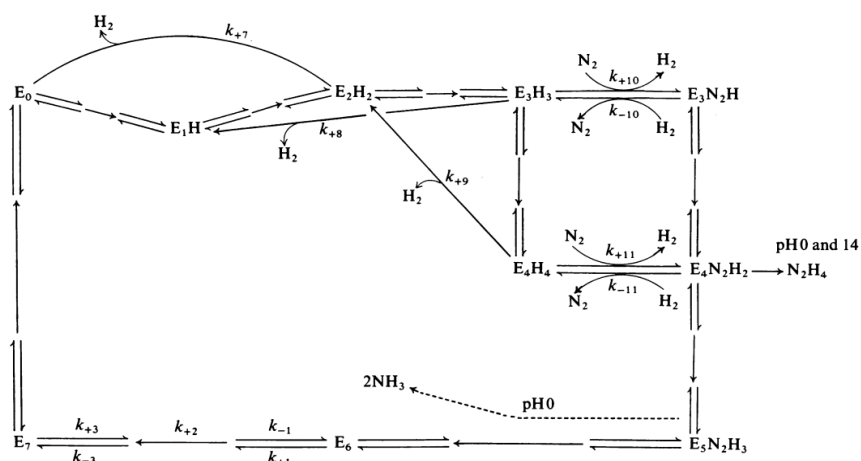


Figure 2.4. Lowe-Thorneley nitrogen reduction reaction mechanism [100] (reproduced by the permission of Portland Press Ltd. Permission to reuse must be obtained from the rights holder)

Varley et al. carried out a DFT study in order to calculate the required energy levels for nitrogen reduction in a very similar reaction mechanism model to Thorneley-Lowe [101]. Their model also consisted of 8  $H^+$  and 8  $e^-$  transfer as well as the obligatory synthesis of hydrogen while reducing the nitrogen molecule. As a result of the DFT calculations, they found out that Fe site was critical in the initiation of the reduction process of nitrogen molecule similar to the traditional iron catalyst. The calculated energy levels also explained the possibility of ammonia synthesis at ambient temperature and atmospheric pressure conditions according to the mechanism proposed by Lowe and Thorneley [100].

Schrock and co-workers also investigated the mechanistic steps of the ammonia synthesis reaction with nitrogenase [102]–[105]. They proposed a mechanism based on the Mo center of the FeMo cofactor involving stepwise addition of protons and electrons. They proposed the mechanism given in Figure 2.5. Before they proposed the nitrogen reduction mechanism, they studied their analogous nitrogenase enzyme system and wanted to isolate and characterize the reaction intermediates during the reaction via X-Ray diffraction. As a result of experimental studies, they showed that

the oxidation states of Mo(III) and Mo(IV) could be responsible for nitrogen reduction in nitrogenase.

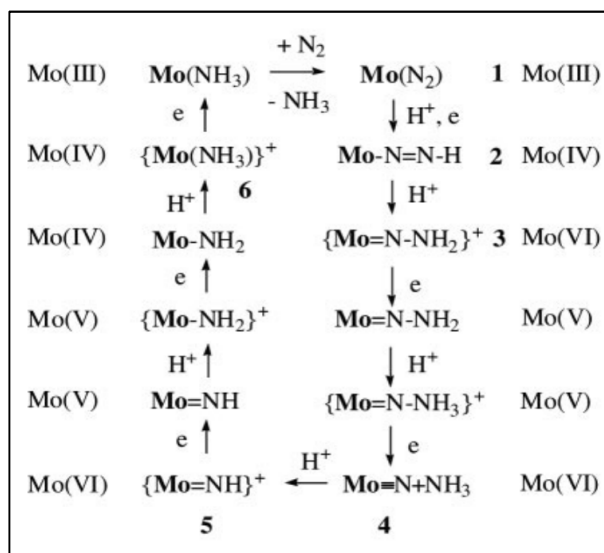


Figure 2.5. Proposed reaction mechanism by Yandulov and Schrock and intermediates in the reduction of dinitrogen at a hypothetical Mo center through the stepwise addition of protons and electrons [106] (reproduced by the permission of Science AAAS. Permission to reuse must be obtained from the rights holder)

## 2.4 Process Intensifications and Energy Improvements

In this part of the literature survey, the improvements on the ammonia production are given throughout the years to increase the efficiency of the process.

Some of the improvements in the ammonia synthesis process can be listed as application of radial flow ammonia synthesis reactors [107]–[113], innovations in H<sub>2</sub> production (synthesis gas production and purification), and heat recovery systems [112]. With the help of these improvements, the energy requirement for ammonia synthesis process has been decreased from ~100 GJ/ton NH<sub>3</sub> to ~28 GJ/ton NH<sub>3</sub>. Although there have been significant developments in the process, there still have been many bottlenecks to overcome the energy efficiency problem of the ammonia production process.

The main cost items of the ammonia synthesis process are synthesis (producer) gas production, the ammonia synthesis loop, and the purification steps [8]. 70% of the energy requirement for the ammonia production process is consumed for synthesis gas preparation and purification, and the rest is needed for compression, ammonia synthesis and refrigeration [8], [114].

There have been several developments in the ammonia production process in terms of energy efficiency in previous years [115]–[119]. Most of the energy saving investigations were performed on the synthesis gas section of the process. Approximately 10-15 GJ/ton NH<sub>3</sub> of energy saving improvement was obtained due to developments in synthesis gas section with the addition of a pre-reformer unit, installation of a gas turbine, modification of coils in the convective heating section of furnace, increased-radiation heating in the furnace, reduction of the steam to carbon ratio, and new developments in CO<sub>2</sub> sequestrations technologies.

## CHAPTER 3

### MATERIALS AND METHODS

#### 3.1 Catalyst Preparation

##### 3.1.1 Incipient Wetness Impregnation Method

1 wt% supported Ru catalysts (Supports: SBA-15, SiO<sub>2</sub> (Merck, granular), carbon nanofiber (CNF) (ElectroVac, Klosterneuburg, Austria), and Vulcan Carbon (Cabot Inc., XC72R)) were prepared using incipient wetness impregnation method. Prior to the catalyst preparation, the amount of water needed to wet the support surface was measured. Ruthenium nitrosyl nitrate (Sigma Aldrich, 1.5 wt% Ru metal) salt was used as metal precursor. 0.67 g ruthenium nitrosyl nitrate salt was dissolved in 2-3 ml/g water to bring about incipient wetness and added to the supports to prepare a slurry to obtain 1.0 g catalyst. Due to the hydrophobic nature of Vulcan, 2-3 droplets of NH<sub>4</sub>OH solution was added to the aqueous ruthenium metal solution. The slurry was mixed until a uniform paste was obtained and dried at room temperature overnight.

For the case of 3 and 5 wt% metal loaded catalysts, initially 1 wt% Ru/Support catalysts were prepared as explained above and required amount of ruthenium nitrosyl nitrate was sequentially added. Then, the slurry was mixed, dried under vacuum conditions and (if needed) the same procedure was applied up to required amount of metal loading was achieved.

##### 3.1.1.1 Synthesis of SBA-15

SBA-15 support material was prepared according to a procedure described by Zhao et al. [120]. In order to synthesize pure SBA-15 molecular sieve, 9 ml of

tetraethoxyorthosilicate (TEOS) was added to 150 ml of 1.6 M HCl solution containing 4 g triblock poly(ethylene oxide)–poly(propylene oxide)–poly(ethylene oxide) (EO<sub>20</sub>-PO<sub>70</sub>EO<sub>20</sub>, Aldrich). The mixture was stirred for 24 h at 40 °C and was allowed to react at 100 °C overnight in Teflon bottles. The solid material obtained after filtering was finally calcined in air flow at 500 °C for 5h.

### 3.1.2 Ion-Exchange Method

1.37 wt% Ru/Zeolite-Y and 1-4 wt% Ru/HAp catalysts were synthesized using ion-exchange method according to the procedure describe elsewhere in [121]<sup>1</sup>.

### 3.1.3 Synthesis of Co<sub>3</sub>Mo<sub>3</sub>N Catalyst

In order to synthesize Co<sub>3</sub>Mo<sub>3</sub>N, required amounts of Co(NO<sub>3</sub>)<sub>2</sub>·6H<sub>2</sub>O and (NH<sub>4</sub>)<sub>6</sub>Mo<sub>7</sub>O<sub>24</sub>·4H<sub>2</sub>O were weighed. Metal salts were dissolved in 200 ml de-ionized water and heated to 80 °C over a magnetic stirrer in a fume cupboard. The indication of the starting of the reaction between metal salts were defined as the color change at high temperature (ca. 80 °C). The color of the aqueous solution changes from red to purple. After the color change occurred, mixing was carried out for 1 h. Then, the solution was filtered and filter cake was washed two times with water and ethanol. The filter cake was dried overnight at room temperature and scratched out from the filter paper. The purple powder was put into watch-glass and dried in oven at 150 °C overnight. After drying process was completed, the cobalt-molybdenum precursor was calcined in a tubular furnace in the presence of air at 500 °C for 3 hours (temperature ramp: 20 °C/min). After calcination, the cobalt-molybdenum oxide powder was put into ammonolysis rig for nitridation process in the presence of 50 ml/min ammonia flow. The details of temperature program is given in Figure 3.1. At the end of the ammonolysis process, catalyst was exposed to 2% O<sub>2</sub> in Ar flow (10 ml/min) for passivation. After passivation, amorphous Co<sub>3</sub>Mo<sub>3</sub>N powder was synthesized. In order

---

<sup>1</sup> The samples were prepared by Serdar Akbayrak

to get crystalline phase  $\text{Co}_3\text{Mo}_3\text{N}$  material, the powder was treated at 700 °C (temperature ramp: 10 °C/min) for 3 h in the presence of  $\text{H}_2:\text{N}_2=3:1$  flow at 60 ml/min.

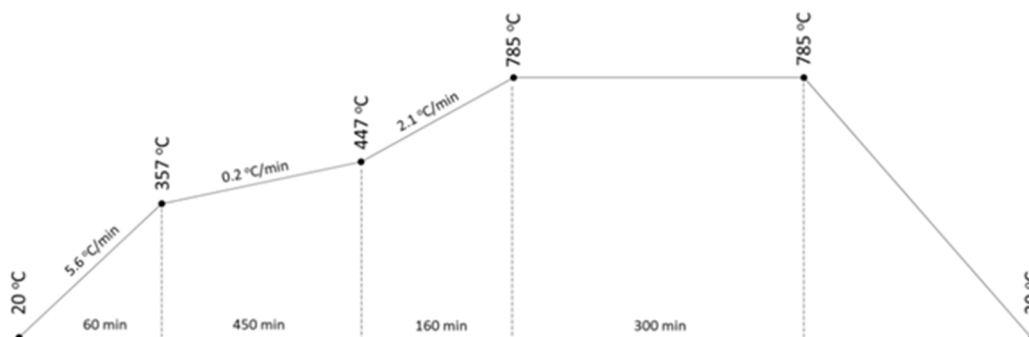


Figure 3.1. Temperature program scheme of ammonolysis process

## 3.2 Catalyst Characterization

### 3.2.1 BET Surface Area Measurements

BET surface area of the support materials were measured using a Micromeritics Tristar II instrument using  $\text{N}_2$  adsorption isotherms determined at 77 K. Prior to the surface area measurement, samples are heated to 120 °C and evacuated for 12 hours.

### 3.2.2 X-Ray Diffraction

Powder diffraction analyses were performed using a Siemens D5000 instrument operating with a  $\text{Cu K}\alpha$  X-ray tube. A  $2\theta$  range between 5° and 85° was scanned using a counting rate of 1 second per step with a step size of 0.02°.

### 3.2.3 CHN Analysis

Elemental analysis of  $\text{Co}_3\text{Mo}_3\text{N}$  was carried out using an Exeter Analytical CE-440 elemental analyzer.

### 3.2.4 ATR-IR Spectroscopy

ATR-IR spectra of Ru/Vulcan catalysts were obtained in a Perkin Elmer Spectrum Two ATR Spectrometer. In all measurements, pure KBr (Sigma Aldrich, FTIR grade)

spectrum was used as background. The samples were diluted to 1/100 wt% with KBr. 32 scans were recorded with  $4\text{ cm}^{-1}$  resolution in the range of  $4000 - 500\text{ cm}^{-1}$  wavenumbers.

### 3.2.5 H<sub>2</sub>-Chemisorption

Volumetric hydrogen chemisorption experiments were conducted in a home-built, constant volume, Pyrex high vacuum manifold (shown in Figure 3.2) equipped with a ultra-high vacuum pump (Pfeiffer, up to  $10^{-9}$  atm), high vacuum Teflon valves (ACE Glass), a capacitance gauge (MKS Baratron, up to 100 or 1000 Torr) at room temperature. Prior to dispersion determination experiments, the catalysts were reduced in the presence of H<sub>2</sub> gas. The step by step reduction procedure as well as measurement of total and weak adsorption isotherms were given in the Appendix C.

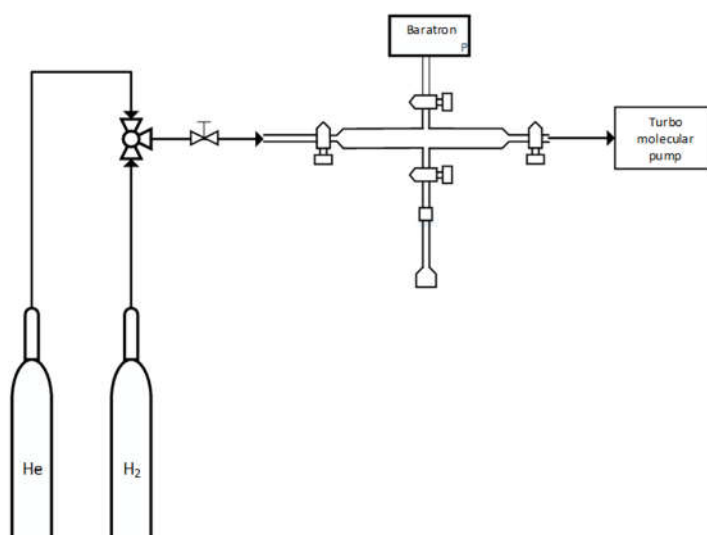


Figure 3.2. Schematic Representation of Chemisorption Manifold

In order to determine the dispersion of the supported Ru catalysts, the difference between the total and weak adsorption isotherms is used to calculate the strong hydrogen amounts. Ru metal dispersion of the catalysts were determined assuming that strongly bound hydrogen to ruthenium metal ratio equal to one (H:Ru=1)

In case of hydrogen chemisorption experiments of  $\text{Co}_3\text{Mo}_3\text{N}$  catalysts, a similar experimental procedure was applied to the sample with an exception that the catalyst was reduced at 773 K.

It is important to note that hydrogen exposure durations are selected to ensure that thermal and chemical equilibrium over the metal is reached, but slower processes are inhibited.

### **3.2.6 Microcalorimetry**

Heat of adsorption measurements are conducted on a Setaram C-80 Tian-Calvet calorimeter coupled to the multiport high-vacuum pyrex glass manifold (Figure 3.3), as described in  $\text{H}_2$ -chemisorption section. A desired amount of sample (~0.50 g) is loaded into the sample cell, which is then attached to one end of the tee connection and inserted into the sample port of the microcalorimeter. The other end of the tee connection is attached to an empty sample cell inserted into the reference port of the microcalorimeter. The reduction procedure that applied in microcalorimeter setup is the same as the  $\text{H}_2$ -chemisorption experiment. The only difference is the reduction temperature of the catalysts. The maximum allowable temperature of the microcalorimeter instrument is 250 °C. Therefore, the catalysts are reduced at 250 °C. The heat of adsorption of hydrogen over supported Ru catalysts is measured at 50 °C. Total adsorption isotherms of the catalysts are also obtained during the heat of adsorption measurements.

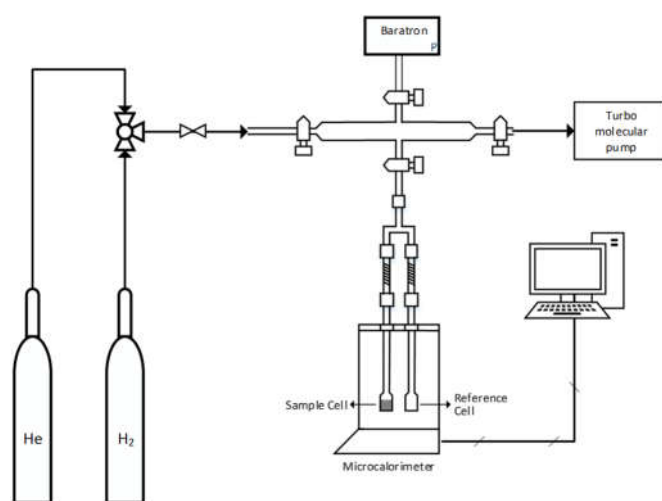


Figure 3.3. Schematic Representation of Chemisorption Manifold and Microcalorimeter

### 3.2.6.1 Measurement of Heat of Adsorption of Ammonia over HAp

Heat of adsorption of ammonia over HAp measurement was also carried out on the adsorption calorimetry setup using pure ammonia (99.9%) gas. Prior to the ammonia adsorption, the dead volume of the sample was measured with He gas and then the temperature of the calorimeter was increased to 383 K with a temperature ramp of 2 °C/min while the manifold was being kept at vacuum. After heat treatment, the temperature was decreased to 323 K and incremental amounts of ammonia was sent to the sample starting from 1.0 Torr of ammonia pressure.

### 3.2.6.2 Measurement of Acidity of HAp, Zeolite-Y and Carbon Vulcan

Acidic properties of bare and commercial support materials (Na-Y, HAp, and Vulcan Carbon) were studied by adsorption calorimetry (Setaram, C80 Tian-Calvent calorimeter, Figure 3.3) using ammonia as a probe molecule at 323 K. In order to measure the heat of adsorption of ammonia in helium gas (5.0% volume NH<sub>3</sub> in He), the same preparation steps were applied with the experiments of the heat of adsorption of H<sub>2</sub> over supported Ru catalysts with excluding the catalyst reduction procedure. After dead volume measurement was performed, the temperature of the calorimeter was set to 383 K and kept 383 K for ca. 2 hours to remove adsorbed moisture and

impurities. After that, the sample (and microcalorimeter) was cooled to 323 K. Following the stabilization of heat flow, 515 Torr of NH<sub>3</sub> in He (5.0% mol NH<sub>3</sub> in He) was sent to the sample. When the system reached the thermal equilibrium, the final pressure inside the manifold was recorded.

### **3.2.7 High Resolution Transmission Electron Microscopy (HR-TEM)**

Surface morphologies and particle size distributions of supported Ru catalysts are investigated using JEOL 2100 F high resolution transmission electron microscopy (HR-TEM). In order to obtain TEM images of the catalysts, suspensions of Ru catalyst samples in ethanol were prepared and sonicated for 15 min. Then, samples are transferred to a Cu grid for TEM analysis.

Ru metal particle size distributions of supported Ru catalysts are obtained by the help of high-resolution TEM images. The diameters of all metal particles are measured against the scale in the image. All particles are assumed spherical. After sizing the metal particles shown in TEM images, histograms of particle size distributions are obtained.

### **3.2.8 Temperature Programmed Analysis**

Temperature programmed analysis experiments are performed in Micromeritics Chemisorb 2720 instrument. Sample holder of the instrument with pre-weighed supported Ru catalyst is connected to the manifold. Temperature programmed reduction (H<sub>2</sub>-TPR) experiment for supported Ru catalysts is carried out under the flow of H<sub>2</sub> in Ar (10% H<sub>2</sub>) at a rate of 25 ml min<sup>-1</sup> and at a temperature ramp of 5 °C min<sup>-1</sup> up to 700 °C. After H<sub>2</sub>-TPR profiles are obtained, immediately the catalysts are cooled to room temperature in the presence of H<sub>2</sub> in Ar (10% H<sub>2</sub>) flow in order to observe the hydrogen uptake behaviors of the catalysts. After room temperature is reached, temperature programmed desorption (TPD) experiment was carried out under

the flow of pure He at a rate of 25 ml min<sup>-1</sup> using a temperature ramp of 5 °C up to 700 °C.

Temperature programmed reduction (TPR) of Co<sub>3</sub>Mo<sub>3</sub>N was carried out under flow of 10% H<sub>2</sub> in Ar gas at a rate of 25 mL/min with a temperature ramp of 10 °C/min up to 900 °C.

The calculations for the temperature programmed reduction was performed using a calibration factor which was determined by the reduction of Ag<sub>2</sub>O reference material. The area under the H<sub>2</sub>-TPR pattern of Ag<sub>2</sub>O reference material was calculated. Then corresponding H<sub>2</sub> consumption for reduction of Ag<sub>2</sub>O to Ag was determined using the reduction stoichiometry as 7.30x10<sup>-5</sup> mol H<sub>2</sub> per unit area that determined under the reduction curve of Ag<sub>2</sub>O to Ag.

### 3.2.8.1 O<sub>2</sub>-Titration

O<sub>2</sub>-titration experiments are performed in Micromeritics Chemisorb 2720 instrument. Prior to the experiment, supported Ru catalysts (supports: SiO<sub>2</sub> and Vulcan) are purged and dehydrated under 25 ml min<sup>-1</sup> He flow up to 150 °C for 30 min. After dehydration, the Ru/SiO<sub>2</sub> catalysts are cooled to room temperature in He flow, oxidized under flow of 25 mL min<sup>-1</sup> O<sub>2</sub> in He (2% O<sub>2</sub>) up to 200 °C, and followed by reduction under 25 ml min<sup>-1</sup> H<sub>2</sub> in Ar (10% H<sub>2</sub>) flow and a temperature ramp of 5 °C min<sup>-1</sup> up to 500 °C. After reduction process is completed, the Ru/SiO<sub>2</sub> are cooled to 25 °C in He flow. Then, Ru/SiO<sub>2</sub> catalysts are oxidized in the flow of 25 ml min<sup>-1</sup> O<sub>2</sub> in He (2% O<sub>2</sub>) with a temperature ramp of 5 °C min<sup>-1</sup> up to 200 °C.

Ru/Vulcan catalysts are oxidized in the flow of 25 ml min<sup>-1</sup> O<sub>2</sub> in He (2% O<sub>2</sub>) at room temperature for 30 min to avoid burning of the carbon based support material. The oxidized catalysts are cooled to room temperature in the presence of He flow. Then, Ru/Vulcan catalysts are re-reduced in the flow of 25 ml min<sup>-1</sup> H<sub>2</sub> in Ar (10% H<sub>2</sub>) with temperature ramp of 5 °C min<sup>-1</sup> up to ca. 300 °C. Hydrogen consumption/Ru atom values are quantified.

### 3.3 Ammonia Synthesis Reaction Studies

#### 3.3.1 In-situ DRIFTS Measurements

DRIFTS measurements are performed in a Perkin Elmer Spectrum 100 DRIFT Spectrometer combined with a Pike reaction cell and the Pike Temperature Control Unit. The schematic representation of experimental setup is given in Figure 3.4. 128 scans are recorded with  $1\text{ cm}^{-1}$  resolution in the range of  $4000 - 450\text{ cm}^{-1}$ . Gas flow rates are adjusted using Teledyne mass flow controllers and Terralab mass flow control unit. The catalysts are pressed into pellets, then crushed to an average diameter of  $\sim 2\text{ mm}$  and about  $50\text{ mg}$  of these pellets is placed in the sample holder covered by an IR transparent window (ZnSe window). The reference DRIFTS spectrum is measured prior to any treatment under  $50\text{ mL min}^{-1}$  Ar flow. The catalyst is first reduced with  $\text{H}_2:\text{Ar}$  (Linde, 99.999%) ( $3:12\text{ mL min}^{-1}$ ) flow with a temperature ramp of  $2\text{ }^\circ\text{C/min}$ . After temperature of the sample holder reached  $250\text{ }^\circ\text{C}$ , reduction continued at this temperature and at same  $\text{H}_2:\text{Ar}$  flow for 2 hours. At the end of 2 hours, the system was cooled to room temperature, still under  $15\text{ mL min}^{-1}$   $\text{H}_2:\text{Ar}$  flow. Finally,  $\text{N}_2$  gas (Linde, 99.999%) is sent to the sample holder at a rate of  $4\text{ mL min}^{-1}$  overnight at room temperature and atmospheric pressure.

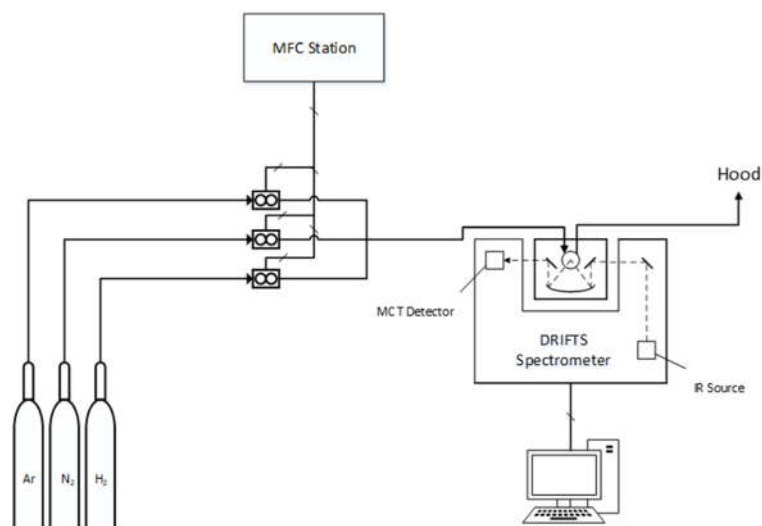


Figure 3.4. Schematic representation of experimental setup for ammonia synthesis using DRIFTS spectrometry

### 3.3.2 Steady State Ammonia Synthesis Reaction

NH<sub>3</sub> synthesis experiments are carried out at 300-400 °C, atmospheric pressure and under 100 mL min<sup>-1</sup> (H<sub>2</sub>:N<sub>2</sub>:Ar=3:1:2) gas flow. Experimental setup for ammonia synthesis reaction under steady flow conditions is represented in Figure 3.5. The flow rates were adjusted by mass flow controllers (MKS) and driven by a control station (Terralab). The 6.0 mm OD reactor was heated in a temperature controlled tubular furnace. 70.0 mg of Ru catalysts with a particle diameter between 38.0 and 106.0 μm are loaded into the reactor. Prior to the activity measurements, the catalysts are reduced under 100 mL min<sup>-1</sup> H<sub>2</sub> in Ar (1:3) flow at 300 °C for 2 hours. The effluent gases are sent to a wash bottle containing 1.10 mM H<sub>2</sub>SO<sub>4</sub> solution. The reaction rate of ammonia synthesis is determined by following the change of conductivity of H<sub>2</sub>SO<sub>4</sub> solution with respect to time at 25 °C and atmospheric pressure. At the end of kinetic measurements, the sample is purged under 100 mL min<sup>-1</sup> pure Ar flow to monitor total amount of NH<sub>3</sub> desorption from the catalysts.

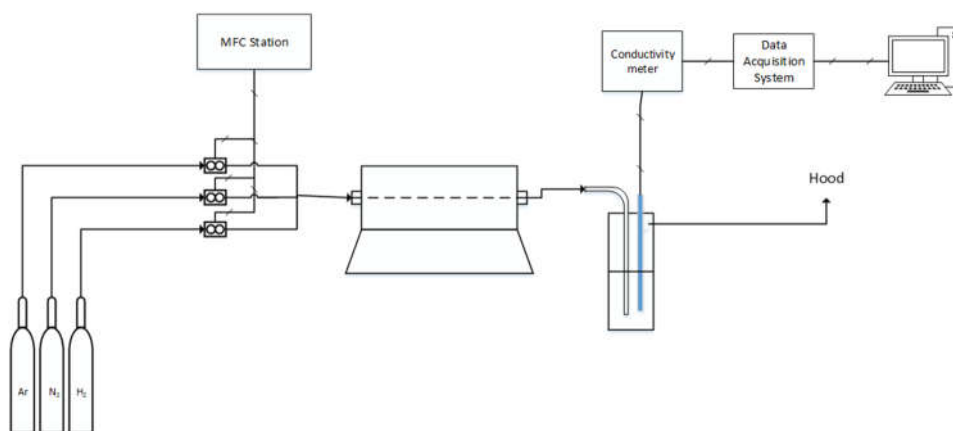


Figure 3.5. Experimental Setup for Ammonia Synthesis Reaction under Steady Flow Conditions.

### 3.3.3 Unsteady State Ammonia Synthesis Reaction

Unsteady state experiments were carried out under 100 mL min<sup>-1</sup> total flow rate by switching between H<sub>2</sub>:N<sub>2</sub> (3:1) and pure N<sub>2</sub> flows. An illustration of experimental setup for ammonia synthesis reaction under pulse flow conditions is given in Figure

3.6. A time controlled 4-way valve (VICI Valco) is used to switch the gas flows. The time period of each reactant streams sent to reactor is selected as 10 min. The ammonia synthesis activity is measured in a similar manner to the steady state reaction tests.

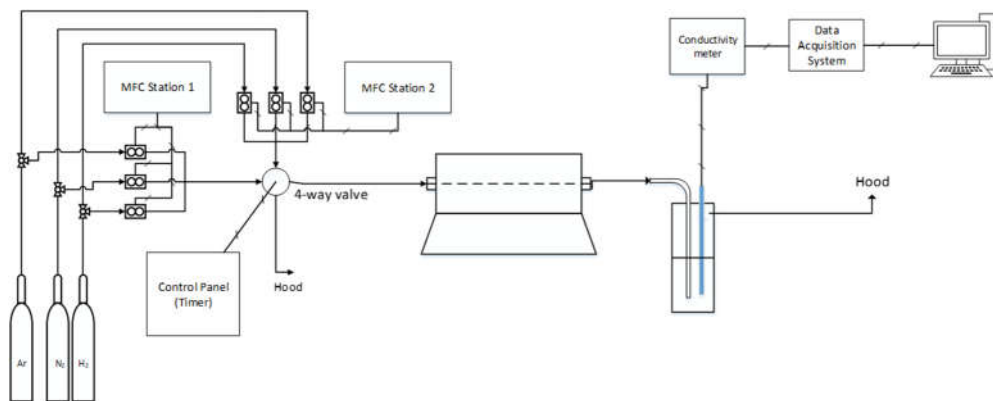


Figure 3.6. Experimental Setup for Ammonia Synthesis Reaction under Unsteady State Flow Conditions



## CHAPTER 4

### FUNDAMENTALS OF HYDROGEN ADSORPTION & STORAGE PROCESSES OVER Ru/SiO<sub>2</sub> AND Ru/Vulcan<sup>2</sup>

#### 4.1 Introduction

Hydrogen is a clean and efficient energy that can be used especially for fuel cell vehicles and portable devices [122]–[124], albeit suffering from problems related to its low density under standard temperatures and pressures [125]. A safe, lightweight and relatively small storage tank is needed for high pressure (700 bar) hydrogen storage for fuel cell cars [126]. Another solution is the solid state storage of hydrogen. The main bottleneck of solid state storage of hydrogen in such materials are the requirement of high pressure (10 bar and above) and/or low temperature (77 K) conditions for storing the hydrogen, high hydrogen release temperatures (200 °C and above) and slow kinetics [127]. US Department of Energy (DOE) started a long term initiative to meet safety, cost and performance needs for onboard vehicle hydrogen storage systems that allow for a driving distance of more than 500 km [128]. US DOE target for 2020 is 4.5 wt% gravimetric hydrogen storage, -40/85 °C for operating temperature and at least 1500 cycles for storing and releasing hydrogen in 3-5 min [16], [129]. Similar targets and projects ensued by European Union (EU). For example, Solid State Hydrogen Storage Testing Facility (SoITEF) of EU is responsible for researching and testing on potential hydrogen storage materials [130].

Hydrogen storage materials reported in the literature can be grouped into four categories as i) adsorbent type materials (*MOF, carbon based materials etc.*) [131]–[134], ii) metal hydrides (*MgH<sub>2</sub>, Mg<sub>2</sub>NiH<sub>4</sub> etc.*) [135]–[140], iii) complex metal

---

<sup>2</sup> This chapter is a slightly modified version of the article published as “M.Y. Aslan and D. Uner, International Journal of Hydrogen Energy, 44 (2019), 18903-18914”

hydrides (*LiBH<sub>4</sub>*, *NaAlH<sub>4</sub>* etc.) [141]–[143], and iv) chemical storage of hydrogen in ammonia borane type materials [144], [145]. In Table 4.1, the hydrogen storage capacities, heats of adsorption values (Table 4.1(a)), hydrogen release temperatures (Table 4.1(b)) and hydrogen solid bond energies (Table 4.1(c)) of various hydrogen storage materials are summarized. Experimentally reported hydrogen storage capacities of materials are changing between 1.3 and 7.5 wt% while theoretical estimates can increase up to 9.0 wt%. Reported heat of adsorption of hydrogen over storage materials are in the range of 4 – 20 kJ/mol.

The studies in the literature showed that one of the best materials for hydrogen storage  $\text{MgH}_2$ , needs Ni addition in order to alter the kinetics of hydrogen storage and release processes [146]. Addition of Ni assist  $\text{H}_2$  dissociation and atomic hydrogen is accommodated very rapidly [135], [147], [148]. Ni (or metals such as Pd, Pt, Ru) doped carbon based materials were used as hydrogen storage material [[132], [149], [150] and references therein], [151]–[153]]. The enhancement in the hydrogen uptake of the material after addition of Ni (or transition metal) was explained with the spillover of dissociated hydrogen from metal surface to support surface. Zhang et al. carried out a DFT study on the effect of Ni addition to the hydrogen storage capacity of  $\text{Mg}_{17}\text{Al}_{12}$  alloy. They found out that hydrogen dissociation energy barrier is calculated as 0.23 eV lower in the presence of Ni [149]. Li and Yang observed the increase on the hydrogen uptake capacity of metal-organic-framework type material (IRMOF) in the presence of Pt metal [132].

Table 4.1. Hydrogen storage materials and reported adsorption/desorption characteristics data

Table 4.1.a. Heat of hydrogen adsorption/desorption of storage materials

<b>Material</b>	<b>Storage Capacity, wt%</b>	<b>Heat of Adsorption/Desorption, kJ/mol</b>	<b>Notes</b>	<b>Reference</b>
<b>NOTT-103</b>	2.56 (1 bar, 78 K)	4-6		[131]
<b>Pt/AC-IRMOF</b>	4.0 (100 bar, 298 K)	20		[132]
<b>Pd/MIL-100 (Al)</b>	1.3 (4 MPa, 77 K)			[133]
<b>Mn<sup>2+</sup> decorated MOF</b>	6.9 (90 bar, 77 K)	10.1	@ Maximum Capacity	[134]
<b>In-based MOF</b>	2.61 (78 K, 1.2 bar)	6.5	Independent of coverage	[154]
<b>MOF-324</b>	4.2 (77 K, 79 bar)	6.2	Near zero coverage	[155]
<b>NU-125</b>	8.8 (100 bar, 77 K to 5 bar, 160 K)	5.1	Calculated	[156]
<b>10 wt% 9Ni-Mg-Y added MgH<sub>2</sub></b>	5.0 (350 °C, 500 s)	78	Measured desorption enthalpy	[157]
<b>Ni-CMK/MgH<sub>2</sub></b>	5.5	74.7	Calculated desorption enthalpy	[137]
<b>Ni<sub>50</sub>Co/MOF-74</b>	3.0 (14 bar, 77 K)	10.0	Initial	[158]
<b>†Ni decorated h-BN</b>	3.0	38.6-49.2		[159]

†Theoretical (DFT) studies

Table 4.1.b. TPD based H<sub>2</sub> release temperatures of storage materials

Material	Storage Capacity, wt%	H <sub>2</sub> release temperature (peak temperature), °C	Reference
2LiBH <sub>4</sub> -MgH <sub>2</sub> /CS	7.5 (@ 400 °C)	150 (starts) 327 (main)	[141]
2LiBH <sub>4</sub> -LiAlH <sub>4</sub> /RFC	5.7 (reversible, 350 °C, 50 bar)	120 (starts) 280 (main)	[142]
LiBH <sub>4</sub>	5.0	470, 200 (SiO <sub>2</sub> addition)	[160]
MgH <sub>2</sub> +V	5.5	235	[136]
Ni-CMK/MgH <sub>2</sub>	5.5	245	[137]
MgH <sub>2</sub> +NbF <sub>5</sub>	3.5	280	[138]
CeH <sub>2.73</sub> -MgH <sub>2</sub> -Ni	4.0	232	[139]
MgH <sub>2</sub> +5.0 wt CeO <sub>2</sub>	4.0	375	[140]
9Ni-Mg-Y/MgH <sub>2</sub> (D1)	3.5 (350 °C, 8 min)	210 (starts)	[161]
<sup>†</sup> Sc-Graphene	8.0	124 - 391	[162]
MWCNT/SnO <sub>2</sub>	0.8	220-510	[163]

<sup>†</sup>Theoretical (DFT) studies

Table 4.1.c. Hydrogen solid surface bond energies of storage materials.

Material	Storage Capacity, wt%	Hydrogen solid surface bond energy, kJ/mol	Reference
<sup>†</sup> Sc-Graphene	8.0	16.4	[162]
<sup>†</sup> Sc-C <sub>60</sub>	7.5	28.9	[164]
<sup>†</sup> Ti-SWNT	8.0	43.4	[165]
<sup>†</sup> Li <sub>12</sub> C <sub>60</sub>	9.0	5.8-17.3	[166]
MWCNT/SnO <sub>2</sub>	0.8	32.8-46.3	[163]
<sup>†</sup> Li decorated Be <sub>3</sub> C <sub>2</sub>	9.3	19.3-25.1	[167]
<sup>†</sup> Mg/Mg <sub>2</sub> Ni interface	6.8	1.9-80.1	[168]
<sup>†</sup> Ti-doped BNNT	7.2	5.8-20.7	[169]

<sup>†</sup>Theoretical (DFT) studies

Hydrogen spillover is defined as the migration of dissociated hydrogen from a hydrogen-rich phase to a hydrogen poor-phase [170]. The phenomenon was first observed through the change of color of  $\text{WO}_3$  from yellow to blue in the presence of  $\text{Pt}/\text{Al}_2\text{O}_3$  [171]. Later, Kramer and Andre demonstrated that hydrogen spillover is an activated surface diffusion process [172]. Roland et al. discussed the proposed ideas on the chemical nature of the spilled over hydrogen species such as atomic H,  $\text{H}^+$ ,  $\text{H}^+$ - $\text{H}^-$  ion pairs, and  $\text{H}_3^+$  and concluded in the light of electrical conductivity and Electron Spin Resonance (ESR) spectroscopy measurements that spilled over hydrogen species is electrically charged. Moreover, H atoms and  $\text{H}^+$  ions coexisted on the support surface [173], [174]. The experimental methods used include  $^1\text{H}$  Nuclear Magnetic Resonance (NMR) [175]–[177] for quantitative identification of adsorbed hydrogen species in different chemical environments, IR [178]–[180], for observing the H-D exchange process, ESR [181], for determining the charge of the noble metal (especially Pt), Inelastic Neutron Scattering (INS) [182]–[184], for the identification of the chemical nature of spilled over hydrogen over support material, and temperature programmed analysis [185]–[187] to study the relation of adsorption-desorption characteristics of the hydrogen with temperature over supported metal catalysts.

Hydrogen spillover is exploited in many industrially important reactions such as hydrocracking and hydroprocessing [188]–[190]. In recent years, it was demonstrated that spilled over hydrogen can also play a crucial role in hydrogen storage technologies [132], [191], [192], Fischer-Tropsch [193], [194] and ammonia synthesis [45], [195] reactions. The studies reported in the literature indicated that, metal particle size [196], [197] presence of hydroxyl groups on the support surface [198], reduction temperature of catalyst [185], and support type [199] influence the rate and amounts of spilled-over  $\text{H}_2$ . Effect of support type on the adsorption-desorption characteristics of hydrogen were studied over various supports [132], [173], [185], [200]. Although the experimental evidence surmounts for hydrogen spillover over supported metal catalysts, the chemical nature and mechanism of the process, especially over non-

reducible support materials, are still waiting to be clarified.

DFT studies report storage capacities and energies of hydrogen atom over a variety of support materials [162], [164]–[169], [201]. Hydrogen spillover on defect free non-reducible oxides such as MgO and SiO<sub>2</sub> are reported to be energetically impossible [202], [203] while contrary findings are also reported [204]–[206]. Spreafico et al. proposed that the main parameters that influence the spillover rate over Pt/TiO<sub>2</sub> and Pt/Al<sub>2</sub>O<sub>3</sub> were the hydrogen partial pressure and thickness of support material [206]. While TiO<sub>2</sub> had a homogeneous spilled over hydrogen coverage due to that spillover rate was not affected by co-adsorbed water molecules and faster compared to Ti(III)/proton migration process, spilled over hydrogen can go up to a few atomic distance from Pt metal particles in the presence of Al<sub>2</sub>O<sub>3</sub> due to having similar diffusion and desorption rates of hydrogen.

In this study, the effect of metal particle size and support material type in terms of H<sub>2</sub> adsorption-desorption characteristics, including surface migrations, over Ru/SiO<sub>2</sub> and Ru/Vulcan materials are reported. Volumetric chemisorption experiments and HR-TEM were used to determine the average metal particle sizes of Ru metal. Temperature programmed analysis techniques were applied to reveal the reduction, H<sub>2</sub> uptake and release characteristics of the catalysts. Experimental results were evaluated in the framework of hydrogen uptake and release conditions of supported Ru hydrogen storage materials.

## **4.2 Results and Discussion**

### **4.2.1 Dispersion of Ru Particles over Ru/SiO<sub>2</sub> and Ru/Vulcan catalysts**

HR-TEM images of 1, 3, and 5 wt% Ru/SiO<sub>2</sub> catalysts were given in Figure 4.1. The particle size distributions of the Ru/SiO<sub>2</sub> catalysts with different metal loadings were given in Figure 4.2. Although some agglomerations were observed in the HR-TEM images of 3 and 5 wt% metal loadings, generally Ru metal distributions were uniform.

HR-TEM images indicated that the average Ru metal particle size increased with increasing metal loading. The average particle diameters of 1, 3, and 5 wt% Ru/SiO<sub>2</sub> were determined as 1.2, 2.1 and 2.5 nm, respectively.

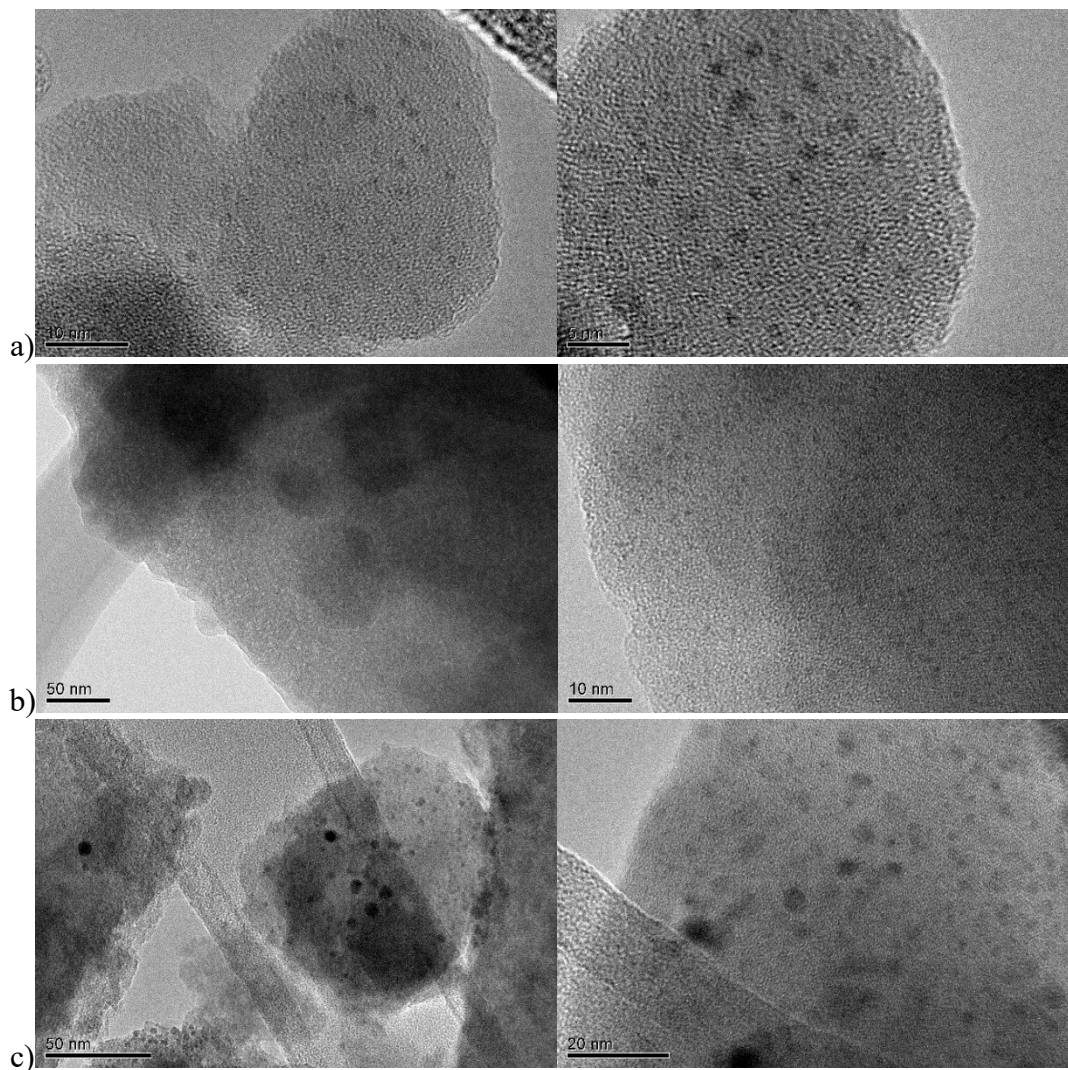


Figure 4.1. HR-TEM images of a) 1 wt% Ru/SiO<sub>2</sub>, b) 3 wt% Ru/SiO<sub>2</sub>, c) 5 wt% Ru/SiO<sub>2</sub>

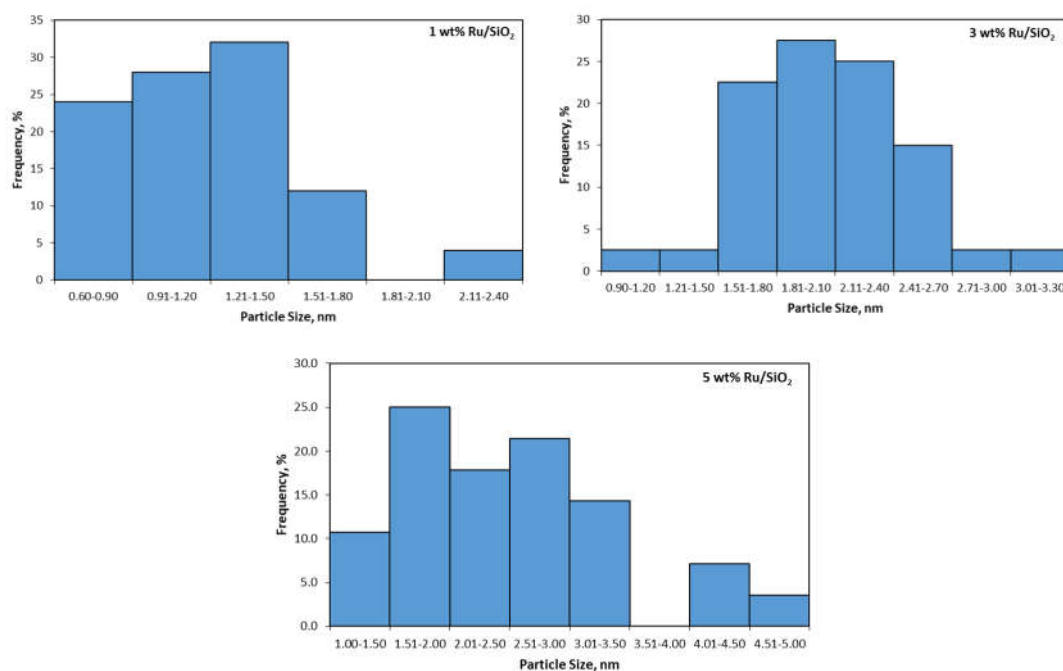


Figure 4.2. Ru metal particle size distributions of Ru/SiO<sub>2</sub> catalysts

HR-TEM images of Ru/Vulcan catalysts were given in Figure 4.3. HR-TEM images of Ru/Vulcan catalysts exhibited well dispersed Ru metal nanoparticles. In addition, some agglomerated particles were observed with increasing metal loading. In Figure 4.4, the average Ru metal particles size distribution of 1, 3 and 5 wt% Ru/Vulcan catalysts determined from HR-TEM images were given. Similar to the Ru/SiO<sub>2</sub>, the average diameter of Ru metal particles were increased with increasing metal loading. The average particle diameters of 1, 3, and 5 wt% Ru/Vulcan were determined as 2.1, 6.3 and 9.4 nm, respectively.

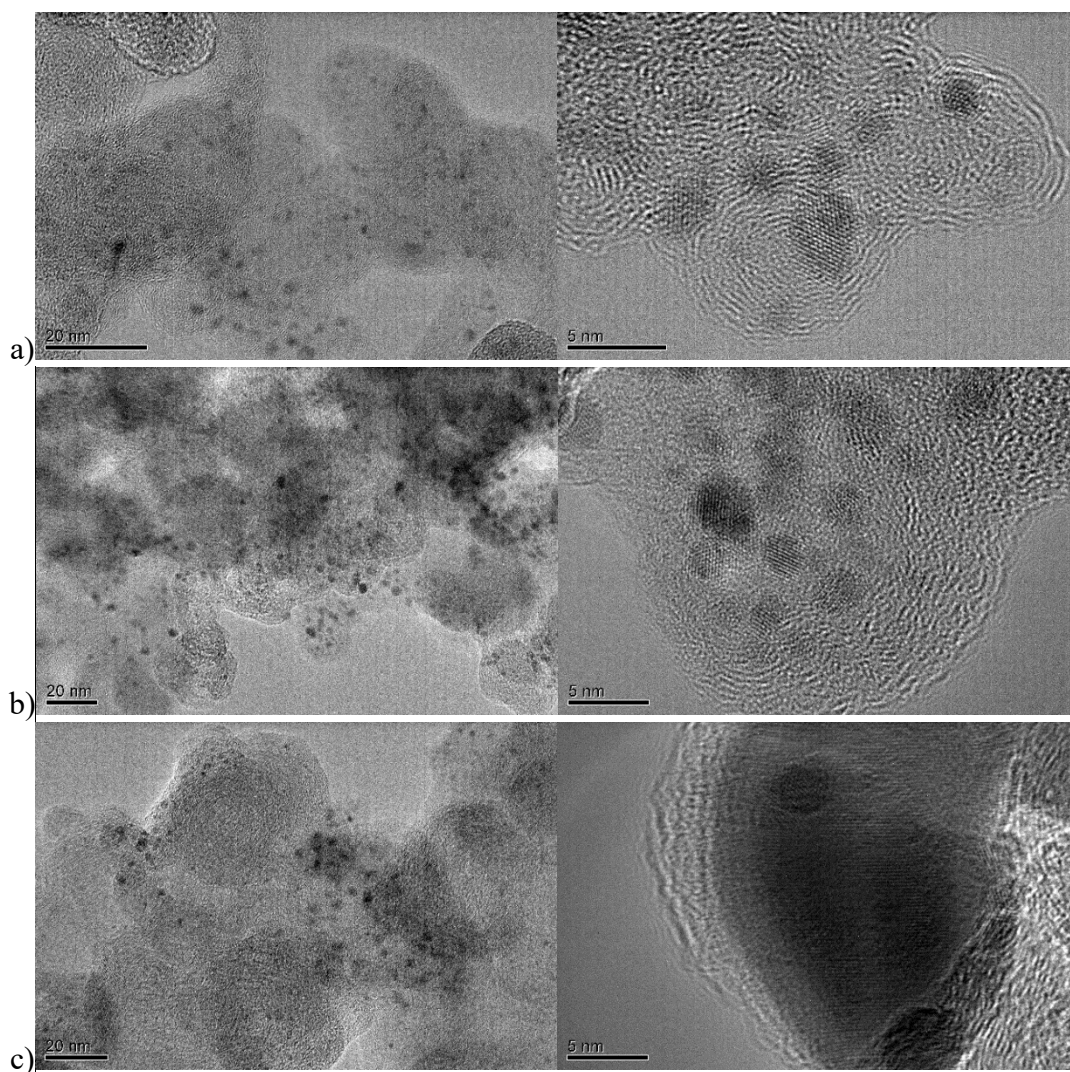


Figure 4.3. HR-TEM images of a) 1 wt% Ru/Vulcan b) 3 wt% Ru/Vulcan, c) 5 wt% Ru/Vulcan

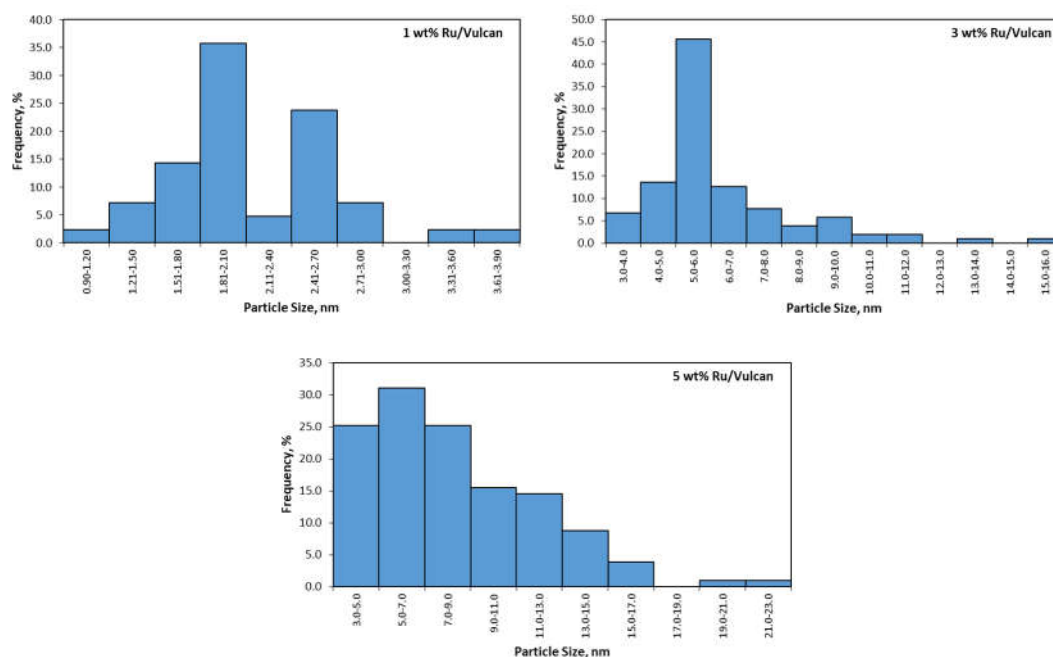


Figure 4.4. Ru metal particle size distributions of Ru/Vulcan catalysts

## 4.2.2 Temperature Programmed Analysis

### 4.2.2.1 Temperature Programmed Reduction

#### Ru/SiO<sub>2</sub>

H<sub>2</sub>-TPR patterns of 1, 3, and 5 wt% Ru/SiO<sub>2</sub> materials were given in Figure 4.5 in the flow of H<sub>2</sub> in Ar (%10 H<sub>2</sub>) at a flow rate of 25 ml min<sup>-1</sup> and with a 5 °C min<sup>-1</sup> temperature ramp. All the Ru/SiO<sub>2</sub> materials have a sharp peak at 194 °C, which was attributed to the reduction temperature of Ru salt (Ru(NO)(NO<sub>3</sub>)<sub>3</sub>) located inside the pores of SiO<sub>2</sub> support. Nurunnabi et al. also reported that the reduction of Ru nitrosyl nitrate precursor over Al<sub>2</sub>O<sub>3</sub> occurred at 199 °C [207]. In addition to this, all catalysts had a small peak before the peak at 194 °C, which may be attributed to the easily accessible Ru salt particles compared to the particles reduced at 194 °C. When the hydrogen consumption amounts were examined in terms of required hydrogen amounts in order to reduce Ru salt, it can be seen that, consumed hydrogen amounts

were higher than theoretical hydrogen amounts. Quantitative analysis of this process is given in Table 4.2

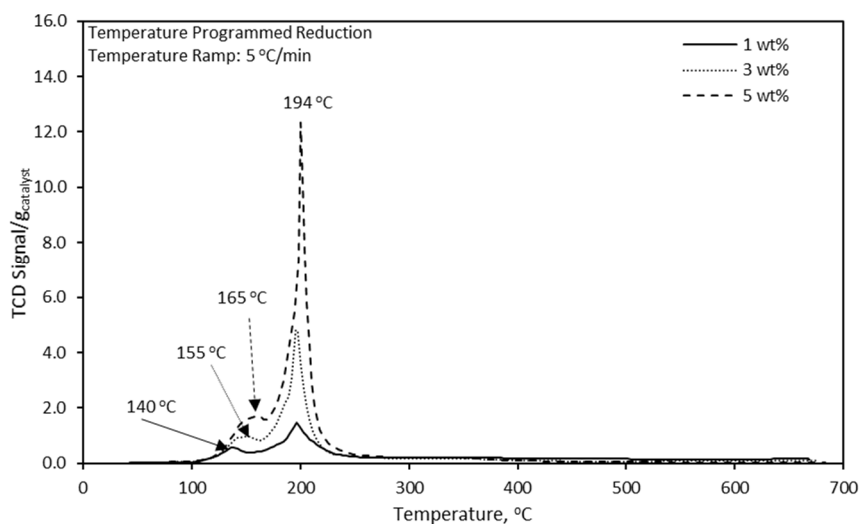


Figure 4.5. Temperature Programmed Reduction of 1,3 and 5 wt% Ru/SiO<sub>2</sub> catalysts.

Table 4.2. H<sub>2</sub> consumption amounts of fresh Ru/SiO<sub>2</sub> catalysts during H<sub>2</sub>-TPR

	H <sub>2</sub> Consumption for Ru(NO)(NO <sub>3</sub> ) <sub>3</sub> reduction, mol/g <sub>catalyst</sub>	Theoretical H <sub>2</sub> Consumption, mol/g <sub>catalyst</sub>
1 wt% Ru/SiO <sub>2</sub>	$2.56 \times 10^{-3}$	$3.96 \times 10^{-4}$
3 wt% Ru/SiO <sub>2</sub>	$3.41 \times 10^{-3}$	$1.19 \times 10^{-3}$
5 wt% Ru/SiO <sub>2</sub>	$5.38 \times 10^{-3}$	$1.98 \times 10^{-3}$

### Ru/Vulcan

In Figure 4.6, H<sub>2</sub>-TPR profiles of 1, 3, and 5 wt% Ru/Vulcan catalysts were given. Two peaks were observed in the H<sub>2</sub>-TPR patterns of Ru/Vulcan catalysts. The peak observed at 190 °C (for 1 and 5 wt% Ru/Vulcan materials 203 °C) can be attributed to the reduction of Ru(NO)(NO<sub>3</sub>)<sub>3</sub>. Another broad peak centered at 540 °C was also observed. The amount of hydrogen consumption during H<sub>2</sub>-TPR analysis were

determined (see Table 4.3) and the results revealed that hydrogen consumption amounts were higher than the required amount of hydrogen to reduce the Ru metal over the Vulcan support. The higher amount of hydrogen required for reduction is attributed to the reduction of carbonyl ( $1840\text{ cm}^{-1}$ ) and hydroxyl ( $1382\text{ cm}^{-1}$ ) groups formed over Vulcan support during impregnation, identified by ATR-IR spectroscopy as shown in Figure 4.7.

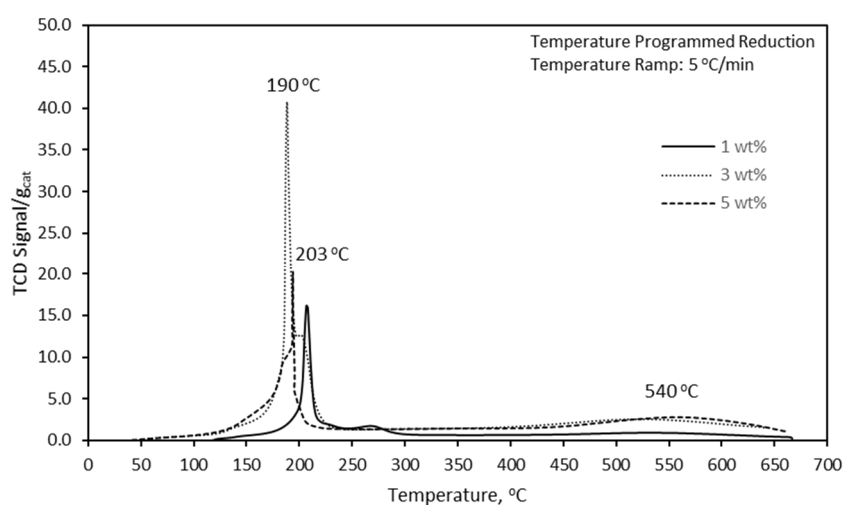


Figure 4.6. Temperature Programmed Reduction of 1,3 and 5 wt% Ru/Vulcan catalysts.

Table 4.3.  $\text{H}_2$  consumption amounts of fresh Ru/Vulcan catalysts during  $\text{H}_2$ -TPR

	$\text{H}_2$ Consumption for $\text{Ru}(\text{NO})(\text{NO}_3)_3$ reduction, $\text{mol/g}_{\text{catalyst}}$	Theoretical $\text{H}_2$ Consumption, $\text{mol/g}_{\text{catalyst}}$
1 wt% Ru/Vulcan	$9.64 \times 10^{-3}$	$3.96 \times 10^{-4}$
3 wt% Ru/Vulcan	$2.38 \times 10^{-2}$	$1.19 \times 10^{-3}$
5 wt% Ru/Vulcan	$1.87 \times 10^{-2}$	$1.98 \times 10^{-3}$

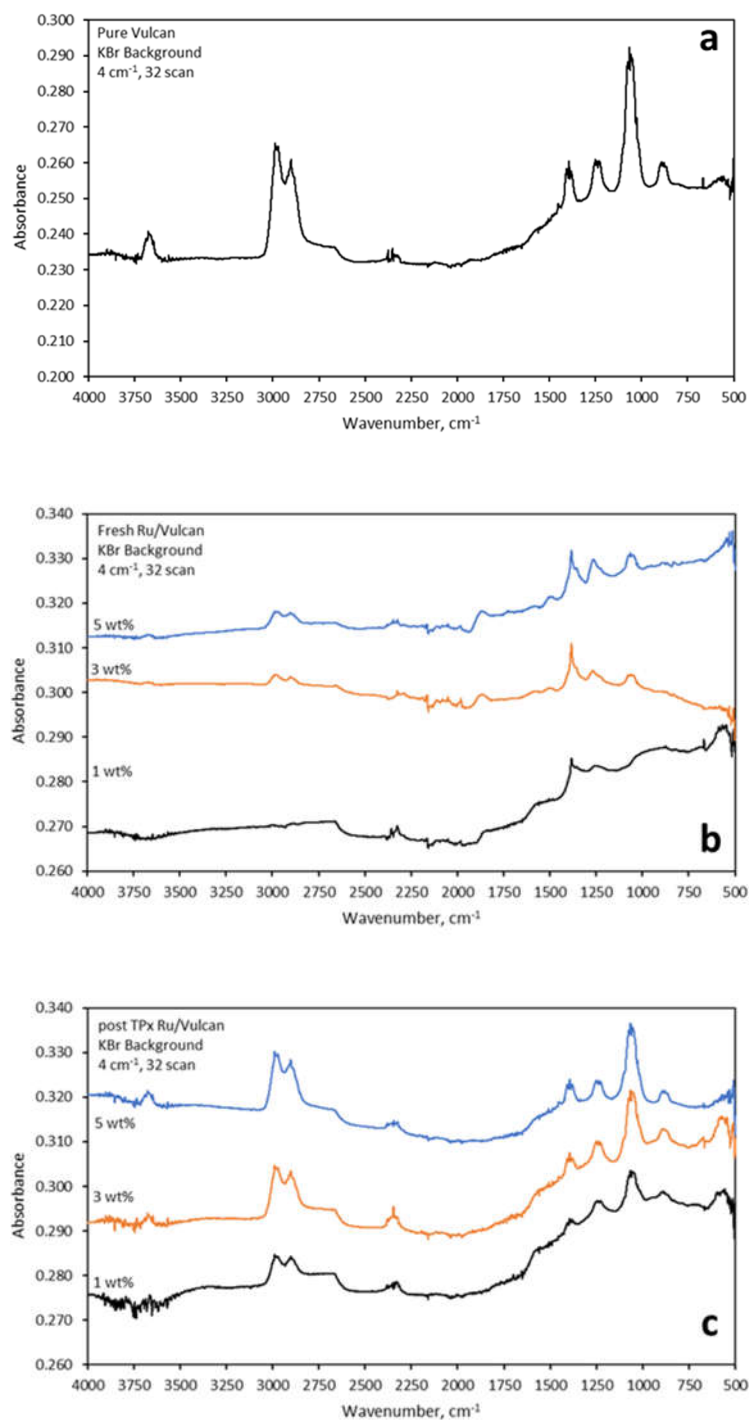


Figure 4.7. ATR-IR spectra of a) pure Vulcan, b) fresh 1, 3, and 5 wt% Ru/Vulcan catalysts, c) 1, 3, 5 wt% Ru/Vulcan catalysts after  $\text{H}_2$ -TPR, TPD and  $\text{O}_2$ -titration experiments

#### 4.2.2.2 Temperature Programmed Desorption and O<sub>2</sub>-Titration

TPD behavior observed in this study is consistent with the similar results in the literature. A low temperature peak attributed to desorption from the metal and a high temperature peak attributed to desorption from the support were consistently observed and reported [185], [187], [208]–[210].

#### Ru/SiO<sub>2</sub>

TPD profiles of the Ru/SiO<sub>2</sub> catalysts were given in Figure 4.8. All of the catalysts exhibit a broad desorption peak at low temperatures (150 – 195 °C). This broad peak never reached the baseline for high metal load samples. For the sample with 1 wt% Ru, a desorption peak centered at 548 °C was also recorded, for over 3 and 5 wt% Ru/SiO<sub>2</sub> catalysts, a second desorption process was initiated at the later stages, but due to the instrumental limitations, the full behavior could not be observed.

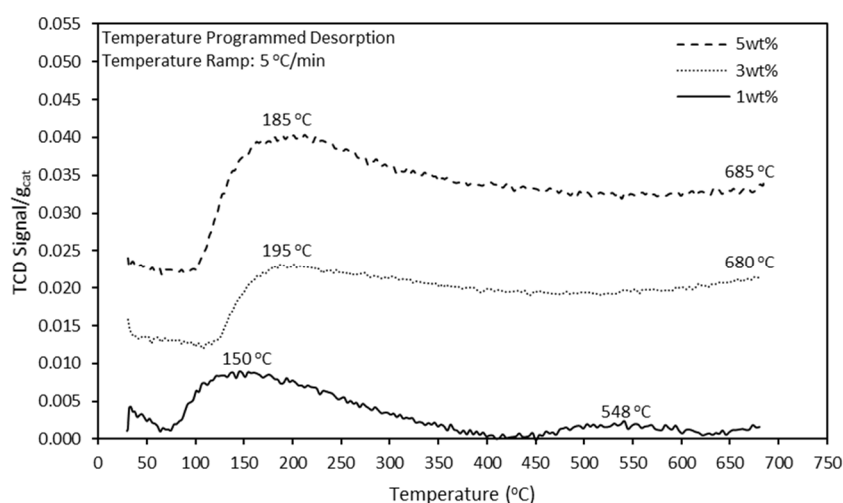


Figure 4.8. Temperature Programmed Desorption profiles of Ru/SiO<sub>2</sub> materials.

Adsorbed(consumed)/desorbed amount of hydrogen during TPD, O<sub>2</sub>-titration and H<sub>2</sub>-chemisorption analyses of Ru/SiO<sub>2</sub> catalysts were compared in terms of their H/Ru ratios for Ru/SiO<sub>2</sub> (Table 4.4) and Ru/Vulcan (Table 4.5). All of the methods indicated

a decrease in dispersion with increased metal loading. The absolute dispersion values determined from oxygen titration and HR-TEM results were in closed agreement. The total amount of hydrogen desorbed from the material was also given in the same table in terms of H/Ru Ratio. It is seen that, over Ru/SiO<sub>2</sub>, the total hydrogen desorbed is not too much, and the amount does not depend on dispersion, suggesting that spillover is not substantial over this material.

Table 4.4. Ru metal dispersions of Ru/SiO<sub>2</sub> catalysts obtained from different methods.

<b>Ru, wt%</b>	H/Ru from TPD	O <sub>2</sub> titration, %	H <sub>2</sub> -chemisorption, %	HR-TEM, %
<b>1</b>	0.59	74	22	83
<b>3</b>	0.56	42	10	48
<b>5</b>	0.50	38	7	40

### **Ru/Vulcan**

TPD profiles of Ru/Vulcan catalysts were given in Figure 4.9. Two hydrogen desorption process were observed: one at a low temperature (around 100 °C) and another one at a high temperature (around 400 °C). When a Redhead analysis [211] on the low temperature desorption peak shown in Figures 4.8 and 4.9, attributed to desorption from the metal sites, with a choice of desorption pre-exponential of 10<sup>13</sup> for a mobile desorption, approximately 100 kJ/mol desorption activation energy was obtained. The high temperature peaks exhibited similar shapes for all Ru/Vulcan materials. Low temperature peak of 3 wt% Ru/Vulcan was significantly higher in area than the corresponding peaks of 1% and 5% samples.

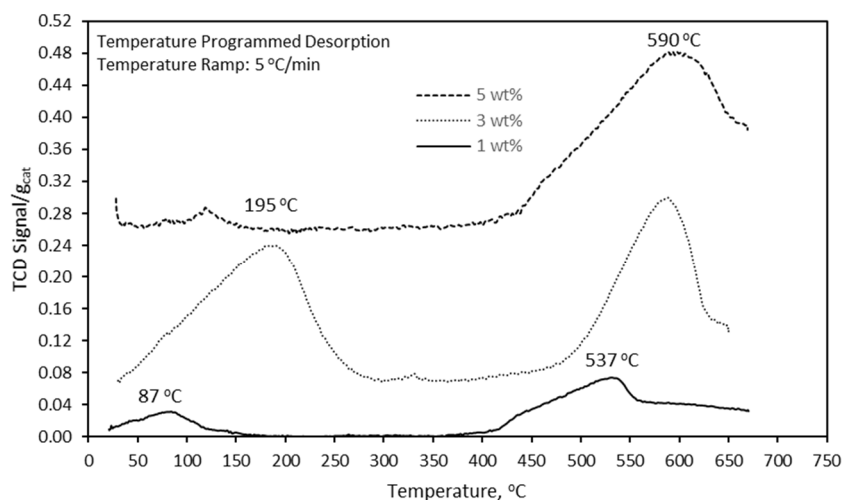


Figure 4.9. Temperature Programmed Desorption profiles of Ru/Vulcan materials.

The comparison of adsorbed(consumed)/desorbed amount of hydrogen obtained from TPD, O<sub>2</sub>-titration and H<sub>2</sub>-chemisorption methods for Ru/Vulcan catalysts were given in Table 4.5. When Table 4.5 was analyzed, it was seen that H/Ru ratio decreased with increasing Ru metal loading. On the other hand, it was obvious that the H/Ru obtained from TPD analysis one order of magnitude higher than the other analysis methods. The high H/Ru ratio can be indication of desorption of hydrogen not only from the Ru metal surface but also from the support surface. This argument can be supported with the observation of high temperature peaks in Figure 4.9, which can represent the back diffusion of spillover hydrogen species from support surface to metal surface at high temperatures.

Table 4.5. Ru metal dispersions of Ru/Vulcan materials obtained from different methods

<b>Ru, wt%</b>	<b>H/Ru from TPD</b>	<b>O<sub>2</sub>-titration, %</b>	<b>H<sub>2</sub>-chemisorption, %</b>	<b>HR-TEM, %</b>
<b>1</b>	4.75	84	28	48
<b>3</b>	4.78	70	5	16
<b>5</b>	2.14	16	4	11

Ru metal dispersions of Ru/Vulcan materials obtained from O<sub>2</sub>-titration, HR-TEM and volumetric chemisorption analysis methods were given in Table 4.5. The dispersion data obtained from these three different methods agree slightly, probably due to the support related influences during O<sub>2</sub>-titration and hydrogen chemisorption.

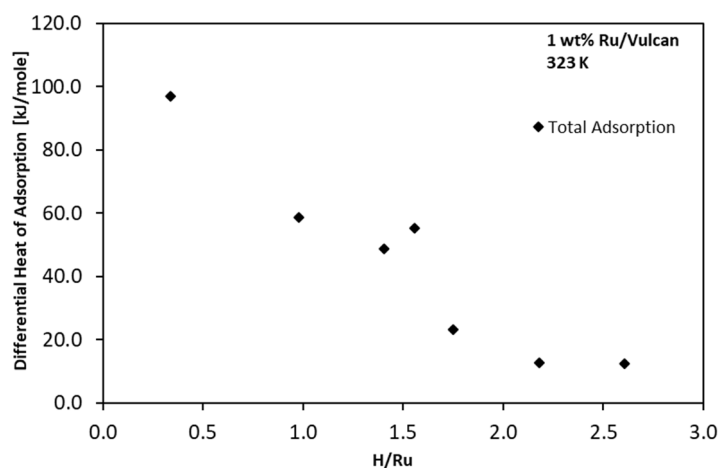


Figure 4.10. Differential heats of adsorption of hydrogen on 1 wt% Ru/Vulcan at 50 °C

In order to differentiate hydrogen on the metal and over the support, adsorption calorimetry measurements were conducted. Coverage dependent differential heats of adsorption over 1 wt% Ru/Vulcan are shown in Figure 4.10. The initial heat of adsorption was approximately 100 kJ/mol H<sub>2</sub>, attributed to Ru sites. This value is consistent with the desorption activation energy obtained by Redhead analysis of the low temperature TPD peaks for both Ru/SiO<sub>2</sub> and Ru/Vulcan. The measurements at increasing coverages indicated a linear decrease in adsorption heats with coverage, until approximately H/Ru ratio was 2. At this coverage, the heats of adsorption were around 10 kJ/mol, indicating a weakly bound state. The isosteric heat of adsorption value of hydrogen on transition metal “promoted” storage materials were reported to be between 4 – 20 kJ/mol [131], [132], [134], [154], [155]. On the other hand, the condensation enthalpy of hydrogen at 20 K and atmospheric pressure was reported as 0.891 kJ/mol [212]. The comparison of the results of adsorption microcalorimetry and

literature findings indicated that the heat of adsorption of hydrogen value are nearly same with the multilayer adsorption of hydrogen over material surface at high hydrogen coverages. In addition to experimental studies, DFT studies also showed that while first hydrogen molecule was dissociately adsorbed on the Pt/SWCNT material, the other hydrogen molecules were adsorbed molecularly on the Pt/SWNT with an increase in H-H bond length [201].

High temperature peaks observed during H<sub>2</sub> TPD experiments indicate a slow and/or highly activated desorption process. Along the same lines with the similar studies in the literature (e.g. ref. [172]), we propose that once dissociated hydrogen leaves the metal and is on the support, its migration will be by diffusion. The reversal of the adsorption, i.e. desorption, will proceed through diffusion as well, but still requiring metal sites for associative desorption (Figure 4.11). High amounts of hydrogen uptake by carbon-based materials in the presence of noble metals was attributed to C-H bond formation [202]. We will particularly note here the XPS study by Bhomwick et al. [213]: Using C 1s region of XPS spectra, they showed C-H bond formation through the suppression of sp<sup>2</sup> hybridization (C-C bonding) with concurrent increase in sp<sup>3</sup> hybridization upon hydrogen exposure over Pt/SWCNT catalyst.

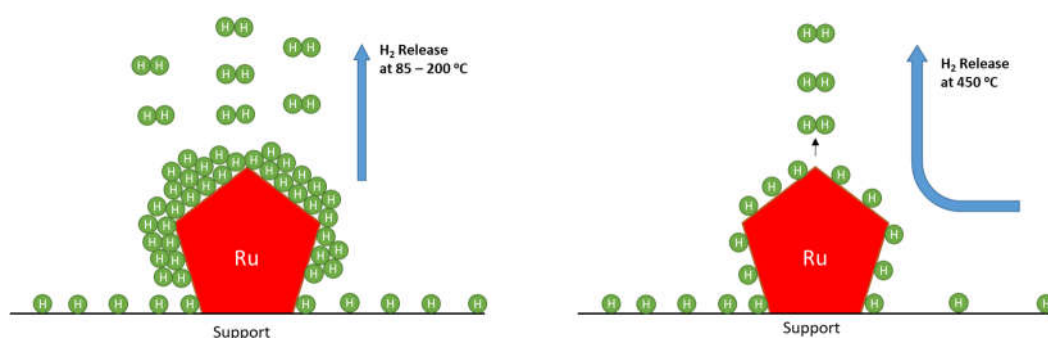


Figure 4.11. Hydrogen release at lower hydrogen coverages is diffusion limited, requiring higher temperatures.

### 4.3 Chapter Summary

The question addressed in this part of the study was to investigate the fundamentals of the hydrogen adsorption and desorption over various support materials promoted with Ru. It was observed that the dissociated hydrogen migration by spillover is a slow process and desorption of spilled over hydrogen may require excessive temperatures (while  $\text{MgH}_2$  releases hydrogen at 300 °C and above, Ru/SiO<sub>2</sub> and Ru/Vulcan based materials need 450 °C and above). The results of hydrogen adsorption by calorimetry performed at 50 °C indicated that after the precious metal surface layer saturates, hydrogen adsorption heat values decrease, but still higher than the heat of condensation of H<sub>2</sub>. In other words, the process is no longer governed by adsorption and migration of the dissociated hydrogen only but also by the multilayer adsorption of hydrogen.



## CHAPTER 5

### SUPPORT EFFECTS IN AMMONIA SYNTHESIS<sup>3</sup>

#### 5.1 Introduction

Ammonia synthesis by Haber-Bosch process consumes ~ 2% of the world energy annually. As a result, it is one of the most energy intensive industrial chemical processes [112], [214]. Primary consumer of synthetic ammonia is the fertilizer industry[1], [7]. Ammonia is also being considered as a hydrogen storage material, as a feedstock for CO-free hydrogen production [215], [216]. The challenge of ammonia synthesis remains to be finding an active catalyst that can improve rates at lower temperatures.



Ammonia synthesis reaction (Equation 5.1) is a thermodynamically limited reaction. Besides, it is established that the rate-determining step of ammonia synthesis reaction is the dissociation of nitrogen step [29], [33], [37], [217], [218]. The following steps in the reaction mechanism are the subsequent hydrogenation of dissociated nitrogen molecules, which are in equilibrium. Therefore, the ammonia synthesis rate can be expressed as the nitrogen activation rate (adsorption rate of N<sub>2</sub> to catalytic metal surface) on the catalyst surface. If a general ammonia synthesis rate expression is derived based on the mechanism of ammonia synthesis over a catalytic surface proposed in the literature [37], [217] assuming Langmuir-Hinshelwood model, it is seen that the concentrations (partial pressures) of both H<sub>2</sub> and NH<sub>3</sub> are appeared in the denominator. It means that hydrogen and ammonia poison the ammonia synthesis reaction. In addition, there are several studies in the literature that reported semi-

---

<sup>3</sup> This chapter is prepared for publication in “Applied Catalysis A: General” with the co-authors of “M.Y.Aslan, S. Akbayrak, S. Özkar, and D. Uner”

empirical ammonia synthesis rate expressions which indicate the poisoning of the ammonia synthesis reaction by ammonia and hydrogen [29], [31], [33], [34], [116], [218]. In a more detailed perspective: when the partial pressure of hydrogen increases, the surface coverage of hydrogen increases over the catalyst surface depending upon the adsorption equilibrium constant of hydrogen. On the other hand, the poisoning effect of ammonia is originated from the surface coverage of ammonia. Ammonia is synthesized during the reaction as a product. As a result, the source of the gas phase ammonia is the ammonia coverage on the catalyst surface. In addition, increase of the surface coverage of ammonia also increases the reverse rate of ammonia synthesis reaction.

Ruthenium is the most active metal among ammonia synthesis catalysts in terms of nitrogen activation at same operating conditions [33], [52], [74], [219], [220]. The ammonia synthesis rates and corresponding apparent activation energies reported in the literature at high temperature (300 – 400 °C) and atmospheric pressure conditions are summarized in Table 6.1 and 6.2. However, the studies reported in the literature reveal that the apparent activity of ruthenium catalysts are in the same order of magnitude with iron [33]. On supported Ru catalysts, the poisoning effect of hydrogen become more prominent [31], [51], [55], [65], [195]. However, the inhibition effect of ammonia can also be another parameter that influences ammonia synthesis rate. Rosowski et al. reported ammonia synthesis rate expressions based on power law kinetics and showed that ammonia inhibited the ammonia synthesis reaction over supported Al<sub>2</sub>O<sub>3</sub> and MgO supported Ru catalysts, respectively. [65]. On the other hand, Siporin and Davis studied on the ammonia synthesis kinetics using power law kinetics over Ru/MgO catalyst that ammonia nearly has no effect on the ammonia synthesis rate [51]. In addition to the poisoning effect of synthesized ammonia on the catalyst (Ru) surface, the possibility of inhibition effect of ammonia retained on the support surface is an open question.

Table 5.1. Ammonia synthesis reaction rates, TOF values and the related operating conditions reported in the literature over supported Ru based catalysts

Reference	Catalyst	Ru loading, wt%	Operating Conditions	Flow Rate (H <sub>2</sub> :N <sub>2</sub> =3:1), mL/min	Catalyst Amount, g	Space Time, s	GHSV, hr <sup>-1</sup>	Rate, μmol /g <sub>cat</sub> -h	TOF <sup>a</sup> , s <sup>-1</sup> (x10 <sup>-4</sup> )
[19]	Ru/Al <sub>2</sub> O <sub>3</sub>	5.0	315 °C, 1 bar	120	0.138	0.02	229000	89	0.3
[19]	Ru/MgO	5.0	315 °C, 1 bar	120	0.138	0.02	229000	684	2.2
[43]	Cs-Ru/HT	10.0	325 °C, 1 bar	167	5.0	0.60	7000	377	0.5
[21]	Ru/MgO	8.0	380 °C, 1 bar	60	0.20	0.05	77200	2017	2.3
[21]	Ru/BHA	8.0	380 °C, 1 bar	60	0.20	0.05	77200	3497	3.3
[221]	Ru/KY	2.5	400 °C, 1 bar	40	0.3	0.20	15500	445	4.8

Table 5.2. The reported apparent activation energies of Ru based catalysts used for ammonia synthesis reaction.

Reference	Catalyst	E <sub>A</sub> , kJ/mol	GHSV, hr <sup>-1</sup>	Conditions
[220]	Ru/MgO	74	13900	1 bar, 270 – 350 °C
[58]	Ru/Al <sub>2</sub> O <sub>3</sub>	63		1 bar
[58]	Ru-CsOH/Al <sub>2</sub> O <sub>3</sub>	116		1 bar
[222]	K-Ru/MgO-CNT	88	31290	2 bar, 325 – 415 °C
[223]	Ru/BaX	113	4800	20.7 atm, 350 – 420 °C
[51]	La-Ru/MgO	86	90240	20.7 atm, 325 – 450 °C
[51]	Ru/MgO	107	90240	20.7 atm, 325 – 450 °C
[31]	Ba(Cs or K)-Ru/C	96	50000	70-100 bar, 360 – 460 °C

Surface acidity of the support materials can be an important parameter on the ammonia synthesis reaction rate which can be related with inhibition effect of ammonia [19], [35], [80], [81], [224]–[226]. According to the studies in the literature, ammonia formation rate in the presence of basic supports are reported to be higher than that of in the presence of acidic supports. It is claimed that basic supports can provide more electrons to Ru metal to dissociate nitrogen molecules effectively [19], [21], [35], [80], [83], [226]. On the other hand, semi-empirical models for the reaction rate expressions that ammonia synthesis reaction is poisoned by ammonia and hydrogen. The surface characteristics of the support materials (either acidic or basic) would affect the surface

coverage of ammonia so that the rate of ammonia formation can be affected accordingly.

In the literature, in order to improve ammonia synthesis rate over various type of catalysts, the unsteady state reactor operation were proposed as one of the solutions. The suggested unsteady state reactor operations were constructed in two basis: i) the removal of ammonia from the reaction environment using an appropriate absorbent and ii) feeding the reactants in a pure and/or mixture form in a cyclic manner. In the light of theoretically derived and published semi-empirical ammonia synthesis rate expression in the literature, the possibility of removing the inhibitory effects of ammonia and hydrogen over supported Ru catalysts (supports: zeolite-Y, HAp, Vulcan Carbon) depended on the acidity of the support during ammonia synthesis reaction is studied. In this framework, the density and the strength of the acidic sites of support materials are measured using differential and single point heat of ammonia adsorption experiments. Ammonia synthesis reaction rates are measured at 300 – 400 °C and atmospheric pressure over zeolite-Y, Vulcan and HAp supported Ru catalysts, under steady and unsteady flow conditions.

## **5.2 Results and Discussion**

The objective of the study is to investigate the possibility of reducing and/or eliminating the inhibitory effects of ammonia and hydrogen over supported Ru catalysts (supports: Zeolite-Y, HAp, Vulcan Carbon) depended on the type (acidity) of the support material during ammonia synthesis reaction using an unsteady state flow strategy. The poisoning effect of hydrogen over supported Ru catalysts are well established. The acidity of the support material can be a parameter for the poisoning of the catalyst by ammonia. The synthesized ammonia can accumulate on the support and/or Ru metal surface. In this framework, differential and single point ammonia adsorption experiments were performed to measure the strength and density of acidic sites of the supports. Ammonia synthesis experiments were conducted in the presence of supported Ru catalysts that having similar Ru metal dispersions to ensure that

ammonia formation rate was not affected by the Ru metal dispersion. Ammonia synthesis reaction experiments were carried out under steady gas flow ( $\text{H}_2:\text{N}_2:\text{Ar}=3:1:2$ ) between 300 and 400 °C and atmospheric pressure. Following the ammonia synthesis experiments under steady flow, total amount of ammonia that accumulated on the catalyst surface was measured under Ar flow. The relation between the total amount of synthesized ammonia within 1 h and total amount of desorbed ammonia over the catalysts revealed the degree of inhibition by ammonia. In order to reduce/eliminate the poisoning effects of both ammonia and hydrogen, an unsteady state flow strategy (forced unsteady state) was proposed such that  $\text{H}_2:\text{N}_2=3:1$  and pure  $\text{N}_2$  flows were sent to the reactor as pulses. The unsteady state flow strategy was tested in the presence of HAp supported Ru catalyst to demonstrate the revival of the ammonia synthesis reaction that inhibited and stopped under steady flow conditions.

## **5.2.1 Support Characterization**

### **5.2.1.1 Support Acidity**

The density and strength of acid sites of bare HAp were measured with two different methods: i) single point ammonia adsorption using 5.0 % (vol.)  $\text{NH}_3$  in He gas mixture, ii) differential heat of adsorption of ammonia using pure ammonia gas. The results of ammonia adsorption performed on bare HAp material with two different methods gave consistent results as shown in Figure 6.1. Therefore, single point heat of ammonia adsorption experiments were also carried out for zeolite-Y and Vulcan supports. Zeolite-Y and Vulcan supports adsorbed higher amounts of ammonia compared to HAp as given in Table 5.3. On the contrary, higher energy release was observed over HAp (28.3 kJ/mol) as compared to Zeolite-Y (7.3 kJ/mol) and Vulcan (3.0 kJ/mol). This indicates the availability of sites with acidic nature over HAp surface. These results are consistent with the reported studies in the literature revealing that HAp represented amphoteric characteristics [227], [228].

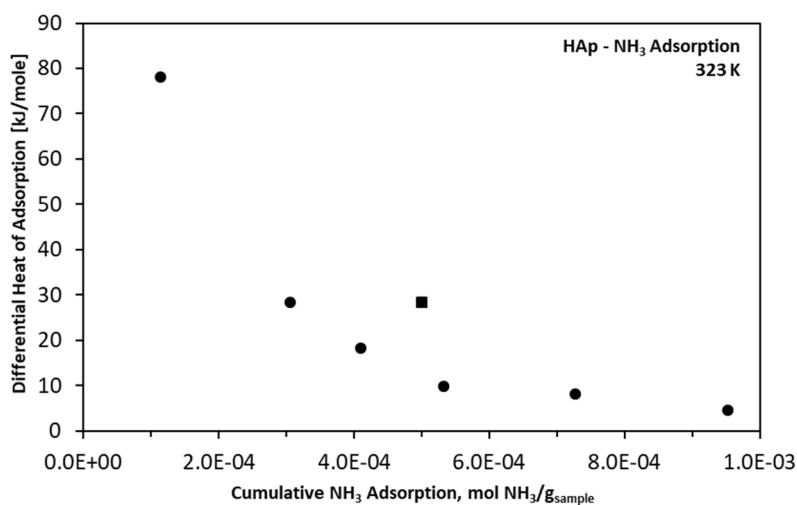


Figure 5.1. Heat of adsorption of ammonia over HAp at 323 K; • belongs to differential heat of adsorption of ammonia, ■ belongs to single point heat of ammonia adsorption at 515 Torr.

### 5.2.1.2 Surface Area of Support

BET surface area, monolayer ammonia adsorption based on the BET surface area, surface area of supports estimated based on ammonia coverage and the kinetic diameter of ammonia were given in Table 5.3 which shows that surface area of HAp material estimated based on ammonia coverage was in a good agreement with the BET surface area. However, monolayer coverage of ammonia estimated from the BET surface area of zeolite-Y and Vulcan were 7-10 times higher compared to experimentally measured amount of ammonia coverage. In summary, single point ammonia adsorption experiments indicate that while adsorbed ammonia covers 100% of HAp surface, only 10-15% of the surface of Zeolite-Y and Vulcan is covered by adsorbed ammonia.

Table 5.3. Comparison of surface area of supports using BET and amounts of adsorbed ammonia

Support	BET surface area of support, m <sup>2</sup> /g	Monolayer coverage <sup>a</sup> , mmol/g	Amount of NH <sub>3</sub> adsorbed, mmol NH <sub>3</sub> /g <sub>support</sub>	Energy Released, kJ/mol NH <sub>3</sub>	Surface Area covered by adsorbed NH <sub>3</sub> <sup>b</sup> , m <sup>2</sup> /g
Zeolite-Y	744	12.4	2.2	7.3	70.3
Vulcan	222	3.7	1.0	3.0	31.9
HAp	13	0.2	0.5	28.3	16.0

<sup>a</sup> Monolayer NH<sub>3</sub> adsorption coverage was calculated based on BET surface area of support with the assumption of 10<sup>15</sup> site/cm<sup>2</sup> [211]

<sup>b</sup> Surface area estimated using the experimentally measured NH<sub>3</sub> adsorption on supports and kinetic diameter of NH<sub>3</sub> [229]

## 5.2.2 Characterization of Ru Nanoparticles

HR-TEM images of Ru/Zeolite-Y, Ru/Vulcan and Ru/HAp (Fig. 5.2a-c) and corresponding particle size distribution histograms (Figure 5.2d-f) show a uniform Ru metal particle size distribution. In Table 5.4, metal loadings determined by ICP-OES and Ru metal dispersions of the catalysts obtained by H<sub>2</sub>-chemisorption and HR-TEM analyses are reported. H<sub>2</sub>-chemisorption based average particle size of the all catalysts are in the range of 3.0 and 3.6 nm slightly bigger than that is estimated from TEM.

Table 5.4. Loading, dispersion and average particle diameter of supported Ru<sup>0</sup> nanoparticles

Catalyst	Ru loading, % wt.	Ru dispersion, % (H <sub>2</sub> -chem.)	Average Ru particle size, nm (H <sub>2</sub> -chem.)	Ru metal dispersion, % (HR-TEM)	Average Ru particle size, nm (HR-TEM)
Ru/Zeolite-Y	1.37*	30	3.3	18	5.5±1.8
Ru/HAp	3.96*	30	3.3	25	4.2±1.3
Ru/HAp	2.00*	12	8.3		
Ru/Vulcan	1.0	28	3.6	48	2.1±0.5

\*determined by ICP-OES analysis

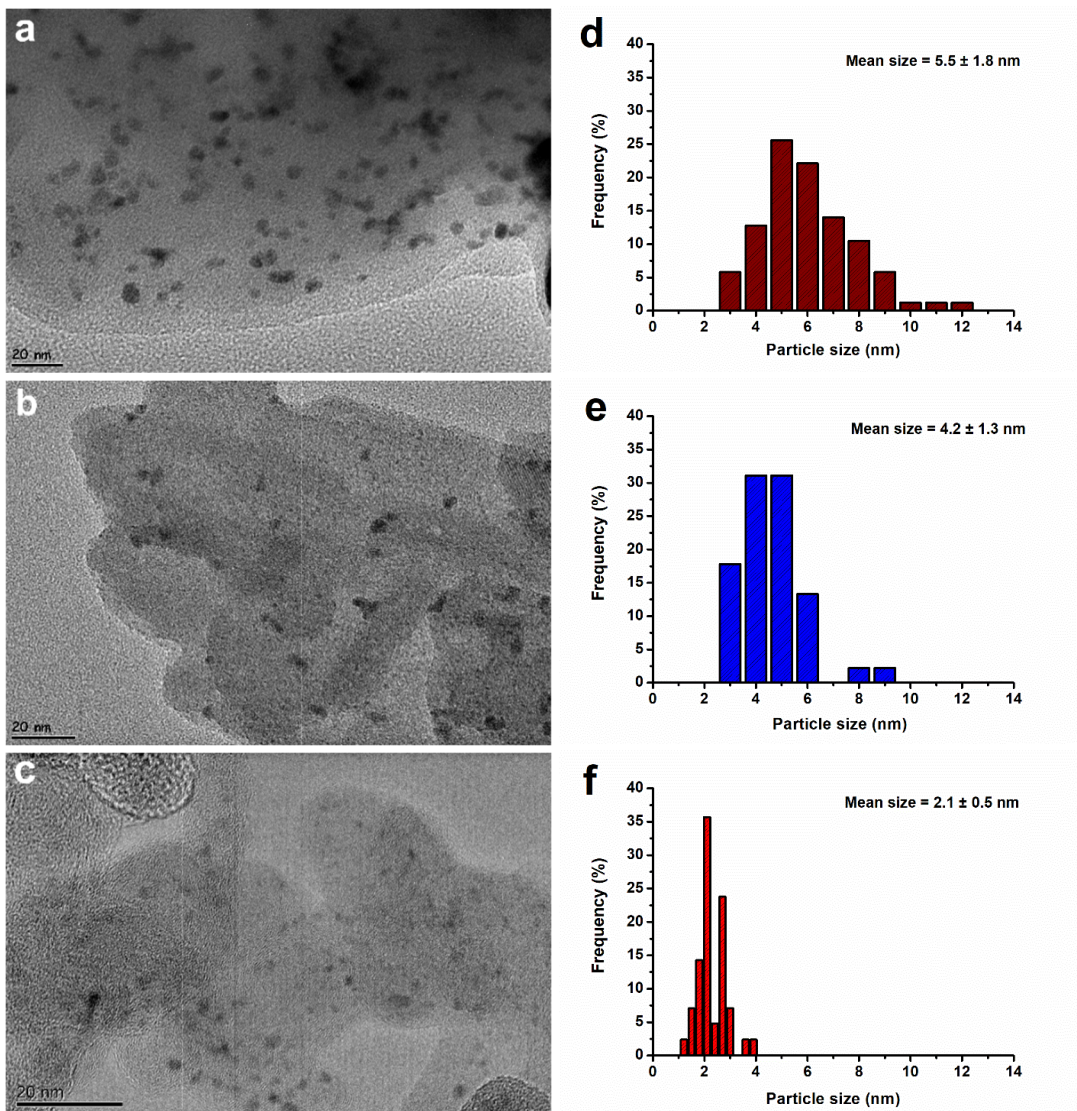


Figure 5.2. HR-TEM images of a) 1.37 wt% Ru/Zelite-Y, b) 4.0 wt% Ru/HAp, c) 1.0 wt% Ru/Vulcan and corresponding particle size distribution histograms of d) 1.37 wt% Ru/Zelite-Y, e) 4.0 wt% Ru/HAp, f) 1.0 wt% Ru/Vulcan

### 5.2.3 Ammonia Formation Rates

Formation rates of ammonia is measured under steady flow of 100 ml/min H<sub>2</sub>:N<sub>2</sub> (3:1) between 300 and 400 °C and atmospheric pressure using a fixed bed reactor. Ammonia synthesis activities reported in Table 5.5 indicate that the catalytic activity of Ru/Vulcan and Ru/Zeolite-Y are similar, while Ru/HAp catalysts have lower activities. Experimentally obtained nitrogen conversions over supported Ru catalysts and equilibrium conversion of ammonia synthesis reaction given in Figure 5.3 shows that the reaction is away from the equilibrium conditions. It must be mentioned here that the rates measured on HAp supported catalysts are independent of metal loading. The values reported in Table 5.5 are consistent with the reported values for atmospheric pressure data given in Table 5.1. High pressure operating conditions [36-38] and alkali promotion [31], [51], [54], [223], [230] or highly basic supports [81]–[83], [225], [231] can give rise to higher rates than that were reported in Table 5.1.

Table 5.5. Initial NH<sub>3</sub> formation rates over supported Ru catalysts (H<sub>2</sub>:N<sub>2</sub>:Ar=3:1:2)

Temperature, °C	Formation Rates, μmol NH <sub>3</sub> /g <sub>cat</sub> -h			
	Ru/HAp (2.0% wt. Ru)	Ru/HAp (4.0% wt. Ru)	Ru/Zeolite-Y (1.37% wt. Ru)	Ru/Vulcan (1.0 wt. Ru)
300	49	103	304	249
325	169	127	323	250
350	229	304	308	316
375	261	321	332	349
400	299	329	468	422
Apparent activation energies, kJ/mol	92.2	63.7	24.7	22.4

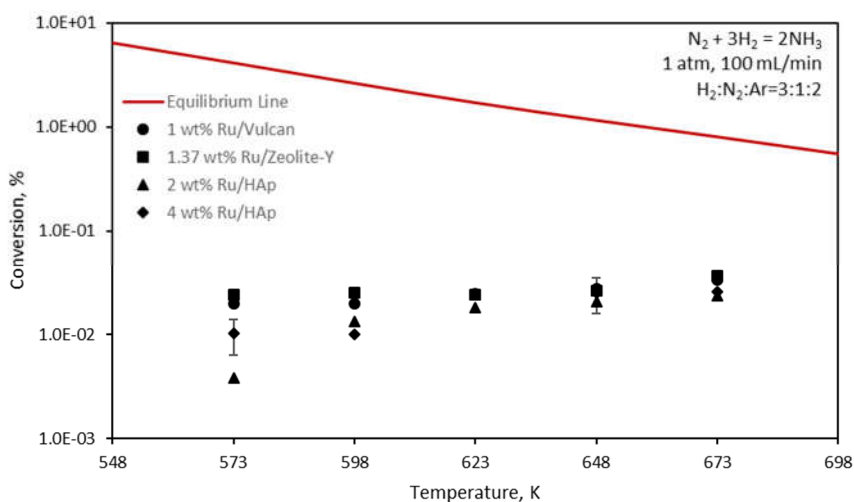


Figure 5.3. Conversion vs. temperature graph of ammonia synthesis reaction over supported Ru catalysts

The apparent activation energies calculated using Arrhenius plot over supported Ru catalysts are also reported in Table 5.5. Apparent activation energies over Ru/Zeolite-Y and Ru/Vulcan catalysts indicated possibility of mass transfer (diffusion) limitations despite the significant precautions taken to overcome these barriers during the experiments. This situation could be the result of the high porosity of Zeolite-Y and Vulcan supports.

#### 5.2.4 Degree of Ammonia Retention

The total amount of ammonia obtained in the reactor exit during one hour excursion of the reaction is presented in Table 5.6. In the same table, post-reaction desorbed ammonia is also reported. The highest and lowest amount of ammonia productions are observed over 1.37 wt% Ru/Zeolite-Y and Ru/HAp catalysts, respectively. The produced and desorbed amounts of ammonia over the catalysts are compared. While the produced and desorbed amounts of ammonia have nearly equal values in the presence of Ru/HAp catalysts, the produced amount of ammonia is higher than desorbed amount of ammonia in the presence of Ru/Zeolite-Y and Ru/Vulcan. These results indicate that significant amount of ammonia accumulation on the surface of the

catalysts are determined, especially over Ru/HAp catalysts, which hint towards an inhibition by ammonia over the catalysts.

Table 5.6. Total amount of NH<sub>3</sub> production during one hour of the synthesis and desorbed amounts after the reaction over supported Ru catalysts.

Temperature, °C	Total amount of NH <sub>3</sub> , μmol NH <sub>3</sub> /g <sub>catalyst</sub>							
	Ru/HAp (2.0% wt. Ru)		Ru/HAp (4.0% wt. Ru)		Ru/Zeolite-Y (1.37% wt. Ru)		Ru/Vulcan (1.0 wt. Ru)	
	produced	desorbed	produced	desorbed	produced	desorbed	produced	desorbed
300	60.0	125	83.0	35	387.0	150	156.0	145
325	115.0	117	75.0	65	265.0	155	118.0	95
350	100.0	108	130.0	155	141.0	100	73.0	80
375	123.0	67	80.0	120	263.0	115	107.0	75
400	96.0	75	160.0	90	212.0	100	200.0	100

The data presented in Table 5.6 are also reported as parity plots in Figure 5.4. A linear correlation can be found between the amount of desorbed ammonia and total amount of ammonia synthesized within 1 h over Ru/HAp catalysts (Figure 5.4.a) at various temperatures. On the other hand, while the total amount of ammonia synthesized increases with increasing temperature, the amount of desorbed ammonia remains constant over Ru/Zeolite-Y and Ru/Vulcan catalysts (Figure 5.4.b). As a result, parity plots reveal a higher degree of inhibition by ammonia over Ru/HAp catalysts compared to Ru/Zeolite-Y and Ru/Vulcan.

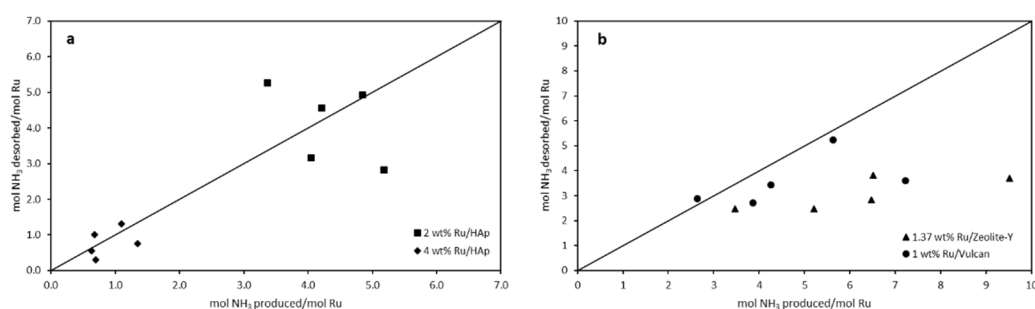


Figure 5.4. Comparison of desorbed amount of ammonia and total amount of synthesized ammonia during reaction tests a) 2 wt% HAp and 4 wt% HAp; b) 1.37 wt% Ru/Zeolite-Y and 1 wt% Ru/Vulcan (Reaction tests were carried out app. for 1 hr.)

### 5.2.5 N<sub>2</sub> Pulse Experiments

The removal of the ammonia accumulated on the surface of the catalysts and/or decreasing the partial pressure of hydrogen in the reaction environment can enhance the ammonia formation rates according to previously reported studies on the unsteady state reactor operation of ammonia synthesis in the literature [74], [232], [233]. In addition, Rambeau *et al.* published a series of papers for unsteady state ammonia synthesis at high temperature and pressures using ruthenium and osmium powders [33], [34]. Their ammonia synthesis rates were with cycles of hydrogenation of preadsorbed nitrogen over ruthenium up to three orders of magnitude larger than the corresponding steady state values. Similarly, Uner and Aslan [195] estimated up to two orders of magnitude higher rates under incremental hydrogen feed flow conditions. Improvement on the ammonia formation rates under pulse/cyclic flow of reactants either in pure or mixture form was also demonstrated by several researchers over various catalysts [75], [234]–[238]. In this framework, use of N<sub>2</sub> pulses can decrease/eliminate the inhibition by ammonia and hydrogen over supported Ru catalysts. In this section, the results of the experiments that performed using unsteady state (pulse) flow strategy intended to remove inhibition by ammonia will be presented.

Ammonia synthesis activity measured under the flow of H<sub>2</sub>:N<sub>2</sub> (3:1) is shown in Figure 5.5. Also in the same figure, N<sub>2</sub> pulses cycled with a time-period of 10 min and steady state H<sub>2</sub>:N<sub>2</sub> (3:1) flow conditions were compared. Ammonia synthesis activity under steady state flow conditions decreased until no activity was observed after about 2 h. However, the production of ammonia under unsteady state flow conditions did not exhibit such inhibitions. After each nitrogen pulse, a constant ammonia production was measured under H<sub>2</sub>:N<sub>2</sub>=3:1 flow.

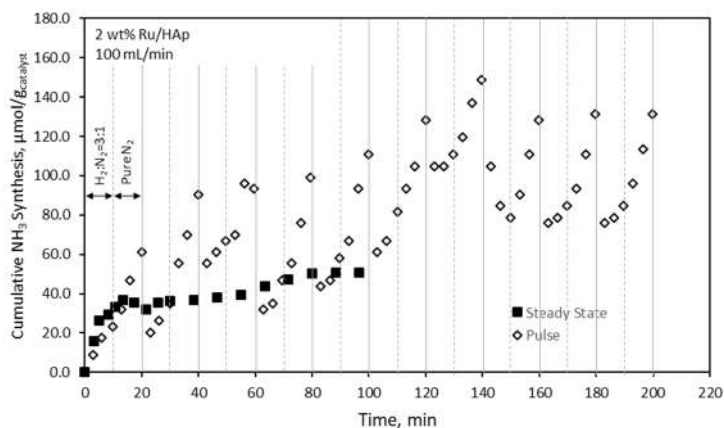


Figure 5.5. Cumulative ammonia synthesis with time under pulse flow ( $H_2:N_2=3:1$  – 10 min &  $N_2$  – 10 min, 100 mL/min) and steady state flow ( $H_2:N_2=3:1$ , 100 mL/min) conditions over 2.0 wt% Ru/HAp at 400 °C. The dashed-vertical lines correspond to end of  $H_2:N_2=3:1$  flow, the straight-vertical lines correspond to end of pure  $N_2$  flow under pulse flow

Whether the activity loss under steady state flow was due to surface modifications of the support was investigated using IR spectra of fresh and used Ru/HAp catalysts. Particular attention was paid if there was any change in the concentration of the phosphate ions located on the HAp surface. The IR spectra of fresh and used Ru/HAp catalysts shown in Figure 5.6 indicated no significant change in the concentration of phosphate ions ( $1200 - 900\text{ cm}^{-1}$  and  $700 - 400\text{ cm}^{-1}$ ).

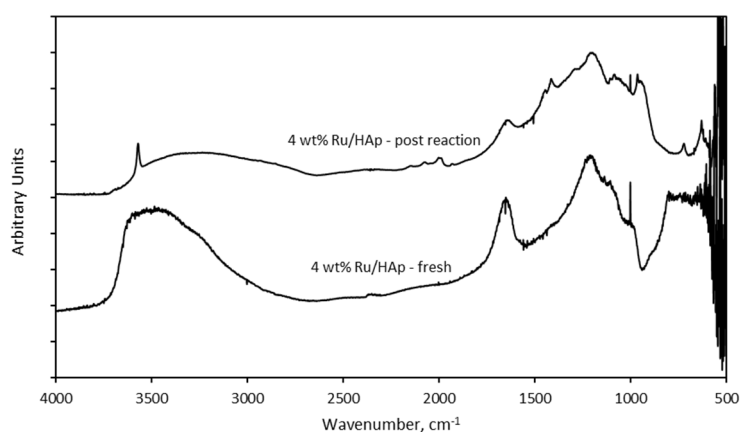


Figure 5.6. IR spectra of fresh and consumed 4 wt% Ru/HAp catalysts

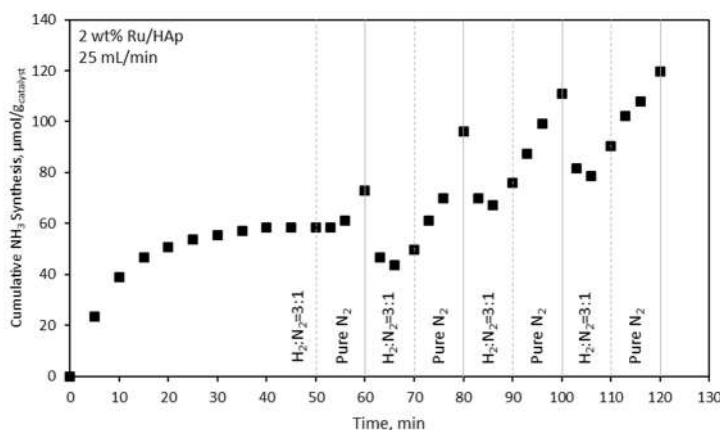


Figure 5.7. Ammonia synthesis reaction over 2.0 wt% Ru/HAp operated under firstly at steady state flow conditions, followed by pulse flow conditions at 400 °C and atmospheric pressure.

In Figure 5.7, ammonia synthesis reaction over 2.0 wt% Ru/HAp was carried out initially at steady flow conditions under 25 mL/min reactant flow ( $H_2:N_2=3:1$ ) at 400 °C and atmospheric pressure. No activity was observed after 50 min under steady state flow condition. At that moment,  $N_2$  pulse was given for 10 min, followed by a pulse of  $H_2:N_2=3:1$  flow. The recovery of ammonia synthesis after the nitrogen pulse was observed (Figure 5.7).

Moreover, ammonia adsorbs very strongly over HAp support surface revealed by the single point ammonia adsorption experiment reported in the previous sections. On the other hand, ammonia synthesis activity over the same catalyst could proceed under flow of  $H_2:N_2$  and  $N_2$  pulses for 3 hours (Figure 5.5). The deactivated ammonia synthesis catalyst could be re-activated with switching from steady state flow to pulse flow (Figure 5.7). These results indicate that the type (acidity) of the support has an important role on the activity of supported Ru catalysts due to the ammonia coverage on the surface of the catalyst. In the same direction, Cussler and his coworkers applied a strategy to remove the synthesized ammonia from the reaction environment by absorbing the ammonia in an absorbent to shift the ammonia synthesis reaction to forward direction (product side) [77], [239]–[241]. In this study, a similar strategy,

removal of the synthesized ammonia from the reaction environment, is applied to decrease the ammonia coverage over supported Ru catalysts by feeding pure N<sub>2</sub> pulses to the reactor. As a result, pulse flow strategy to enhance the ammonia synthesis rates can be applied due to decreasing the poisoning effects of hydrogen and ammonia.

### **5.3 Chapter Summary**

Ammonia synthesis reaction was carried out at high temperature and atmospheric pressure conditions over Zeolite-Y, HAp, and Vulcan supported Ru catalysts. The differential and single point ammonia adsorption experiments showed that HAp support material has monolayer ammonia coverage with a relatively high-energy release while Zeolite-Y and Vulcan supports had lower ammonia coverage with low amount of energy release. Total amount of synthesized ammonia and amount of desorbed ammonia after obtained ammonia synthesis experiments showed that the degree of inhibition by ammonia is higher over Ru/HAp catalysts compared to Ru/Zeolite-Y and Ru/Vulcan due to acidic nature of HAp surface. Forced unsteady state conditions imposed on the reactor by giving periodic N<sub>2</sub> pulses could sweep ammonia adsorbed on the surface and decrease the surface coverage of ammonia, increasing productivity by suppressing ammonia inhibition.



## CHAPTER 6

### NH<sub>3</sub> SYNTHESIS over Co<sub>3</sub>Mo<sub>3</sub>N UNDER TIME INTERRUPTED CONDITIONS<sup>4</sup>

#### 6.1 Introduction

Ammonia production is one of the most energy intensive chemical processes and it consumes approximately 2% of the world energy production [112], [214]. One of the main operating costs that influence the price of ammonia is the cost of hydrogen. According to the analysis of U.S. Department of Energy (DOE) in one of their reports, the percent cost of H<sub>2</sub> per ton of produced NH<sub>3</sub> is about 70% [242]. Moreover, according to the estimation of International Energy Agency, 70% of CO<sub>2</sub> emissions is sourced from the common production method of hydrogen, steam methane reforming, is the raw material of ammonia manufacturing [243].

So far in this thesis, it is established that catalytic ammonia synthesis reaction is poisoned by hydrogen [32], [51], [65]. Zeinalipour et al. carried out a study on the mechanism of ammonia synthesis reaction over Co<sub>3</sub>Mo<sub>3</sub>N catalyst using DFT[244] and showed that Eley-Riedal/Mars van Krevelen mechanism is energetically favorable compared to Langmuir-Hinshelwood mechanism which both of the mechanisms include the hydrogen adsorption step. In contrary to this fact, Kojima and Aika reported an ammonia synthesis rate expression over Co<sub>3</sub>Mo<sub>3</sub>N catalyst at 673 K and 31 bar operation conditions based on power law kinetics that the order of hydrogen was 0.8 [87]. Therefore, the effect of partial pressure of hydrogen on the ammonia formation rate over Co<sub>3</sub>Mo<sub>3</sub>N catalysts is in a conflicting situation. In this circumstance, a question can be asked as to whether limiting the use of hydrogen (in terms of sending

---

<sup>4</sup> This chapter is prepared for publication in Faraday Discussions with the co-authors “M.Y.Aslan, J.S. Justin Hargreaves, and D. Uner”. Abstract is submitted to “Reaction Mechanism in Catalysis: Faraday Discussions” which will be held on 22-24<sup>th</sup>, April 2020

to the reactor) can improve the bottlenecks of ammonia synthesis using an unsteady state reactor operation strategy over  $\text{Co}_3\text{Mo}_3\text{N}$  catalysts.

Unsteady state reactor operation was suggested in the literature for ammonia synthesis over various types of catalysts in order to improve the efficiency of the reaction [33], [234], [235], [238]. Some rate improvements were achieved in all of the studies at different cyclic operation conditions based on the type of the catalyst. Furthermore, Cussler and coworkers studied the absorption of synthesized ammonia on an absorbent. Their studies showed that supported absorbents (e.g.  $\text{MgCl}_2$  supported on zeolite-Y) can be used in a packed column instead of using a high pressure condenser in order to separate ammonia at high temperature and low pressure process conditions [77], [78], [245]–[247].

$\text{Co}_3\text{Mo}_3\text{N}$  catalysts are promising for application as a nitrogen transfer agents. It was known from the earlier studies that molybdenum nitrides possess activity for ammonia synthesis [248], [249]. Volpe and Boudart showed that high surface area  $\text{Mo}_2\text{N}$  materials can be synthesized using temperature programmed reaction of  $\text{MoO}_3$  and  $\text{NH}_3$ , which is named ammonolysis, between 25 °C to 710 °C [84]. They emphasized that a low value of temperature ramp should be selected such as 0.01 °C/second during the ammonolysis reaction to obtain high surface area  $\text{Mo}_2\text{N}$ . Kojima and Aika [87] used  $\text{Co}_3\text{Mo}_3\text{N}$  for ammonia synthesis and observed significant  $\text{NH}_3$  synthesis rates at 300–400 °C and atmospheric pressure. Kojima and Aika also reported the apparent activation energy of ammonia synthesis over  $\text{Co}_3\text{Mo}_3\text{N}$  as 56 kJ/mol between 315 and 400 °C and 31 bar [87]. Hargreaves and coworkers showed while ammonia synthesis reaction under flow of  $\text{H}_2:\text{N}_2$  can be carried out for longer times, in the presence of  $\text{Ar}:\text{H}_2$  flow initially ammonia production was observed then the productivity of the catalyst disappeared due to phase change from  $\text{Co}_3\text{Mo}_3\text{N}$  to  $\text{Co}_6\text{Mo}_6\text{N}$  [89], [90], [250]. They also reported the regeneration of  $\text{Co}_6\text{Mo}_6\text{N}$  to  $\text{Co}_3\text{Mo}_3\text{N}$  [91]. Recently, Zeinalipour-Yazdi et al. worked on the mechanism of ammonia synthesis over  $\text{Co}_3\text{Mo}_3\text{N}$  using DFT calculations [244], [251], [252]. The results of DFT calculations showed that the ammonia synthesis reaction should proceed over  $\text{Co}_3\text{Mo}_3\text{N}$  obeying

Mars-van Krevelen mechanism due to that it has the lowest energy required reaction pathway [244].

The studies in the literature showed that ammonia synthesis reaction can be carried out at lower  $H_2:N_2$  ratios ( $H_2:N_2 < 3.0$ ) due to that hydrogen adsorption to catalytic surface is not a rate determining step. In this study, the possibility of operating the ammonia synthesis reaction over  $Co_3Mo_3N$  at lower  $H_2:N_2$  ratios is investigated in terms from the perspective of economics of the ammonia production process. In this scope, hydrogen adsorption characteristic over  $Co_3Mo_3N$  surface is determined at different temperatures. Steady state ammonia synthesis experiments were performed at different  $H_2:N_2$  ratios in the light of  $H_2$  adsorption experiments. Forced unsteady state ammonia synthesis experiments were performed to verify that higher ammonia synthesis rates can be obtained in the presence of intermittent hydrogen pulses in the light of steady flow experiments.

## **6.2 Results and Discussion**

### **6.2.1 Characterization**

#### **6.2.1.1 XRD and Elemental Analysis**

The XRD pattern of  $Co_3Mo_3N$  material is given in Figure 6.1. The main peak that determine the formation of Co-Mo-N structure is obtained at  $42.4^\circ$ . The other peaks observed in the XRD pattern are labeled with their corresponding planes as given in JCPDS-ICDD standard ( $Co_3Mo_3N$ : 89-7953) which are in agreement with the literature [85], [89].

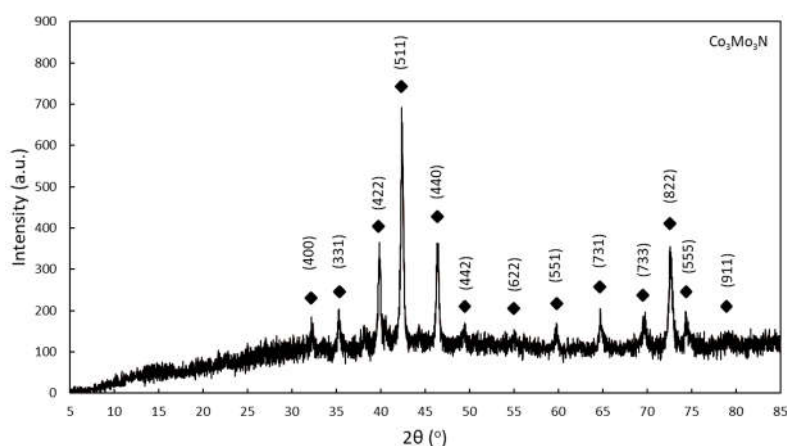


Figure 6.1. XRD Pattern of  $\text{Co}_3\text{Mo}_3\text{N}$  (the peaks marked with a diamond belong to  $\text{Co}_3\text{Mo}_3\text{N}$ )

Elemental analysis of  $\text{Co}_3\text{Mo}_3\text{N}$  given in Table 6.1 showed that the theoretical and experimentally measured amount of nitrogen is in reasonable agreement. When the data given in Figure 6.1 and Table 6.1 were evaluated together, it can be said that  $\text{Co}_3\text{Mo}_3\text{N}$  was successfully synthesized.

Table 6.1. Elemental analysis results (nitrogen content) of  $\text{Co}_3\text{Mo}_3\text{N}$

Material	MW, g/mol	Theoretical,	Experiment 1,	Experiment 2,
		%	%	%
		N	N	N
$\text{Co}_3\text{Mo}_3\text{N}$	478.52	2.93	2.70	2.70

### 6.2.1.2 Temperature Programmed Reduction

$\text{H}_2$ -TPR profile of  $\text{Co}_3\text{Mo}_3\text{N}$  catalyst is given in Figure 6.2 under flow of  $\text{H}_2$  in Ar (10 %  $\text{H}_2$  in Ar) at a rate of 25 mL/min with a temperature ramp of 10 °C/min. It is observed two peaks at 475 °C and 495 °C, respectively. The hydrogen consumption is calculated as  $3.0 \times 10^{-3} \text{ mol H}_2 \text{ g}_{\text{catalyst}}^{-1}$  using the calibration experiment of reduction of  $\text{Ag}_2\text{O}$  to Ag (the calculation details is given in Appendix G).

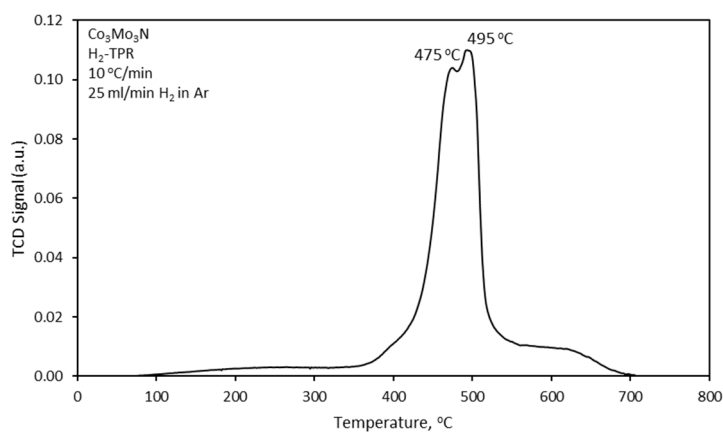


Figure 6.2. H<sub>2</sub>-TPR pattern of Co<sub>3</sub>Mo<sub>3</sub>N

It is known that the surface of Co<sub>3</sub>Mo<sub>3</sub>N catalyst is passivated with oxygen as a part of the preparation procedure. The possible oxide structures on the oxidized surface can be said as CoO, MoO<sub>3</sub>, and CoMoO<sub>4</sub>. In this framework, the consumed amount of hydrogen can be compared with the amount of oxygen sites on the surface of the oxides to determine which type of oxide can be dominant on Co<sub>3</sub>Mo<sub>3</sub>N surface before reduction. In Table 6.2, the required amount of hydrogen for reduction of each possible oxide type given. It is noted that BET surface area of passivated Co<sub>3</sub>Mo<sub>3</sub>N catalyst is measured as 9 m<sup>2</sup> g<sup>-1</sup>. The values in Table 6.2 is lower compared to amount of H<sub>2</sub> consumption during H<sub>2</sub>-TPR experiment. Therefore, the peaks can be attributed to both the reduction of surface oxide species and atomic nitrogen species on the structure of Co<sub>3</sub>Mo<sub>3</sub>N.

Table 6.2. Comparison of required amount of H<sub>2</sub> to reduce the possible oxides on passivated Co<sub>3</sub>Mo<sub>3</sub>N surface

Oxide type	Crystal Structure	<sup>a</sup> Amount of oxygen sites, O sites/cm <sup>2</sup>	Required amount of H <sub>2</sub> , mol H <sub>2</sub> /g <sub>catalyst</sub>
CoO	Simple cubic	0.55x10 <sup>15</sup>	8.2x10 <sup>-5</sup>
MoO <sub>3</sub>	Orthorhombic	1.70x10 <sup>15</sup> (Plane 1)	2.5x10 <sup>-5</sup>
		0.58x10 <sup>15</sup> (Plane 2)	8.7x10 <sup>-5</sup>
CoMoO <sub>4</sub>	Orthorhombic	0.54x10 <sup>15</sup> (Plane 1)	8.1x10 <sup>-5</sup>
		0.48x10 <sup>15</sup> (Plane 2)	7.2x10 <sup>-5</sup>

<sup>a</sup> The amount of oxygen sites per cm<sup>2</sup> is calculated using the crystal structures of the oxides

### 6.2.1.3 H<sub>2</sub> Adsorption Isotherm

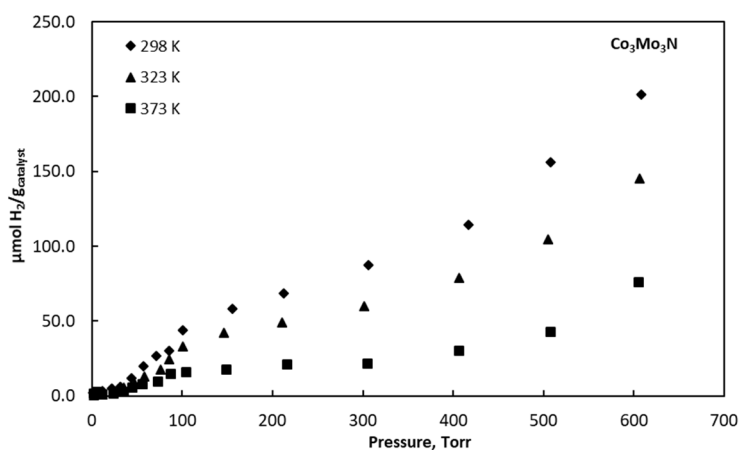


Figure 6.3. H<sub>2</sub> adsorption isotherms of Co<sub>3</sub>Mo<sub>3</sub>N at 25 °C, 50 °C, and 100 °C

H<sub>2</sub> adsorption isotherms of Co<sub>3</sub>Mo<sub>3</sub>N catalyst at 25 °C, 50 °C and 100 °C given in Figure 6.3 show that the amount of H<sub>2</sub> adsorption with temperature decreases. In addition, a plateau is observed after 100 Torr H<sub>2</sub> pressure especially at 373 K. This plateau is interpreted as the saturation of the catalyst surface with strongly bound hydrogen.

## 6.2.2 Kinetic Studies

### 6.2.2.1 NH<sub>3</sub> Synthesis Experiments under Steady State Flow

Ammonia formation rates experiments measured between 400 – 475 °C and atmospheric pressure are given in Table 6.3. The apparent activation energy calculated from the kinetic data is also given in Table 6.3. The reported ammonia synthesis rate over Co<sub>3</sub>Mo<sub>3</sub>N in the literature was 167 μmol/g<sub>cat</sub>-h at 400 °C[89]. The low ammonia synthesis rate at 400 °C reported in Table 6.3. can be justified with the experimental operating conditions such as space velocity.

Table 6.3. Measured ammonia formation rates and calculated apparent activation energy over Co<sub>3</sub>Mo<sub>3</sub>N catalyst

Temperature, °C	Ammonia Formation Rate, μmol/g <sub>cat</sub> -h	Apparent Activation Energy, kJ/mol
400	115	89.9
425	182	
450	330	
475	571	

### 6.2.2.2 NH<sub>3</sub> Synthesis Experiments at Different H<sub>2</sub>:N<sub>2</sub> Ratio

Ammonia synthesis rate measurements performed with different H<sub>2</sub>:N<sub>2</sub> ratios under constant flow of 100 mL/min at 400 °C and atmospheric pressure are reported in Figure 7.4. No significant change was observed with the change of H<sub>2</sub>:N<sub>2</sub> ratio on the ammonia synthesis rate when H<sub>2</sub>:N<sub>2</sub> ratio is greater than 0.5. The corresponding partial hydrogen pressures between H<sub>2</sub>:N<sub>2</sub>=3.0 and H<sub>2</sub>:N<sub>2</sub>=0.5 are 570 and 253 Torr, respectively. On the other hand, ammonia synthesis rate decreases with decreasing H<sub>2</sub>:N<sub>2</sub> ratio, when H<sub>2</sub>:N<sub>2</sub> ratio is lower than 0.5. When the decrease in the ammonia formation rate at lower H<sub>2</sub>:N<sub>2</sub> ratios (H<sub>2</sub>:N<sub>2</sub> <0.5) and the hydrogen adsorption behavior over Co<sub>3</sub>Mo<sub>3</sub>N at lower hydrogen pressures (P<sub>H<sub>2</sub></sub> < 100 Torr) are evaluated together (Figure 6.4), it is observed a direct relationship between the amount of adsorbed hydrogen on Co<sub>3</sub>Mo<sub>3</sub>N surface and ammonia formation rate. Therefore, it

can be said that the strongly bound hydrogen is the reactive form over  $\text{Co}_3\text{Mo}_3\text{N}$  catalyst for ammonia synthesis reaction.

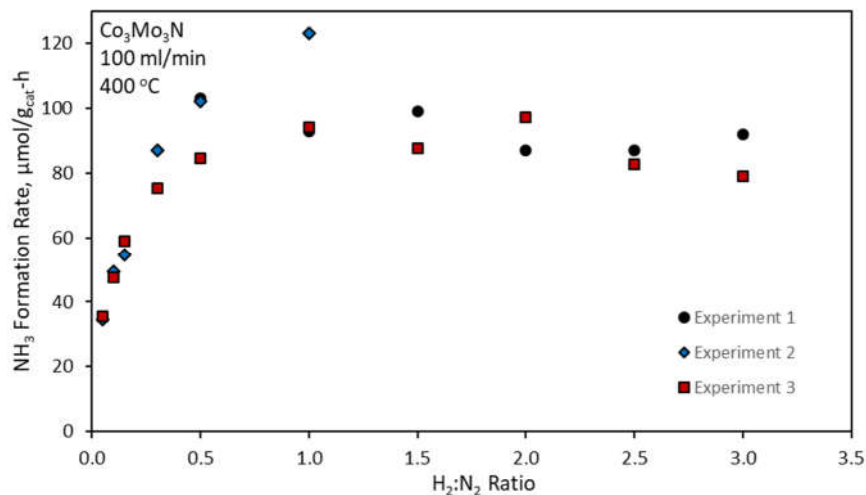


Figure 6.4. Effect of  $\text{H}_2:\text{N}_2$  ratio on the ammonia formation rate over  $\text{Co}_3\text{Mo}_3\text{N}$  catalyst at  $400\text{ }^\circ\text{C}$

After it was observed that ammonia synthesis rate over  $\text{Co}_3\text{Mo}_3\text{N}$  catalyst was not a function of  $\text{H}_2:\text{N}_2$  ratio when  $\text{H}_2:\text{N}_2$  ratio is 0.5 or above, it was decided to carry out ammonia synthesis reaction under pulse flow with different  $\text{H}_2:\text{N}_2$  ratios while pure  $\text{N}_2$  flow remained constant as shown in Figure 6.5. In the first experiment, 100 mL/min of  $\text{H}_2:\text{N}_2=3:1$  and pure  $\text{N}_2$  pulses were sent to the reactor with a time period of 10 min. In the second experiment, the same procedure was applied with  $\text{H}_2:\text{N}_2=0.5:1$ . It was observed that cumulative ammonia synthesis was slightly higher in the presence of  $\text{H}_2:\text{N}_2=3:1$  &  $\text{N}_2$  pulse flow with respect to  $\text{H}_2:\text{N}_2=0.5:1$  &  $\text{N}_2$  pulse flow. The results of  $\text{H}_2$  adsorption isotherms and ammonia synthesis experiments under steady and unsteady flow conditions indicated that when  $\text{H}_2:\text{N}_2$  ratio is above 0.5:1, the strongly bound hydrogen coverage over  $\text{Co}_3\text{Mo}_3\text{N}$  surface did not change significantly. Therefore varying the  $\text{H}_2:\text{N}_2$  ratio between 0.5:1 and 3:1 did not influence the ammonia synthesis rate under different operating conditions due to presence of required amount of hydrogen on the catalyst surface.

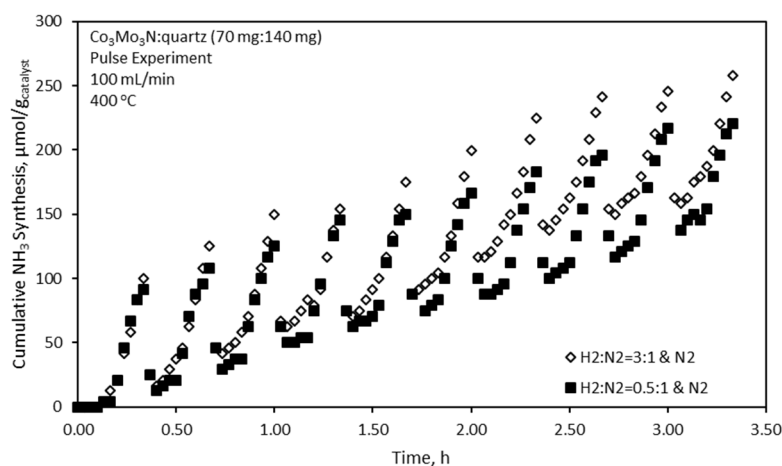


Figure 6.5. Cumulative ammonia synthesis with time under pulse flow of  $\text{H}_2:\text{N}_2=3:1$  &  $\text{N}_2$  and  $\text{H}_2:\text{N}_2=0.5:1$  &  $\text{N}_2$  under 100 mL/min at 400 °C. The valve switching time was 10 min.

### 6.2.2.3 Pulse Flow Experiments

Prior to pulse flow experiments, ammonia synthesis reaction experiment was performed in a manner that initially steady state  $\text{H}_2:\text{N}_2=3:1$  flow was fed to the reactor as shown in Figure 6.6. After steady state ammonia synthesis was observed, the flow was switched from  $\text{H}_2:\text{N}_2=3:1$  to pure  $\text{N}_2$  at constant gas flow of 100 mL/min. Under pure  $\text{N}_2$  flow, an increase was initially observed and then cumulative amount of synthesized ammonia remained constant. The increase in the synthesized amount of ammonia for a limited time can be explained by the desorption of ammonia from  $\text{Co}_3\text{Mo}_3\text{N}$  surface. After the sweeping of ammonia from the catalyst surface again flow was switch from pure  $\text{N}_2$  to  $\text{H}_2:\text{N}_2=3:1$ . This cycle was repeated for two times. The results represented in Figure 6.6 revealed that amount of synthesized ammonia can be increased under  $\text{N}_2$  pulses.

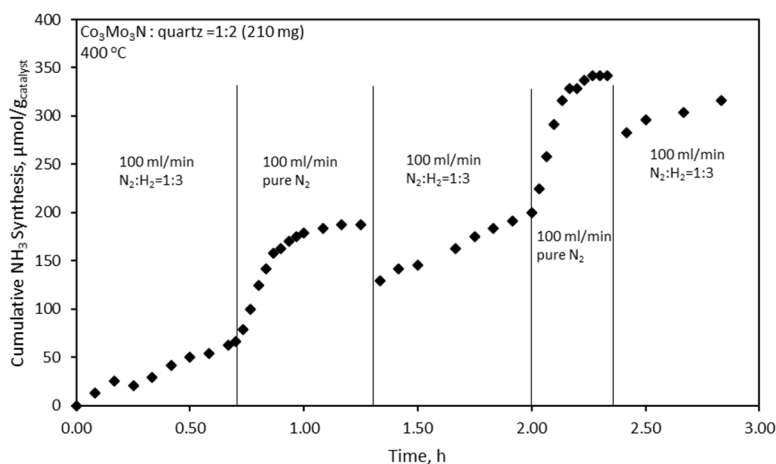


Figure 6.6. Cumulative NH<sub>3</sub> synthesis under 100 mL/min H<sub>2</sub>:N<sub>2</sub>=3:1 and pure N<sub>2</sub> flows over Co<sub>3</sub>Mo<sub>3</sub>N at 400 °C and atmospheric pressure

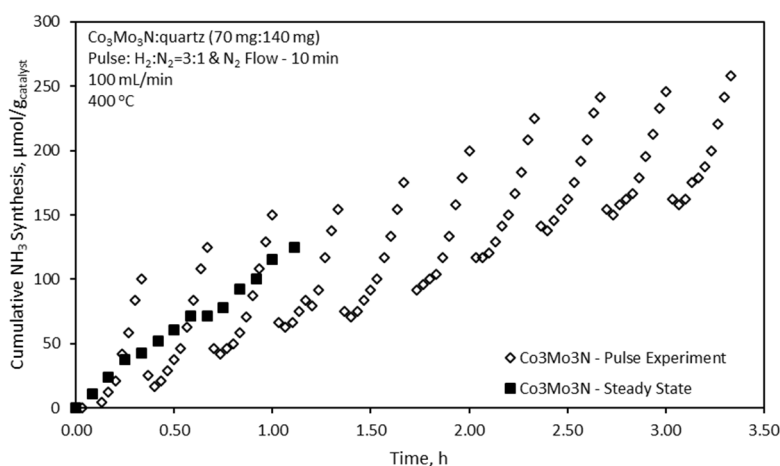


Figure 6.7. Cumulative ammonia synthesis with time under pulse flow (H<sub>2</sub>:N<sub>2</sub>=3:1 – 10 min & N<sub>2</sub> – 10 min, 100 mL/min) and steady state flow (H<sub>2</sub>:N<sub>2</sub>=3:1, 100 mL/min) conditions over Co<sub>3</sub>Mo<sub>3</sub>N at 400 °C.

Unsteady state ammonia synthesis experiments under 100 mL/min pulsed flow of H<sub>2</sub>:N<sub>2</sub>=3:1 for 10 min and followed by pure N<sub>2</sub> flow for 10 min are shown in Figure 6.7. The results of ammonia synthesis experiment under steady flow (H<sub>2</sub>:N<sub>2</sub>=3:1) was also given in Figure 6.7 for comparison. It was observed similar ammonia synthesis rates under steady flow and pulse flow. It should be noted that in case of steady flow

continuously  $H_2:N_2=3:1$  was sent to the reactor while  $H_2:N_2=3:1$  flow was fed to the reaction interruptedly in pulse flow. It means that although half of the reactant was sent to the reactor in pulse flow compared to the steady flow, similar yields were obtained.

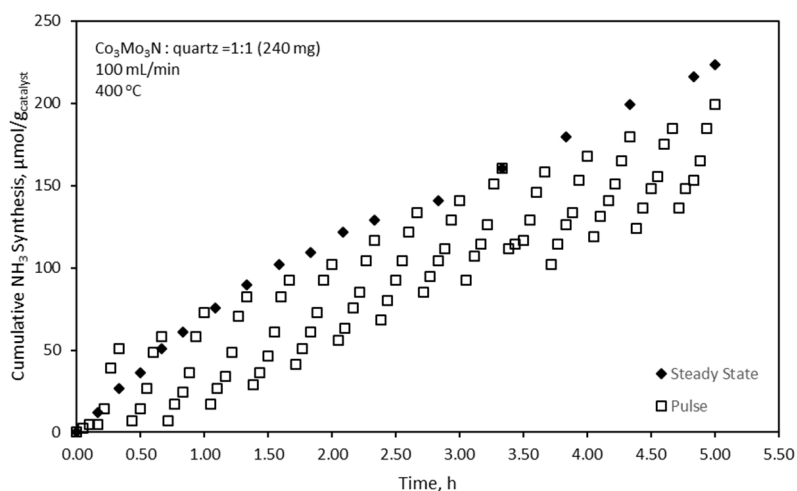


Figure 6.8. Cumulative ammonia synthesis for long period of times under pulse flow ( $H_2:N_2=3:1$  – 10 min &  $N_2$  – 10 min, 100 mL/min) and steady state flow ( $H_2:N_2=3:1$ , 100 mL/min) conditions over  $Co_3Mo_3N$  at 400 °C.

The ammonia synthesis rates were observed for steady and pulse flow conditions for longer time reaction operation (5 h). In Figure 6.8, the cumulative amount of ammonia synthesized under steady and pulse flow were given. No significant change in ammonia synthesis rates was observed. After the reaction operation experiments, 100 ml/min Ar flow was fed to the reactor in order to sweep the adsorbed ammonia on the catalyst surface. The total amount of synthesized ammonia and desorbed amount of ammonia under Ar flow are given in Table 6.4. A significant amount of ammonia was desorbed after  $H_2:N_2=3:1$  steady flow operation compared to desorbed amount of ammonia after pulse flow of  $H_2:N_2=3:1$  and pure  $N_2$  flow conditions. When the desorbed amount of ammonia after previously performed for small time periods (1-2

h) was taken into account, similar amounts of ammonia were measured. Therefore, it can be said that the amount of ammonia accumulated on the  $\text{Co}_3\text{Mo}_3\text{N}$  surface under steady flow conditions did not change with reaction time.

Table 6.4. Summary of amount of formed and desorbed  $\text{NH}_3$  during/after reactor operation

	Steady State Operation	Pulse Operation
Cumulative Amount of $\text{NH}_3$ Formation, $\mu\text{mol}/\text{g}_{\text{cat}}$	223.5	199.2
Amount of Desorbed $\text{NH}_3$ , $\mu\text{mol}/\text{g}_{\text{cat}}$	108.3	20.8
Total, $\mu\text{mol}/\text{g}_{\text{cat}}$	331.8	220

### 6.3 Chapter Summary

$\text{H}_2$  adsorption isotherms over  $\text{Co}_3\text{Mo}_3\text{N}$  catalyst were obtained at 25 °C, 50 °C, and 100 °C.  $\text{H}_2$  adsorption isotherms revealed that  $\text{Co}_3\text{Mo}_3\text{N}$  surface saturated with strongly bound hydrogen at 100 Torr pressure. Ammonia synthesis was carried out over a  $\text{Co}_3\text{Mo}_3\text{N}$  catalyst under steady and pulse flow conditions at atmospheric pressure and high temperatures (400 °C and above) and the apparent activation energy was calculated as 89.9 kJ/mol. It was observed that there is no effect of  $\text{H}_2:\text{N}_2$  ratio on the ammonia synthesis reaction under steady flow conditions between the  $\text{H}_2:\text{N}_2$  ratio of 3.0 and 0.5. At lower  $\text{H}_2:\text{N}_2$  ratios than 0.5, ammonia synthesis rate decreased with decreasing  $\text{H}_2:\text{N}_2$  ratio. Pulse flow experiments were also conducted but no improvement was observed on ammonia synthesis rate with respect to steady flow experiments. As a result, ammonia synthesis reaction can be operated over  $\text{Co}_3\text{Mo}_3\text{N}$  catalyst with  $\text{H}_2:\text{N}_2$  ratio of 0.5 instead of 3.0, which can improve the efficiency of process in terms of hydrogen consumption.

## CHAPTER 7

### CONCLUSIONS

The objective of this thesis study was to suggest a solution to improve the sustainability of the ammonia synthesis reaction based on time interrupted flow conditions at lower temperature and pressure with respect to operation conditions of Haber-Bosch process. In this framework:

The hydrogen adsorption and spillover characteristics over supported Ru catalysts (Support: Vulcan and SiO<sub>2</sub>) was investigated with different Ru metal loadings. It was demonstrated that Ru metal dispersion decreased with increasing Ru metal loading. It was observed that hydrogen migration from metal surface to support surface is a slow process and desorption of spilled over hydrogen from the catalyst surface required high temperatures.

The inhibition effect of ammonia over supported Ru catalysts was studied over support materials with different surface acidic characteristics. The steady flow experiment over supported Ru catalysts (Support: HAp, zeolite-Y, Vulcan) showed explicitly the poisoning effect of ammonia. The poisoning effect of ammonia over supported Ru catalyst was eliminated by using a N<sub>2</sub> pulse strategy. In this way, the adsorbed ammonia over the support surface was swept and the deactivated catalyst was revived.

Ammonia synthesis experiments were carried out under steady flow conditions over Co<sub>3</sub>Mo<sub>3</sub>N under atmospheric pressures. It was demonstrated that similar ammonia synthesis rates can be achieved with a H<sub>2</sub>:N<sub>2</sub> ratio of 0.5 instead of 3.0 under steady flow conditions. The forced unsteady state (pulse) flow strategy was also applied ammonia synthesis reaction over Co<sub>3</sub>Mo<sub>3</sub>N catalysts to investigate if higher ammonia formation rates could be measured with the use of lower amount of hydrogen, but no improvement was obtained. As a result, it can be concluded that use of lower amount

of hydrogen compared to stoichiometric amount can be beneficial in terms of process economy.

To sum up, the inhibitory effects of hydrogen and ammonia was tried to be diminished over ammonia synthesis catalysts under specific applications of time interrupted flow conditions. The findings obtained in this study indicated that unsteady state reactor operation can be a good way to find solutions to get rid of inhibitory effects that influence the reactions such as ammonia synthesis.

## CHAPTER 8

### RECOMMENDATIONS

In the scope of this thesis study, ammonia synthesis reaction experiments were carried out under atmospheric pressure conditions. It is known that industrial ammonia synthesis is carried out at elevated pressures such as 100 – 300 bar. The positive effect of pulse flow strategy on support Ru catalysts under high pressure conditions can be investigated whether similar results were obtained.

Ammonia synthesis reaction experiments in this thesis study was carried out at low conversions (< 1%). Similar to the investigation of the high pressure effect, the operation of ammonia synthesis at higher conversions condition would be beneficial of implementation of pulse flow strategy at pilot/industrial conditions.

Ammonia synthesis experiments that will be operated at high pressures and conversions will reveal if pulse strategy is meaningful. If the results of the experiments is promising then a pilot scale ammonia synthesis can be constructed to investigate heat and mass transfer effects.

It was shown that while pulse flow strategy is found as an effective method to improve ammonia synthesis rates over supported Ru catalysts, it is not found as an effective method over  $\text{Co}_3\text{Mo}_3\text{N}$  catalyst. Operating ammonia synthesis reaction over a supported  $\text{Co}_3\text{Mo}_3\text{N}$  catalyst may improve the rates.



## REFERENCES

- [1] R. Schlögl, “Catalytic synthesis of ammonia - A ‘never-ending story’?,” *Angew. Chemie - Int. Ed.*, vol. 42, no. 18, pp. 2004–2008, Apr. 2003.
- [2] J. W. Erisman, M. A. Sutton, J. Galloway, Z. Klimont, and W. Winiwarter, “How a century of ammonia synthesis changed the world,” *Nat. Geosci.*, vol. 1, pp. 636–639, Apr. 2008.
- [3] H. Ritchie, “How many people does synthetic fertilizer feed?,” *Our World in Data*, 25-Dec-2017. [Online]. Available: <https://ourworldindata.org/how-many-people-does-synthetic-fertilizer-feed>.
- [4] “Technology Roadmap: Energy and GHG Reductions in the Chemical Industry via Catalytic Processes,” 2018. [Online]. Available: [https://dechema.de/dechema\\_media/Downloads/Positionspapiere/IndustrialCatalysis/Chemical\\_Roadmap\\_2013\\_Final\\_WEB-called\\_by-dechema-original\\_page-136220-original\\_site-dechema\\_eV-view\\_image-1-p-4584.pdf](https://dechema.de/dechema_media/Downloads/Positionspapiere/IndustrialCatalysis/Chemical_Roadmap_2013_Final_WEB-called_by-dechema-original_page-136220-original_site-dechema_eV-view_image-1-p-4584.pdf). [Accessed: 07-Oct-2019].
- [5] J. Baltrusaitis, “Sustainable Ammonia Production,” *ACS Sustain. Chem. Eng.*, vol. 5, no. 11, p. 9527, Apr. 2017.
- [6] “Grand Challenges - 14 Grand Challenges for Engineering,” 2018. [Online]. Available: <http://www.engineeringchallenges.org/challenges.aspx>. [Accessed: 07-Oct-2019].
- [7] J. Paull, “A Century of Synthetic Fertilizer: 1909-2009,” *Elem. J. Bio-Dynamics Tasmania*, no. 94, pp. 16–21, Apr. 2009.
- [8] A. Max, “Ammonia, 2. Production Processes,” in *Ullmann’s Encyclopedia of Industrial Chemistry*, 2000, pp. 174–179.
- [9] C. Adams, “Applied Catalysis: A Predictive Socioeconomic History,” *Top. Catal.*, vol. 52, no. 8, pp. 924–934, Apr. 2009.
- [10] B. K. Burgess and D. J. Lowe, “Mechanism of Molybdenum Nitrogenase,” *Chem. Rev.*, vol. 96, no. 7, pp. 2983–3012, Apr. 2002.
- [11] A. Vojvodic *et al.*, “Exploring the limits: A low-pressure, low-temperature Haber-Bosch process,” *Chem. Phys. Lett.*, vol. 598, pp. 108–112, Apr. 2014.
- [12] A. R. Singh *et al.*, “Electrochemical Ammonia Synthesis—The Selectivity Challenge,” *ACS Catal.*, vol. 7, no. 1, pp. 706–709, Apr. 2017.
- [13] X. Sun, D. Jiang, L. Zhang, S. Sun, and W. Wang, “Enhanced Nitrogen Photofixation over LaFeO<sub>3</sub> via Acid Treatment,” *ACS Sustain. Chem. Eng.*, vol. 5, no. 11, pp. 9965–9971, Mar. 2017.

- [14] R. Michalsky, A. M. Avram, B. A. Peterson, P. H. Pfromm, and A. A. Peterson, "Chemical looping of metal nitride catalysts: low-pressure ammonia synthesis for energy storage," *Chem. Sci.*, vol. 6, no. 7, pp. 3965–3974, Apr. 2015.
- [15] B. Hinnemann and J. K. Nørskov, "Catalysis by Enzymes: The Biological Ammonia Synthesis," *Top. Catal.*, vol. 37, no. 1, pp. 55–70, Apr. 2006.
- [16] "DOE Targets for Onboard Hydrogen Storage Systems for Light-Duty Vehicles | Department of Energy," 2018. [Online]. Available: <https://www.energy.gov/eere/fuelcells/doe-technical-targets-onboard-hydrogen-storage-light-duty-vehicles>. [Accessed: 07-Oct-2019].
- [17] F. Mertens, G. Wolf, and F. Baitalow, "Ammonia Borane and Related Compounds as Hydrogen Source Materials," *Handb. Hydrog. Storage New Mater. Futur. Energy Storage*, pp. 215–247, Apr. 2010.
- [18] A. Max, "Ammonia, 2. Production Process," in *Ullmann's Encyclopedia of Industrial Chemistry*, Wiley-VCH Verlag GmbH & Co. KGaA, 2000, p. 140.
- [19] O. Hinrichsen, F. Rosowski, A. Hornung, M. Muhler, and G. Ertl, "The Kinetics of Ammonia Synthesis over Ru-Based Catalysts: 1. The Dissociative Chemisorption and Associative Desorption of N<sub>2</sub>," *J. Catal.*, vol. 165, no. 1, pp. 33–44, Apr. 1997.
- [20] D. Szmigielski *et al.*, "The Kinetics of Ammonia Synthesis over Ruthenium-Based Catalysts: The Role of Barium and Cesium," *J. Catal.*, vol. 205, no. 1, pp. 205–212, Mar. 2002.
- [21] Z. You, K. Inazu, K. Aika, and T. Baba, "Electronic and structural promotion of barium hexaaluminate as a ruthenium catalyst support for ammonia synthesis," *J. Catal.*, vol. 251, no. 2, pp. 321–331, Apr. 2007.
- [22] M. Hara, M. Kitano, and H. Hosono, "Ru-Loaded C<sub>12</sub>A<sub>7</sub>:e<sup>-</sup> Electride as a Catalyst for Ammonia Synthesis," *ACS Catal.*, vol. 7, no. 4, pp. 2313–2324, Apr. 2017.
- [23] J. S. J. Hargreaves and D. McKay, "A comparison of the reactivity of lattice nitrogen in Co<sub>3</sub>Mo<sub>3</sub>N and Ni<sub>2</sub>Mo<sub>3</sub>N catalysts," *J. Mol. Catal. A Chem.*, vol. 305, no. 1, pp. 125–129, Apr. 2009.
- [24] R. Kojima and K. I. Aika, "Cobalt molybdenum bimetallic nitride catalysts for ammonia synthesis Part 3. Reactant gas treatment," *Appl. Catal. A Gen.*, vol. 219, no. 1–2, pp. 157–170, Apr. 2001.
- [25] C. Leterme, C. Fernández, P. Eloy, E. M. Gaigneaux, and P. Ruiz, "The inhibitor role of NH<sub>3</sub> on its synthesis process at low temperature, over Ru catalytic nanoparticles," *Catal. Today*, vol. 286, pp. 85–100, Apr. 2017.
- [26] S. R. Tennison, "Alternative Noniron Catalysts," in *Catalytic Ammonia Synthesis*, Springer, Boston, MA, 1991, pp. 303–364.

- [27] T. W. Hansen, J. B. Wagner, P. L. Hansen, S. Dahl, H. Topsøe, and C. J. H. Jacobsen, "Atomic-resolution in situ transmission electron microscopy of a promoter of a heterogeneous catalyst," *Science* (80-. ), vol. 294, no. 5546, pp. 1508–1510, Jan. 2001.
- [28] G. Gramatica and N. Pernicone, "Kinetics of Ammonia Synthesis and Influence on Converter Design," in *Catalytic Ammonia Synthesis: Fundamentals and Practice*, J. R. Jennings, Ed. Springer Science & Business Media, 1991, pp. 211–251.
- [29] A. Ozaki, H. Taylor, and M. Boudart, "Kinetics and mechanism of the ammonia synthesis," *Proc. R. Soc. London. Ser. A. Math. Phys. Sci.*, vol. 258, no. 1292, pp. 47–62, Dec. 1960.
- [30] A. Cappelli and A. Collina, "Preparation of Kinetic Models for Synthesis of Ammonia on various Industrial Catalysts," 1972, p. 10.
- [31] I. Rossetti, N. Pernicone, F. Ferrero, and L. Forni, "Kinetic Study of Ammonia Synthesis on a Promoted Ru/C Catalyst," *Ind. Eng. Chem. Res.*, vol. 45, no. 12, pp. 4150–4155, Apr. 2006.
- [32] G. Rambeau and H. Amariglio, "Ammonia-Synthesis on Iron Conceived as an Auto-Catalytic Reaction. 2. Reaction-Mechanism and Quantitative Description of Self-Activation," *J. Chim. Phys. Physico-Chimie Biol.*, vol. 75, no. 4, pp. 397–405, 1978.
- [33] G. Rambeau and H. Amariglio, "Ammonia synthesis on ruthenium powder from 100 to 500 °C and hydrogenation of preadsorbed nitrogen down to -70 °C," *J. Catal.*, vol. 72, no. 1, pp. 1–11, Apr. 1981.
- [34] G. Rambeau, A. Jorti, and H. Amariglio, "Ammonia synthesis on osmium powder and hydrogenation of preadsorbed nitrogen from 100 to 500 °C," *J. Catal.*, vol. 74, no. 1, pp. 110–120, Apr. 1982.
- [35] K. Aika, J. Kubota, Y. Kadowaki, Y. Niwa, and Y. Izumi, "Molecular sensing techniques for the characterization and design of new ammonia catalysts," *Appl. Surf. Sci.*, vol. 121–122, pp. 488–491, Apr. 1997.
- [36] A. Kotarba, J. Dmytrzyk, W. Raróg-Pilecka, and Z. Kowalczyk, "Surface heterogeneity and ionization of Cs promoter in carbon-based ruthenium catalyst for ammonia synthesis," *Appl. Surf. Sci.*, vol. 207, no. 1, pp. 327–333, Apr. 2003.
- [37] O. Hinrichsen, F. Rosowski, M. Muhler, and G. Ertl, "The microkinetics of ammonia synthesis catalyzed by cesium-promoted supported ruthenium," *Chem. Eng. Sci.*, vol. 51, no. 10, pp. 1683–1690, Dec. 1996.
- [38] C. J. H. Jacobsen *et al.*, "Structure sensitivity of supported ruthenium catalysts for ammonia synthesis," *J. Mol. Catal. A Chem.*, vol. 163, no. 1–2, pp. 19–26, Apr. 2000.

- [39] S. Dahl, J. Sehested, C. J. H. Jacobsen, E. Törnqvist, and I. Chorkendorff, "Surface science based microkinetic analysis of ammonia synthesis over ruthenium catalysts," *J. Catal.*, vol. 192, no. 2, pp. 391–399, Dec. 2000.
- [40] R. van Hardeveld and A. van Montfoort, "The influence of crystallite size on the adsorption of molecular nitrogen on nickel, palladium and platinum: An infrared and electron-microscopic study," *Surf. Sci.*, vol. 4, no. 4, pp. 396–430, Apr. 1966.
- [41] J. Ni, B. Jing, J. Lin, B. Lin, Z. Zhao, and L. Jiang, "Effect of rare earth on the performance of Ru/MgAl-LDO catalysts for ammonia synthesis," *J. Rare Earths*, vol. 36, no. 2, pp. 135–141, Apr. 2018.
- [42] B. Lin, K. Wei, J. Lin, and J. Ni, "Effect of treatment conditions on ruthenium particle size and ammonia synthesis activity of ruthenium catalyst," *Catal. Commun.*, vol. 39, pp. 14–19, Apr. 2013.
- [43] P. Seetharamulu, V. Siva Kumar, A. H. Padmasri, B. David Raju, and K. S. Rama Rao, "A highly active nano-Ru catalyst supported on novel Mg–Al hydrotalcite precursor for the synthesis of ammonia," *J. Mol. Catal. A Chem.*, vol. 263, no. 1, pp. 253–258, Apr. 2007.
- [44] W. Raróg-Pilecka, E. Miśkiewicz, D. Szmigiel, and Z. Kowalczyk, "Structure sensitivity of ammonia synthesis over promoted ruthenium catalysts supported on graphitised carbon," *J. Catal.*, vol. 231, no. 1, pp. 11–19, Apr. 2005.
- [45] C. Fernández, C. Pezzotta, E. M. Gaigneaux, N. Bion, D. Duprez, and P. Ruiz, "Disclosing the synergistic mechanism in the catalytic activity of different-sized Ru nanoparticles for ammonia synthesis at mild reaction conditions," *Catal. Today*, vol. 251, pp. 88–95, Apr. 2015.
- [46] C. Fernández *et al.*, "Insights in the mechanism of deposition and growth of RuO<sub>2</sub> colloidal nanoparticles over alumina. Implications on the activity for ammonia synthesis," *Appl. Catal. A Gen.*, vol. 502, pp. 48–56, Apr. 2015.
- [47] C. Fernández, C. Sassoie, D. P. Debecker, C. Sanchez, and P. Ruiz, "Effect of the size and distribution of supported Ru nanoparticles on their activity in ammonia synthesis under mild reaction conditions," *Appl. Catal. A Gen.*, vol. 474, pp. 194–202, Apr. 2014.
- [48] A. M. Karim *et al.*, "Correlating Particle Size and Shape of Supported Ru/ $\gamma$ -Al<sub>2</sub>O<sub>3</sub> Catalysts with NH<sub>3</sub> Decomposition Activity," *J. Am. Chem. Soc.*, vol. 131, no. 34, pp. 12230–12239, Apr. 2009.
- [49] A. Ishikawa, T. Doi, and H. Nakai, "Catalytic performance of Ru, Os, and Rh nanoparticles for ammonia synthesis: A density functional theory analysis," *J. Catal.*, vol. 357, pp. 213–222, Apr. 2018.
- [50] D. J. Dooling, R. J. Nielsen, and L. J. Broadbelt, "A density-functional study

- of the interaction of nitrogen with ruthenium clusters,” *Chem. Eng. Sci.*, vol. 54, no. 15, pp. 3399–3409, Apr. 1999.
- [51] S. E. Siporin and R. J. Davis, “Use of kinetic models to explore the role of base promoters on Ru/MgO ammonia synthesis catalysts,” *J. Catal.*, vol. 225, no. 2, pp. 359–368, Nov. 2004.
- [52] M. Muhler, F. Rosowski, O. Hinrichsen, A. Hornung, and G. Ertl, “Ruthenium as catalyst for ammonia synthesis,” in *Studies in Surface Science and Catalysis*, vol. 101, J. W. Hightower, W. Nicholas Delgass, E. Iglesia, and A. T. Bell, Eds. Elsevier, 1996, pp. 317–326.
- [53] A. Mittasch and W. Frankenburg, “Early Studies of Multicomponent Catalysts,” in *Advances in Catalysis*, vol. 2, no. C, W. G. Frankenburg, V. I. Komarewsky, and E. K. Rideal, Eds. Academic Press, 1950, pp. 81–104.
- [54] K. Aika, H. Hori, and A. Ozaki, “Activation of nitrogen by alkali metal promoted transition metal I. Ammonia synthesis over ruthenium promoted by alkali metal,” *J. Catal.*, vol. 27, no. 3, pp. 424–431, Apr. 1972.
- [55] K. Aika *et al.*, “Support and promoter effect of ruthenium catalyst: I. Characterization of alkali-promoted ruthenium/alumina catalysts for ammonia synthesis,” *J. Catal.*, vol. 92, no. 2, pp. 296–304, Apr. 1985.
- [56] S. Murata and K. Aika, “Preparation and characterization of chlorine-free ruthenium catalysts and the promoter effect in ammonia synthesis 2. A lanthanide oxide-promoted Ru/Al<sub>2</sub>O<sub>3</sub> catalyst,” *J. Catal.*, vol. 136, no. 1, pp. 118–125, Apr. 2004.
- [57] Y. Niwa and K.-I. Aika, “The promoter effect of lanthana on MgO supported ruthenium catalysts for ammonia synthesis,” *Res. Chem. Intermed.*, vol. 24, no. 5, pp. 593–603, Apr. 1998.
- [58] Y. Kadowaki and K. Aika, “Promoter Effect of Sm<sub>2</sub>O<sub>3</sub> on Ru/Al<sub>2</sub>O<sub>3</sub> in Ammonia Synthesis,” *J. Catal.*, vol. 161, no. 1, pp. 178–185, Apr. 1996.
- [59] T. Bécue, R. J. Davis, and J. M. Garces, “Effect of Cationic Promoters on the Kinetics of Ammonia Synthesis Catalyzed by Ruthenium Supported on Zeolite X,” *J. Catal.*, vol. 179, no. 1, pp. 129–137, Apr. 1998.
- [60] I. Rossetti, N. Pernicone, and L. Forni, “Promoters effect in Ru/C ammonia synthesis catalyst,” *Appl. Catal. A Gen.*, vol. 208, no. 1–2, pp. 271–278, Apr. 2001.
- [61] Z. Kowalczyk, M. Krukowski, W. Raróg-Pilecka, D. Szmigiel, and J. Zielinski, “Carbon-based ruthenium catalyst for ammonia synthesis: Role of the barium and caesium promoters and carbon support,” *Appl. Catal. A Gen.*, vol. 248, no. 1, pp. 67–73, Apr. 2003.
- [62] M. Guraya, S. Sprenger, W. Rarog-Pilecka, D. Szmigiel, Z. Kowalczyk, and

- M. Muhler, "The effect of promoters on the electronic structure of ruthenium catalysts supported on carbon," *Appl. Surf. Sci.*, vol. 238, no. 1, pp. 77–81, Apr. 2004.
- [63] N. B. Shitova *et al.*, "Formation of Ru - M/sibunit catalysts for ammonia synthesis," *Kinet. Catal.*, vol. 45, no. 3, pp. 414–421, Apr. 2004.
- [64] Y. V Larichev, D. A. Shlyapin, P. G. Tsyrl'nikov, and V. I. Bukhtiyarov, "Comparative Study of Rubidium and Cesium as Promoters in Carbon-supported Ruthenium Catalysts for Ammonia Synthesis," *Catal. Letters*, vol. 120, no. 3–4, pp. 204–209, Apr. 2008.
- [65] F. Rosowski, A. Hornung, O. Hinrichsen, D. Herein, M. Muhler, and G. Ertl, "Ruthenium catalysts for ammonia synthesis at high pressures: Preparation, characterization, and power-law kinetics," *Appl. Catal. A Gen.*, vol. 151, no. 2, pp. 443–460, Apr. 1997.
- [66] K. ichi Aika, T. Takano, and S. Murata, "Preparation and characterization of chlorine-free ruthenium catalysts and the promoter effect in ammonia synthesis. 3. A magnesia-supported ruthenium catalyst," *J. Catal.*, vol. 136, no. 1, pp. 126–140, Apr. 1992.
- [67] D. O. Uner, N. Savargoankar, M. Pruski, and T. S. King, "The effects of alkali promoters on the dynamics of hydrogen chemisorption and syngas reaction kinetics on Ru/SiO<sub>2</sub> surfaces," in *Dynamics of Surfaces and Reaction Kinetics in Heterogeneous Catalysis*, vol. 109, G. F. Froment and K. C. Waught, Eds. Amsterdam: Elsevier Science Publ B V, 2007, pp. 315–324.
- [68] D. O. Uner, "A sensible mechanism of alkali promotion in Fischer-Tropsch synthesis: Adsorbate mobilities," *Ind. Eng. Chem. Res.*, vol. 37, no. 6, pp. 2239–2245, Apr. 1998.
- [69] D. O. Uner, M. Pruski, and T. S. King, "The role of alkali promoters in Fischer-Tropsch synthesis on Ru/SiO<sub>2</sub> surfaces," *Top. Catal.*, vol. 2, no. 1–4, pp. 59–69, Apr. 1995.
- [70] C. Pedrero, T. Waku, and E. Iglesia, "Oxidation of CO in H<sub>2</sub>-CO mixtures catalyzed by platinum: alkali effects on rates and selectivity," *J. Catal.*, vol. 233, no. 1, pp. 242–255, Apr. 2005.
- [71] G. K. Boreskov and Y. U. S. Matros, "Unsteady-State Performance of Heterogeneous Catalytic Reactions," *Catal. Rev.*, vol. 25, no. 4, pp. 551–590, Apr. 1983.
- [72] Y. S. Matros, "Performance of catalytic processes under unsteady conditions," *Chem. Eng. Sci.*, vol. 45, no. 8, pp. 2097–2102, Apr. 1990.
- [73] Y. S. Matros, "Forced Unsteady-state Processes in Heterogeneous Catalytic Reactors," *Can. J. Chem. Eng.*, vol. 74, no. 5, pp. 566–579, Feb. 1996.

- [74] G. Rambeau and H. Amariglio, "Improvement of the catalytic performance of a ruthenium powder in ammonia synthesis by the use of a cyclic procedure," *Appl. Catal.*, vol. 1, no. 5, pp. 291–302, Apr. 1981.
- [75] H. D. Wilson and R. G. Rinker, "Concentration forcing in ammonia synthesis-I Controlled cyclic operation," *Chem. Eng. Sci.*, vol. 37, no. 3, pp. 343–355, Apr. 1982.
- [76] A. K. Jain, R. R. Hudgins, and L. P. Silveston, "Adsorption/desorption models: How useful for predicting reaction rates under cyclic operation," *Can. J. Chem. Eng.*, vol. 61, no. 1, pp. 46–49, Apr. 1983.
- [77] H. H. Himstedt, M. S. Huberty, A. V. McCormick, L. D. Schmidt, and E. L. Cussler, "Ammonia synthesis enhanced by magnesium chloride absorption," *AIChE J.*, vol. 61, no. 4, pp. 1364–1371, Jan. 2015.
- [78] M. S. Huberty, A. L. Wagner, A. V. McCormick, and E. L. Cussler, "Ammonia absorption at haber process conditions," *AIChE J.*, vol. 58, no. 11, pp. 3526–3532, Apr. 2012.
- [79] M. Reese *et al.*, "Performance of a Small-Scale Haber Process," *Ind. Eng. Chem. Res.*, vol. 55, no. 13, pp. 3742–3750, Apr. 2016.
- [80] S. Dahl, A. Logadottir, C. J. H. Jacobsen, and J. K. Nørskov, "Electronic factors in catalysis: the volcano curve and the effect of promotion in catalytic ammonia synthesis," *Appl. Catal. A Gen.*, vol. 222, no. 1, pp. 19–29, Apr. 2001.
- [81] Y. V. Larichev, B. L. Moroz, and V. I. Bukhtiyarov, "Electronic state of ruthenium deposited onto oxide supports: An XPS study taking into account the final state effects," *Appl. Surf. Sci.*, vol. 258, no. 4, pp. 1541–1550, Apr. 2011.
- [82] Y. V. Larichev *et al.*, "XPS and TEM studies on the role of the support and alkali promoter in Ru/MgO and Ru-Cs+ZMgO catalysts for ammonia-synthesis," *J. Phys. Chem. C*, vol. 111, no. 26, pp. 9427–9436, Apr. 2007.
- [83] Z. Wang, J. Lin, R. Wang, and K. Wei, "Ammonia synthesis over ruthenium catalyst supported on perovskite type BaTiO<sub>3</sub>," *Catal. Commun.*, vol. 32, pp. 11–14, Apr. 2013.
- [84] L. Volpe and M. Boudart, "Ammonia synthesis on molybdenum nitride," *J. Phys. Chem.*, vol. 90, no. 20, pp. 4874–4877, Apr. 1986.
- [85] R. Kojima and K. Aika, "Cobalt molybdenum bimetallic nitride catalysts for ammonia synthesis: Part 1. Preparation and characterization," *Appl. Catal. A Gen.*, vol. 215, no. 1, pp. 149–160, Apr. 2001.
- [86] A.-M. Alexander and J. S. J. Hargreaves, "Alternative catalytic materials: carbides, nitrides, phosphides and amorphous boron alloys," *Chem. Soc. Rev.*, vol. 39, no. 11, pp. 4388–4401, Apr. 2010.

- [87] R. Kojima and K. I. Aika, "Cobalt molybdenum bimetallic nitride catalysts for ammonia synthesis: Part 2. Kinetic study," *Appl. Catal. A Gen.*, vol. 218, no. 1–2, pp. 121–128, Apr. 2001.
- [88] R. Kojima and K. Aika, "Cobalt Molybdenum Bimetallic Nitride Catalysts for Ammonia Synthesis," *Chem. Lett.*, vol. 29, no. 5, pp. 514–515, Apr. 2000.
- [89] D. Mckay, J. S. J. Hargreaves, J. L. Rico, J. L. Rivera, and X.-L. Sun, "The influence of phase and morphology of molybdenum nitrides on ammonia synthesis activity and reduction characteristics," *J. Solid State Chem.*, vol. 181, no. 2, pp. 325–333, Apr. 2008.
- [90] D. Mckay, D. H. Gregory, J. S. J. Hargreaves, S. M. Hunter, and X. Sun, "Towards nitrogen transfer catalysis: reactive lattice nitrogen in cobalt molybdenum nitride," *Chem. Commun.*, vol. 0, no. 29, pp. 3051–3053, Apr. 2007.
- [91] D. H. Gregory, J. S. J. Hargreaves, and S. M. Hunter, "On the Regeneration of Co<sub>3</sub>Mo<sub>3</sub>N from Co<sub>6</sub>Mo<sub>6</sub>N with N<sub>2</sub>," *Catal. Letters*, vol. 141, no. 1, pp. 22–26, Apr. 2011.
- [92] N. Perret *et al.*, "Synthesis, characterisation and hydrogenation performance of ternary nitride catalysts," *Appl. Catal. A Gen.*, vol. 488, pp. 128–137, Apr. 2014.
- [93] S. M. Hunter, D. H. Gregory, J. S. J. Hargreaves, M. Richard, D. Duprez, and N. Bion, "A study of <sup>15</sup>N/<sup>14</sup>N isotopic exchange over cobalt molybdenum nitrides," *ACS Catal.*, vol. 3, no. 8, pp. 1719–1725, Apr. 2013.
- [94] J. Kirn and D. C. Rees, "Crystallographic structure and functional implications of the nitrogenase molybdenum-iron protein from *Azotobacter vinelandii*," *Nature*, vol. 360, no. 6404, pp. 553–560, Apr. 1992.
- [95] J. Kim and D. C. Rees, "Structural models for the metal centers in the nitrogenase molybdenum-iron protein," *Science (80-. )*, vol. 257, no. 5077, pp. 1677–1682, Apr. 1992.
- [96] T. Spatzal, "The center of biological nitrogen fixation: FeMo-cofactor," *Zeitschrift fur Anorg. und Allg. Chemie*, vol. 641, no. 1, pp. 10–17, Apr. 2015.
- [97] J. Rosing and E. C. Slater, "The value of  $\Delta G^\circ$  for the hydrolysis of ATP," *BBA - Bioenerg.*, vol. 267, no. 2, pp. 275–290, Jul. 1972.
- [98] H. Schindelin, C. Kisker, J. L. Schlessman, J. B. Howard, and D. C. Rees, "Structure of ADP·AlF<sub>4</sub><sup>-</sup>-stabilized nitrogenase complex and its implications for signal transduction," *Nature*, vol. 387, no. 6631, pp. 370–376, Apr. 1997.
- [99] F. E. H. Katz, C. P. Owens, and F. A. Tezcan, "Electron Transfer Reactions in Biological Nitrogen Fixation," *Isr. J. Chem.*, vol. 56, no. 9–10, pp. 682–692, Apr. 2016.

- [100] D. J. Lowe and R. N. Thorneley, "The mechanism of *Klebsiella pneumoniae* nitrogenase action. Pre-steady-state kinetics of H<sub>2</sub> formation.," *Biochem. J.*, vol. 224, no. 3, pp. 877–886, Apr. 1984.
- [101] J. B. Varley, Y. Wang, K. Chan, F. Studt, and J. K. Nørskov, "Mechanistic insights into nitrogen fixation by nitrogenase enzymes," *Phys. Chem. Chem. Phys.*, vol. 17, no. 44, pp. 29541–29547, Apr. 2015.
- [102] R. R. Schrock, "Catalytic reduction of dinitrogen to ammonia at a single molybdenum center," *Acc. Chem. Res.*, vol. 38, no. 12, pp. 955–962, Apr. 2005.
- [103] R. R. Schrock, "Catalytic reduction of dinitrogen to ammonia by molybdenum: Theory versus experiment," *Angew. Chemie - Int. Ed.*, vol. 47, no. 30, pp. 5512–5522, Apr. 2008.
- [104] D. V. Yandulov and R. R. Schrock, "Reduction of dinitrogen to ammonia at a well-protected reaction site in a molybdenum triamidoamine complex," *J. Am. Chem. Soc.*, vol. 124, no. 22, pp. 6252–6253, Apr. 2002.
- [105] R. R. Schrock, "Catalytic reduction of dinitrogen to ammonia at well-defined single metal sites," *Philos. Trans. R. Soc. A Math. Phys. Eng. Sci.*, vol. 363, no. 1829, pp. 959–969, Apr. 2005.
- [106] D. V. Yandulov and R. R. Schrock, "Catalytic Reduction of Dinitrogen to Ammonia at a Single Molybdenum Center," *Science (80-. )*, vol. 301, no. 5629, pp. 76–78, Apr. 2003.
- [107] H. H. Jurgen, "Process and apparatus for performing reactions in the gaseous phase," US3372988A, 1968.
- [108] U. Zardi, "Axial-radial reactor for heterogeneous synthesis," US4372920A, 1983.
- [109] H. Laukel, "Method and apparatus for reaction heat recovery in catalytic high-pressure synthesis, particularly in ammonia and methanol synthesis," US3622266A, 1971.
- [110] G. Pagani, "Radial-flow reactor for the synthesis of ammonia with production of high thermal-level steam," US4101281A, 1978.
- [111] R. B. Peterson, R. Finello, and G. A. Denavit, "Horizontal ammonia converter," 03-Apr-1984.
- [112] I. Rafiqul, C. Weber, B. Lehmann, and A. Voss, "Energy efficiency improvements in ammonia production—perspectives and uncertainties," *Energy*, vol. 30, no. 13, pp. 2487–2504, Apr. 2005.
- [113] V. Věk, "Optimization of Large Reactors with Extremely Active Catalysts," *Ind. Eng. Chem. Process Des. Dev.*, vol. 16, no. 3, pp. 412–424, Apr. 1977.
- [114] M. Appl, "Ammonia, 3. Production Plants," in *Ullmann's Encyclopedia of*

- Industrial Chemistry*, Weinheim: Wiley-VCH Verlag GmbH & Co. KGaA, 2011, p. 229.
- [115] D. B. Crawford, C. L. Becker, and J. R. LeBlanc, "Parallel steam reformers to provide low energy process," US4162290A, 1977.
- [116] A. Nielsen, J. B. Hansen, J. Houken, and E. A. Gam, "Revamp of ammonia plants," *Plant/Operations Prog.*, vol. 1, no. 3, pp. 186–190, Apr. 2004.
- [117] "New Ammonia Process Reduces Costs.," *Chem. Eng. Prog.*, vol. 79, no. 5, pp. 62–66, Apr. 1983.
- [118] I. Dybkjaer, "Ammonia Production Processes," in *Ammonia*, Springer, Berlin, Heidelberg, 1995, pp. 199–327.
- [119] J. D. Figueroa, T. Fout, S. Plasynski, H. McIlvried, and R. D. Srivastava, "Advances in CO<sub>2</sub> capture technology—The U.S. Department of Energy's Carbon Sequestration Program," *Int. J. Greenh. Gas Control*, vol. 2, no. 1, pp. 9–20, Apr. 2008.
- [120] D. Zhao, Q. Huo, J. Feng, B. F. Chmelka, and G. D. Stucky, "Nonionic triblock and star diblock copolymer and oligomeric surfactant syntheses of highly ordered, hydrothermally stable, mesoporous silica structures," *J. Am. Chem. Soc.*, vol. 120, no. 24, pp. 6024–6036, 1998.
- [121] M. Zahmakiran and S. Özkar, "Zeolite-confined ruthenium(0) nanoclusters catalyst: Record catalytic activity, reusability, and lifetime in hydrogen generation from the hydrolysis of sodium borohydride," *Langmuir*, vol. 25, no. 5, pp. 2667–2678, Mar. 2009.
- [122] S. Satyapal, J. Petrovic, C. Read, G. Thomas, and G. Ordaz, "The U.S. Department of Energy's National Hydrogen Storage Project: Progress towards meeting hydrogen-powered vehicle requirements," *Catal. Today*, vol. 120, no. 3-4 SPEC. ISS., pp. 246–256, Jun. 2007.
- [123] N. Armaroli and V. Balzani, "The hydrogen issue," *ChemSusChem*, vol. 4, no. 1, pp. 21–36, Jun. 2011.
- [124] C. Liu, F. Li, M. Lai-Peng, and H. M. Cheng, "Advanced materials for energy storage," *Adv. Mater.*, vol. 22, no. 8, pp. E28–E62, Jul. 2010.
- [125] L. Zou and H. C. Zhou, "Hydrogen storage in metal-organic frameworks," *Nanostructured Mater. Next-Generation Energy Storage Convers. Hydrog. Prod. Storage, Util.*, vol. 128, pp. 143–170, Jun. 2017.
- [126] A. Züttel and L. Schlapbach, "Hydrogen-storage materials for mobile applications.," *Nature*, vol. 414, no. 6861. pp. 353–358, 02-Jul-2001.
- [127] X. Yao *et al.*, "Mg-based nanocomposites with high capacity and fast kinetics for hydrogen storage," *J. Phys. Chem. B*, vol. 110, no. 24, pp. 11697–11703, Jul. 2006.

- [128] “Hydrogen Storage,” *Energy.gov*, 14-May-2019. [Online]. Available: <https://www.energy.gov/eere/fuelcells/hydrogen-storage>. [Accessed: 02-Jul-2018].
- [129] “Materials-Based Hydrogen Storage,” *Energy.gov*, 15-May-2019. [Online]. Available: <https://www.energy.gov/eere/fuelcells/materials-based-hydrogen-storage>. [Accessed: 02-Jul-2018].
- [130] E. Commission, “HYSAST - Hydrogen Safety in Storage and Transport.” [Online]. Available: <https://iet.jrc.ec.europa.eu/hysast-hydrogen-safety-storage-and-transport#SoITeF>. [Accessed: 02-Jul-2018].
- [131] X. Lin *et al.*, “High capacity hydrogen adsorption in Cu(II) tetracarboxylate framework materials: The role of pore size, ligand functionalization, and exposed metal sites,” *J. Am. Chem. Soc.*, vol. 131, no. 6, pp. 2159–2171, Jun. 2009.
- [132] Y. Li and R. T. Yang, “Hydrogen Storage in Metal–Organic Frameworks by Bridged Hydrogen Spillover,” *J. Am. Chem. Soc.*, vol. 128, no. 25, pp. 8136–8137, Apr. 2006.
- [133] C. Zlotea *et al.*, “Pd nanoparticles embedded into a metal-organic framework: Synthesis, structural characteristics, and hydrogen sorption properties,” *J. Am. Chem. Soc.*, vol. 132, no. 9, pp. 2991–2997, Jun. 2010.
- [134] M. Dinča, A. Dailly, Y. Liu, C. M. Brown, D. A. Neumann, and J. R. Long, “Hydrogen storage in a microporous metal-organic framework with exposed Mn<sup>2+</sup> coordination sites,” *J. Am. Chem. Soc.*, vol. 128, no. 51, pp. 16876–16883, Jun. 2006.
- [135] A. Seiler, L. Schlapbach, T. von Waldkirch, D. Shaltiel, and F. Stucki, “Surface Analysis of Mg<sub>2</sub>Ni-Mg, Mg<sub>2</sub>Ni AND Mg<sub>2</sub>Cu,” *J. less-common Met.*, vol. 73, no. 1, pp. 193–199, Jul. 1980.
- [136] G. Liang, J. Huot, S. Boily, A. Van Neste, and R. Schulz, “Catalytic effect of transition metals on hydrogen sorption in nanocrystalline ball milled MgH<sub>2</sub>-Tm (Tm = Ti, V, Mn, Fe and Ni) systems,” *J. Alloys Compd.*, vol. 292, no. 1–2, pp. 247–252, Jun. 1999.
- [137] G. Chen, Y. Zhang, J. Chen, X. Guo, Y. Zhu, and L. Li, “Enhancing hydrogen storage performances of MgH<sub>2</sub> by Ni nano-particles over mesoporous carbon CMK-3,” *Nanotechnology*, vol. 29, no. 26, p. 265705, Jun. 2018.
- [138] S. A. Pighin, B. Coco, H. Troiani, F. J. Castro, and G. Urretavizcaya, “Effect of additive distribution in H<sub>2</sub> absorption and desorption kinetics in MgH<sub>2</sub> milled with NbH<sub>0.9</sub> or NbF<sub>5</sub>,” *Int. J. Hydrogen Energy*, vol. 43, no. 15, pp. 7430–7439, Jun. 2018.
- [139] L. Z. Ouyang *et al.*, “Enhanced hydrogen storage kinetics and stability by synergistic effects of in situ formed CeH<sub>2.73</sub> and Ni in CeH<sub>2.73</sub>-MgH<sub>2</sub>-Ni

- nanocomposites,” *J. Phys. Chem. C*, vol. 118, no. 15, pp. 7808–7820, Jun. 2014.
- [140] N. S. Mustafa and M. Ismail, “Hydrogen sorption improvement of MgH<sub>2</sub> catalyzed by CeO<sub>2</sub> nanopowder,” *J. Alloys Compd.*, vol. 695, pp. 2532–2538, Jun. 2017.
- [141] D. Peng *et al.*, “Effect of LiBH<sub>4</sub> on hydrogen storage properties of magnesium hydride-carbon composite,” *J. Alloys Compd.*, vol. 711, pp. 104–110, Jun. 2017.
- [142] H. Zhou, X. Wang, H. Liu, and M. Yan, “Enhanced hydrogen storage properties of 2LiBH<sub>4</sub>-LiAlH<sub>4</sub> nanoconfined in resorcinol formaldehyde carbon aerogel,” *J. Alloys Compd.*, vol. 726, pp. 525–531, Jun. 2017.
- [143] S. I. Orimo, Y. Nakamori, J. R. Eliseo, A. Züttel, and C. M. Jensen, “Complex hydrides for hydrogen storage,” *Chem. Rev.*, vol. 107, no. 10, pp. 4111–4132, Jun. 2007.
- [144] F. H. Stephens, V. Pons, and R. Tom Baker, “Ammonia–borane: The hydrogen source par excellence?,” *J. Chem. Soc. Dalt. Trans.*, vol. 0, no. 25, pp. 2613–2626, Jul. 2007.
- [145] C. W. Hamilton, R. T. Baker, A. Staubitz, and I. Manners, “B-N compounds for chemical hydrogen storage,” *Chem. Soc. Rev.*, vol. 38, no. 1, pp. 279–293, Jun. 2009.
- [146] J. J. Rewlly and R. H. Wiswall, “The Reaction of Hydrogen with Alloys of Magnesium and Nickel and the Formation of Mg<sub>2</sub>NiH<sub>4</sub>,” *Inorg. Chem.*, vol. 7, no. 11, pp. 2254–2256, 1968.
- [147] M. Y. Song, M. Pezat, B. Darriet, and P. Hagenmuller, “Hydriding mechanism of Mg<sub>2</sub>Ni in the presence of oxygen impurity in hydrogen,” *J. Mater. Sci.*, vol. 20, no. 8, pp. 2958–2964, Jul. 1985.
- [148] K. J. Gross, D. Chartouni, E. Leroy, A. Züttel, and L. Schlapbach, “Mechanically milled Mg composites for hydrogen storage: The relationship between morphology and kinetics,” *J. Alloys Compd.*, vol. 269, no. 1–2, pp. 259–270, Jul. 1998.
- [149] Z. Zhang, X. Zhou, C. Liu, J. Guo, and H. Ning, “Hydrogen adsorption and dissociation on nickel-adsorbed and -substituted Mg<sub>17</sub>Al<sub>12</sub> (100) surface: A density functional theory study,” *Int. J. Hydrogen Energy*, vol. 43, no. 2, pp. 793–800, Jul. 2018.
- [150] D. S. Pyle, E. M. A. Gray, and C. J. Webb, “Hydrogen storage in carbon nanostructures via spillover,” *Int. J. Hydrogen Energy*, vol. 41, no. 42, pp. 19098–19113, Oct. 2016.
- [151] Y. J. Han and S. J. Park, “Influence of nickel nanoparticles on hydrogen storage

- behaviors of MWCNTs,” *Appl. Surf. Sci.*, vol. 415, pp. 85–89, Oct. 2017.
- [152] Y. Wang *et al.*, “Surface functionalization-enhanced spillover effect on hydrogen storage of Ni-B nanoalloy-doped activated carbon,” *Int. J. Hydrogen Energy*, vol. 36, no. 21, pp. 13663–13668, Oct. 2011.
- [153] L. Zubizarreta, J. A. Menéndez, J. J. Pis, and A. Arenillas, “Improving hydrogen storage in Ni-doped carbon nanospheres,” *Int. J. Hydrogen Energy*, vol. 34, no. 7, pp. 3070–3076, Oct. 2009.
- [154] Y. Liu *et al.*, “Assembly of Metal-Organic Frameworks (MOFs) based on indium-trimer building blocks: A porous MOF with soc topology and high hydrogen storage,” *Angew. Chemie - Int. Ed.*, vol. 46, no. 18, pp. 3278–3283, Jul. 2007.
- [155] D. Himsl and M. Hartmann, “Hydrogen storage in li-doped metal-organic frameworks,” *DGMK Tagungsbericht*, vol. 2010, no. 3, pp. 157–164, Jun. 2010.
- [156] P. García-Holley *et al.*, “Benchmark Study of Hydrogen Storage in Metal-Organic Frameworks under Temperature and Pressure Swing Conditions,” *ACS Energy Lett.*, vol. 3, no. 3, pp. 748–754, Jun. 2018.
- [157] M. Pourabdoli, S. Raygan, H. Abdizadeh, and D. Uner, “Determination of kinetic parameters and hydrogen desorption characteristics of MgH<sub>2</sub>-10 wt% (9Ni-2Mg-Y) nano-composite,” *Int. J. Hydrogen Energy*, vol. 38, no. 27, pp. 11910–11919, Jun. 2013.
- [158] J. A. Villajos, G. Orcajo, C. Martos, J. Á. Botas, J. Villacañas, and G. Calleja, “Co/Ni mixed-metal sited MOF-74 material as hydrogen adsorbent,” *Int. J. Hydrogen Energy*, vol. 40, no. 15, pp. 5346–5352, 2015.
- [159] X. Zhou, W. Chu, Y. Zhou, W. Sun, and Y. Xue, “DFT simulation on H<sub>2</sub> adsorption over Ni-decorated defective h-BN nanosheets,” *Appl. Surf. Sci.*, vol. 439, pp. 246–253, Oct. 2018.
- [160] A. Züttel *et al.*, “Hydrogen storage properties of LiBH<sub>4</sub>,” *J. Alloys Compd.*, vol. 356–357, pp. 515–520, Jun. 2003.
- [161] M. Pourabdoli, S. Raygan, H. Abdizadeh, and D. Uner, “A comparative study for synthesis methods of nano-structured (9Ni-2Mg-Y) alloy catalysts and effect of the produced alloy on hydrogen desorption properties of MgH<sub>2</sub>,” *Int. J. Hydrogen Energy*, vol. 38, no. 36, pp. 16090–16097, Jun. 2013.
- [162] E. Durgun, S. Ciraci, and T. Yildirim, “Functionalization of carbon-based nanostructures with light transition-metal atoms for hydrogen storage,” *Phys. Rev. B - Condens. Matter Mater. Phys.*, vol. 77, no. 8, p. 85405, Jun. 2008.
- [163] L. Vellingiri, K. Annamalai, R. Kandasamy, and I. Kombiah, “Characterization and hydrogen storage properties of SnO<sub>2</sub> functionalized MWCNT

- nanocomposites,” *Int. J. Hydrogen Energy*, vol. 43, no. 22, pp. 10396–10409, Sep. 2018.
- [164] T. Yildirim, J. Íñiguez, and S. Ciraci, “Molecular and dissociative adsorption of multiple hydrogen molecules on transition metal decorated C60,” *Phys. Rev. B - Condens. Matter Mater. Phys.*, vol. 72, no. 15, p. 153403, Jun. 2005.
- [165] T. Yildirim and S. Ciraci, “Titanium-decorated carbon nanotubes as a potential high-capacity hydrogen storage medium,” *Phys. Rev. Lett.*, vol. 94, no. 17, p. 175501, Jun. 2005.
- [166] Q. Sun, P. Jena, Q. Wang, and M. Marquez, “First-principles study of hydrogen storage on Li12C60,” *J. Am. Chem. Soc.*, vol. 128, no. 30, pp. 9741–9745, Jun. 2006.
- [167] L. Chen, X. Chen, J. Liu, P. Xiang, F. Zhuge, and B. Xiao, “Li decorated Be 3 C 2 as light-weight host material for reversible hydrogen storage,” *Appl. Surf. Sci.*, vol. 459, pp. 217–223, Oct. 2018.
- [168] Y. Chen, J. Dai, and Y. Song, “Stability and hydrogen adsorption properties of Mg/Mg2Ni interface: A first principles study,” *Int. J. Hydrogen Energy*, vol. 43, no. 34, pp. 16598–16608, Oct. 2018.
- [169] M. R. Mananghaya, “Hydrogen saturation limit of Ti-doped BN nanotube with B-N defects: An insight from DFT calculations,” *Int. J. Hydrogen Energy*, vol. 43, no. 22, pp. 10368–10375, Oct. 2018.
- [170] W. C. Conner and J. L. Falconer, “Spillover in Heterogeneous Catalysis,” *Chem. Rev.*, vol. 95, no. 3, pp. 759–788, Apr. 1995.
- [171] S. Khoobiar, “Particle to Particle Migration of Hydrogen Atoms on Platinum—Alumina Catalysts from Particle to Neighboring Particles,” *J. Phys. Chem.*, vol. 68, no. 2, pp. 411–412, Apr. 1964.
- [172] R. Kramer and M. Andre, “Adsorption of atomic hydrogen on alumina by hydrogen spillover,” *J. Catal.*, vol. 58, no. 2, pp. 287–295, Apr. 1979.
- [173] U. Roland, T. Braunschweig, and F. Roessner, “On the nature of spilt-over hydrogen,” *J. Mol. Catal. A Chem.*, vol. 127, no. 1, pp. 61–84, Jan. 1997.
- [174] T. Braunschweig, U. Roland, and H. Winkler, “Electrical conductivity study of hydrogen spillover on TiO2,” in *Studies in Surface Science and Catalysis*, vol. 77, T. Inui, K. Fujimoto, T. Uchijima, and M. Masai, Eds. Elsevier, 1993, pp. 183–188.
- [175] T. S. King, X. Wu, and B. C. Gerstein, “Direct evidence for spillover of hydrogen from ruthenium to copper in supported copper-ruthenium/silica catalysts: a study by NMR of chemisorbed hydrogen,” *J. Am. Chem. Soc.*, vol. 108, no. 19, pp. 6056–6058, Jan. 1986.
- [176] M. A. Chesters, K. J. Packer, H. E. Viner, M. A. P. Wright, and D. Lennon,

- “Variable-temperature,  $^1\text{H}$  NMR study of hydrogen chemisorption on EuroPt-1,” *J. Chem. Soc. Faraday Trans.*, vol. 92, no. 23, pp. 4709–4716, Jan. 1996.
- [177] T.-C. Sheng and I. D. Gay, “Proton magnetic resonance of hydrogen adsorbed on supported platinum catalysts,” *J. Catal.*, vol. 71, no. 1, pp. 119–126, Apr. 1981.
- [178] R. R. Cavanagh and J. T. Yates, “Hydrogen spillover on alumina—A study by infrared spectroscopy,” *J. Catal.*, vol. 68, no. 1, pp. 22–26, Jan. 1981.
- [179] U. Roland, R. Salzer, and S. Stolle, “Investigation of Hydrogen and Deuterium Spillover on Y Zeolites by FT-IR Microscopy – Rate Determining Steps,” in *Studies in Surface Science and Catalysis*, vol. 84, J. Weitkamp, H. G. Karge, H. Pfeifer, and W. Hölderich, Eds. Elsevier, 1994, pp. 1231–1238.
- [180] J. L. Blackburn *et al.*, “Spectroscopic Identification of Hydrogen Spillover Species in Ruthenium-Modified High Surface Area Carbons by Diffuse Reflectance Infrared Fourier Transform Spectroscopy,” *J. Phys. Chem. C*, vol. 116, no. 51, pp. 26744–26755, Jan. 2012.
- [181] A. Gutsze, U. Roland, and H. G. Karge, “Evidence for a charge transfer from spilt-over hydrogen to platinum by means of ESR spectroscopy,” in *Studies in Surface Science and Catalysis*, vol. 112, C. Li and Q. Xin, Eds. Elsevier, 1997, pp. 417–424.
- [182] P. C. H. Mitchell, A. J. Ramirez-Cuesta, S. F. Parker, and J. Tomkinson, “Inelastic neutron scattering in spectroscopic studies of hydrogen on carbon-supported catalysts-experimental spectra and computed spectra of model systems,” *J. Mol. Struct.*, vol. 651–653, pp. 781–785, Apr. 2003.
- [183] P. Albers, R. Burmeister, K. Seibold, G. Prescher, S. F. Parker, and D. K. Ross, “Investigations of palladium catalysts on different carbon supports,” *J. Catal.*, vol. 181, no. 1, pp. 145–154, Apr. 1999.
- [184] C.-S. Tsao *et al.*, “Hydrogen Spillover Effect of Pt-Doped Activated Carbon Studied by Inelastic Neutron Scattering,” *J. Phys. Chem. Lett.*, vol. 2, no. 18, pp. 2322–2325, Jan. 2011.
- [185] J. T. Miller, B. L. Meyers, F. S. Modica, G. S. Lane, M. Vaarkamp, and D. C. Koningsberger, “Hydrogen Temperature-Programmed Desorption ( $\text{H}_2$  TPD) of Supported Platinum Catalysts,” *J. Catal.*, vol. 143, no. 2, pp. 395–408, Apr. 1993.
- [186] B. Lin, R. Wang, X. Yu, J. Lin, F. Xie, and K. Wei, “Physicochemical Characterization and  $\text{H}_2$ -TPD Study of Alumina Supported Ruthenium Catalysts,” *Catal. Letters*, vol. 124, no. 3–4, pp. 178–184, Apr. 2008.
- [187] Z. Hu, K. Kunimori, and T. Uchijima, “Interaction of hydrogen and oxygen with niobia-supported and niobia-promoted rhodium catalysts,” *Appl. Catal.*,

- vol. 69, no. 1, pp. 253–268, Jan. 1991.
- [188] G. M. Pajonk, “Contribution of spillover effects to heterogeneous catalysis,” *Appl. Catal. A Gen.*, vol. 202, no. 2, pp. 157–169, Apr. 2000.
- [189] F. Roessner, U. Mroczek, and A. Hagen, “Hydrogen spillover in the conversion of cyclohexane on ZSM-5 zeolites,” in *Studies in Surface Science and Catalysis*, vol. 77, T. Inui, K. Fujimoto, T. Uchijima, and M. Masai, Eds. Elsevier, 1993, pp. 151–158.
- [190] J. M. Parera, E. M. Traffano, J. C. Musso, and C. L. Pieck, “Hydrogen and Oxygen Spillover on Pt/Al<sub>2</sub>O<sub>3</sub> During Naphtha Reforming,” in *Studies in Surface Science and Catalysis*, vol. 17, G. M. Pajonk, S. J. Teichner, and J. E. Germain, Eds. Elsevier, 1983, pp. 101–108.
- [191] J. Sculley, D. Yuan, and H. C. Zhou, “The current status of hydrogen storage in metal-organic frameworks - Updated,” *Energy Environ. Sci.*, vol. 4, no. 8, pp. 2721–2735, Apr. 2011.
- [192] Y. Li and R. T. Yang, “Significantly Enhanced Hydrogen Storage in Metal–Organic Frameworks via Spillover,” *J. Am. Chem. Soc.*, vol. 128, no. 3, pp. 726–727, Jan. 2006.
- [193] D. Nabaho, J. W. (Hans. Niemantsverdriet, M. Claeys, and E. van Steen, “Hydrogen spillover in the Fischer–Tropsch synthesis: An analysis of gold as a promoter for cobalt–alumina catalysts,” *Catal. Today*, vol. 275, pp. 27–34, 2016.
- [194] S. Sun, N. Tsubaki, and K. Fujimoto, “The reaction performances and characterization of Fischer-Tropsch synthesis Co/SiO<sub>2</sub> catalysts prepared from mixed cobalt salts,” *Appl. Catal. A Gen.*, vol. 202, no. 1, pp. 121–131, Jan. 2000.
- [195] D. Üner and M. Y. Aslan, “Using spilled over hydrogen in NH<sub>3</sub> synthesis over supported Ru catalysts,” *Catal. Today*, vol. 272, pp. 49–57, Apr. 2016.
- [196] L. Wang, N. R. Stuckert, H. Chen, and R. T. Yang, “Effects of Pt Particle Size on Hydrogen Storage on Pt-Doped Metal–Organic Framework IRMOF-8,” *J. Phys. Chem. C*, vol. 115, no. 11, pp. 4793–4799, Apr. 2011.
- [197] H. Shen, X. Wu, D. Jiang, X. Li, and J. Ni, “Identification of active sites for hydrogenation over Ru/SBA-15 using in situ Fourier-transform infrared spectroscopy,” *Chinese J. Catal.*, vol. 38, no. 9, pp. 1597–1602, Jan. 2017.
- [198] T.-Y. Chung, C.-S. Tsao, H.-P. Tseng, C.-H. Chen, and M.-S. Yu, “Effects of oxygen functional groups on the enhancement of the hydrogen spillover of Pd-doped activated carbon,” *J. Colloid Interface Sci.*, vol. 441, pp. 98–105, Apr. 2015.
- [199] W. Karim *et al.*, “Catalyst support effects on hydrogen spillover,” *Nature*, vol.

541, no. 7635, pp. 68–71, Apr. 2017.

- [200] L. Wang and R. T. Yang, “New sorbents for hydrogen storage by hydrogen spillover - A review,” *Energy Environ. Sci.*, vol. 1, no. 2, pp. 268–279, Apr. 2008.
- [201] S. Dag, Y. Ozturk, S. Ciraci, and T. Yildirim, “Adsorption and dissociation of hydrogen molecules on bare and functionalized carbon nanotubes,” *Phys. Rev. B - Condens. Matter Mater. Phys.*, vol. 72, no. 15, p. 155404, Jun. 2005.
- [202] R. Prins, “Hydrogen spillover. Facts and fiction,” *Chem. Rev.*, vol. 112, no. 5, pp. 2714–2738, Mar. 2012.
- [203] R. Prins, V. K. Palfi, and M. Reiher, “Hydrogen spillover to nonreducible supports,” *J. Phys. Chem. C*, vol. 116, no. 27, pp. 14274–14283, Apr. 2012.
- [204] H. Shin, M. Choi, and H. Kim, “A mechanistic model for hydrogen activation, spillover, and its chemical reaction in a zeolite-encapsulated Pt catalyst,” *Phys. Chem. Chem. Phys.*, vol. 18, no. 10, pp. 7035–7041, Feb. 2016.
- [205] J. Im, H. Shin, H. Jang, H. Kim, and M. Choi, “Maximizing the catalytic function of hydrogen spillover in platinum-encapsulated aluminosilicates with controlled nanostructures,” *Nat. Commun.*, vol. 5, p. 3370, Feb. 2014.
- [206] C. Spreafico, W. Karim, Y. Ekinici, J. A. Van Bokhoven, and J. Van De Vondele, “Hydrogen Adsorption on Nanosized Platinum and Dynamics of Spillover onto Alumina and Titania,” *J. Phys. Chem. C*, vol. 121, no. 33, pp. 17862–17872, Jan. 2017.
- [207] M. Nurunnabi, K. Murata, K. Okabe, T. Hanaoka, T. Miyazawa, and K. Sakanishi, “Effects of ruthenium precursors on Ru/Mn/Al<sub>2</sub>O<sub>3</sub> and Ru/Al<sub>2</sub>O<sub>3</sub> catalysts for Fischer-Tropsch synthesis,” *J. Japan Pet. Inst.*, vol. 53, no. 2, pp. 75–82, Oct. 2010.
- [208] H. Y. Lin and Y. W. Chen, “The kinetics of H<sub>2</sub> adsorption on supported ruthenium catalysts,” *Thermochim. Acta*, vol. 419, no. 1–2, pp. 283–290, Jan. 2004.
- [209] J. Hájek *et al.*, “Ruthenium-modified MCM-41 mesoporous molecular sieve and Y zeolite catalysts for selective hydrogenation of cinnamaldehyde,” *Appl. Catal. A Gen.*, vol. 251, no. 2, pp. 385–396, Jan. 2003.
- [210] Q. Yao *et al.*, “Ultrafine Ru nanoparticles embedded in SiO<sub>2</sub> nanospheres: Highly efficient catalysts for hydrolytic dehydrogenation of ammonia borane,” *J. Power Sources*, vol. 257, pp. 293–299, Jan. 2014.
- [211] R. I. Masel, *Principles of Adsorption and Reaction on Solid Surfaces.*, 1st ed. USA: John Wiley & Sons, Ltd, 1996.
- [212] M. Klell, “Storage of Hydrogen in the Pure Form,” in *Handbook of Hydrogen Storage: New Materials for Future Energy Storage*, John Wiley & Sons, Ltd,

- 2010, pp. 1–37.
- [213] R. Bhowmick *et al.*, “Hydrogen Spillover in Pt-Single-Walled Carbon Nanotube Composites: Formation of Stable C–H Bonds,” *J. Am. Chem. Soc.*, vol. 133, no. 14, pp. 5580–5586, Feb. 2011.
- [214] N. Saadatjou, A. Jafari, and S. Sahebdehfar, “Ruthenium Nanocatalysts for Ammonia Synthesis: A Review,” *Chem. Eng. Commun.*, vol. 202, no. 4, pp. 420–448, Apr. 2015.
- [215] S. Giddey, S. P. S. Badwal, C. Munnings, and M. Dolan, “Ammonia as a Renewable Energy Transportation Media,” *ACS Sustain. Chem. Eng.*, vol. 5, no. 11, pp. 10231–10239, Mar. 2017.
- [216] C. H. Christensen, T. Johannessen, R. Z. Sørensen, and J. K. Nørskov, “Towards an ammonia-mediated hydrogen economy?,” *Catal. Today*, vol. 111, no. 1–2, pp. 140–144, Sep. 2006.
- [217] Á. Logadóttir and J. K. Nørskov, “Ammonia synthesis over a Ru(0001) surface studied by density functional calculations,” *J. Catal.*, vol. 220, no. 2, pp. 273–279, Dec. 2003.
- [218] V. Temkin, M.I. Pyzhev, “Kinetics of ammonia synthesis on promoted iron catalyst,” *Acta Phys. Chim. USSR*, vol. 12, pp. 327–356, 1940.
- [219] A. Ozaki, K. Aika, and H. Hori, “A New Catalyst System for Ammonia Synthesis,” *Bull. Chem. Soc. Jpn.*, vol. 44, no. 11, pp. 3216–3216, Apr. 2006.
- [220] H. Bielawa, O. Hinrichsen, A. Birkner, and M. Muhler, “The Ammonia-Synthesis Catalyst of the Next Generation: Barium-Promoted Oxide-Supported Ruthenium,” *Angew. Chemie Int. Ed.*, vol. 40, no. 6, pp. 1061–1063, Mar. 2001.
- [221] K. Chao, L. Lin, and M. Yang, “The influence of the precursor form on the ammonia synthesis activity of ruthenium zeolite catalysts,” *Catal. Letters*, vol. 38, no. 3–4, pp. 279–282, Mar. 1996.
- [222] Q. C. Xu, J. D. Lin, J. Li, X. Z. Fu, Y. Liang, and D. W. Liao, “Microwave-assisted synthesis of MgO-CNTs supported ruthenium catalysts for ammonia synthesis,” *Catal. Commun.*, vol. 8, no. 12, pp. 1881–1885, Oct. 2007.
- [223] B. C. McClaine, T. Becue, C. Lock, and R. J. Davis, “Kinetic analysis of ammonia synthesis catalyzed by barium-promoted ruthenium supported on zeolite X,” *J. Mol. Catal. A Chem.*, vol. 163, no. 1–2, pp. 105–116, Mar. 2000.
- [224] P. Seetharamulu, K. Hari Prasad Reddy, A. H. Padmasri, K. S. Rama Rao, and B. David Raju, “Role of promoters on highly active nano-Ru catalyst supported on Mg-Al hydrotalcite precursor for the synthesis of ammonia,” *Catal. Today*, vol. 141, no. 1–2, pp. 94–98, Dec. 2009.
- [225] S. F. Yin, B. Q. Xu, S. J. Wang, and C. T. Au, “Nanosized Ru on high-surface-area superbasic ZrO<sub>2</sub>-KOH for efficient generation of hydrogen via ammonia

- decomposition,” *Appl. Catal. A Gen.*, vol. 301, no. 2, pp. 202–210, Dec. 2006.
- [226] Y. Horiuchi, G. Kamei, M. Saito, and M. Matsuoka, “Development of Ruthenium-loaded Alkaline-earth Titanates as Catalysts for Ammonia Synthesis,” *Chem. Lett.*, vol. 42, no. 10, pp. 1282–1284, Dec. 2013.
- [227] D. Stošić *et al.*, “Glycerol dehydration over calcium phosphate catalysts: Effect of acidic-basic features on catalytic performance,” *Appl. Catal. A Gen.*, vol. 447–448, pp. 124–134, Dec. 2012.
- [228] A. Venugopal and M. S. Scurrall, “Hydroxyapatite as a novel support for gold and ruthenium catalysts: Behaviour in the water gas shift reaction,” *Appl. Catal. A Gen.*, vol. 245, no. 1, pp. 137–147, Mar. 2003.
- [229] M. Kanezashi, A. Yamamoto, T. Yoshioka, and T. Tsuru, “Characteristics of ammonia permeation through porous silica membranes,” *AIChE J.*, vol. 56, no. 5, pp. 1204–1212, Sep. 2010.
- [230] K. Aika, “Role of alkali promoter in ammonia synthesis over ruthenium catalysts—Effect on reaction mechanism,” *Catal. Today*, vol. 286, pp. 14–20, Apr. 2017.
- [231] Z. Q. Wang, Y. C. Ma, and J. X. Lin, “Ruthenium catalyst supported on high-surface-area basic ZrO<sub>2</sub> for ammonia synthesis,” *J. Mol. Catal. A Chem.*, vol. 378, pp. 307–313, Dec. 2013.
- [232] G. Rambeau, A. Jorti, and H. Amariglio, “Improvement of the catalytic performance of an osmium powder in ammonia synthesis by the use of a cyclic procedure,” *Appl. Catal.*, vol. 3, no. 3, pp. 273–282, Nov. 1982.
- [233] H. Amariglio and G. Rambeau, “On the possibility of rate improvements by a periodic operation of catalytic reactors,” *Chemical Engineering Science*, vol. 39, no. 9, p. 1433, 1984.
- [234] B. D. Unger and R. G. Rinker, “Ammonia-Synthesis Reaction in the Chromatographic Regime,” *Ind. Eng. Chem. Fundam.*, vol. 15, no. 3, pp. 225–227, Nov. 1976.
- [235] A. K. Jain, R. R. Hudgins, and P. L. Silveston, “Influence of forced feed composition cycling on the rate of ammonia synthesis over an industrial iron catalyst part I — Effect of cycling parameters and mean composition,” *Can. J. Chem. Eng.*, vol. 61, no. 6, pp. 824–832, Apr. 1983.
- [236] L. Chiao, R. G. Rinker, F. K. Zack, and J. Thullie, “Concentration Forcing in Ammonia Synthesis: Plug-Flow Experiments at High Temperature and Pressure,” *Chem. Eng. Commun.*, vol. 49, no. 4–6, pp. 273–289, Apr. 1987.
- [237] L. Chiao and R. G. Rinker, “A kinetic study of ammonia synthesis: modeling high-pressure steady-state and forced-cycling behavior,” *Chem. Eng. Sci.*, vol. 44, no. 1, pp. 9–19, Apr. 1989.

- [238] T. Egyházy, J. Kovács, and J. Scholtz, “Experimental study of flow reversal ammonia synthesis,” *Chem. Eng. Technol.*, vol. 21, no. 12, pp. 967–974, Apr. 1998.
- [239] M. S. Huberty, A. L. Wagner, A. McCormick, and E. Cussler, “Ammonia absorption at haber process conditions,” *AIChE J.*, vol. 58, no. 11, pp. 3526–3532, Jan. 2012.
- [240] C. Smith, A. V. McCormick, and E. L. Cussler, “Optimizing the Conditions for Ammonia Production Using Absorption,” *ACS Sustain. Chem. Eng.*, vol. 7, no. 4, pp. 4019–4029, Jan. 2019.
- [241] C. Smith, M. Malmali, C. Y. Liu, A. V. McCormick, and E. L. Cussler, “Rates of Ammonia Absorption and Release in Calcium Chloride,” *ACS Sustain. Chem. Eng.*, vol. 6, no. 9, pp. 11827–11835, Jan. 2018.
- [242] G. Thomas and G. Parks, “Potential Roles of Ammonia in a Hydrogen Economy,” *Energy*, 2006. [Online]. Available: [https://www.energy.gov/sites/prod/files/2015/01/f19/fcto\\_nh3\\_h2\\_storage\\_white\\_paper\\_2006.pdf](https://www.energy.gov/sites/prod/files/2015/01/f19/fcto_nh3_h2_storage_white_paper_2006.pdf). [Accessed: 07-Oct-2019].
- [243] S. D. Minter, P. Christopher, and S. Linic, “Recent Developments in Nitrogen Reduction Catalysts: A Virtual Issue,” *ACS Energy Lett.*, vol. 4, no. 1, pp. 163–166, Aug. 2019.
- [244] C. D. Zeinalipour-Yazdi, J. S. J. Hargreaves, and C. R. A. Catlow, “Low-T Mechanisms of Ammonia Synthesis on Co<sub>3</sub>Mo<sub>3</sub>N,” *J. Phys. Chem. C*, vol. 122, no. 11, pp. 6078–6082, Apr. 2018.
- [245] M. Malmali, Y. Wei, A. McCormick, and E. L. Cussler, “Ammonia Synthesis at Reduced Pressure via Reactive Separation,” *Ind. Eng. Chem. Res.*, vol. 55, no. 33, pp. 8922–8932, Jan. 2016.
- [246] E. Cussler, A. McCormick, M. Reese, and M. Malmali, “Ammonia Synthesis at Low Pressure,” *J. Vis. Exp.*, no. 126, p. e55691, Jan. 2017.
- [247] M. Palys, A. McCormick, E. Cussler, and P. Daoutidis, “Modeling and Optimal Design of Absorbent Enhanced Ammonia Synthesis,” *Processes*, vol. 6, no. 7, p. 91, Jan. 2018.
- [248] K. Aika and A. Ozaki, “Mechanism of Ammonia Synthesis over Molybdenum Nitride,” *Bull. Chem. Soc. Jpn.*, vol. 41, no. 11, p. 2818, Apr. 1968.
- [249] G. K. Boreskov, V. M. Kolchanova, E. E. Rachkovskii, S. N. Filimonova, and A. V. Khasin, “Nitrogen activation mechanism in the catalytic synthesis of ammonia on iron and molybdenum nitride,” *Kinet. Catal. (USSR) (Engl. Transl.)*; (*United States*), vol. 16:5, Apr. 1975.
- [250] S. M. Hunter, D. McKay, R. I. Smith, J. S. J. Hargreaves, and D. H. Gregory, “Topotactic nitrogen transfer: Structural transformation in cobalt molybdenum

- nitrides,” *Chem. Mater.*, vol. 22, no. 9, pp. 2898–2907, Apr. 2010.
- [251] C. D. Zeinalipour-Yazdi, J. S. J. Hargreaves, and C. R. A. Catlow, “DFT-D3 Study of Molecular N<sub>2</sub> and H<sub>2</sub> Activation on Co<sub>3</sub>Mo<sub>3</sub>N Surfaces,” *J. Phys. Chem. C*, vol. 120, no. 38, pp. 21390–21398, Apr. 2016.
- [252] C. D. Zeinalipour-Yazdi, J. S. J. Hargreaves, and C. R. A. Catlow, “Nitrogen Activation in a Mars–van Krevelen Mechanism for Ammonia Synthesis on Co<sub>3</sub>Mo<sub>3</sub>N,” *J. Phys. Chem. C*, vol. 119, no. 51, pp. 28368–28376, Apr. 2015.
- [253] A. K. Santra, B. K. Min, C. W. Yi, K. Luo, T. V. Choudhary, and D. W. Goodman, “Decomposition of NH<sub>3</sub> on Ir(100): A temperature programmed desorption study,” *J. Phys. Chem. B*, vol. 106, no. 2, pp. 340–344, Mar. 2002.
- [254] S. Scirè, R. Fiorenza, A. Gulino, A. Cristaldi, and P. M. Riccobene, “Selective oxidation of CO in H<sub>2</sub>-rich stream over ZSM5 zeolites supported Ru catalysts: An investigation on the role of the support and the Ru particle size,” *Appl. Catal. A Gen.*, vol. 520, pp. 82–91, Mar. 2016.
- [255] S. Scirè, G. Burgio, C. Crisafulli, and S. Minicò, “Dehydroisomerization of n-butane over H-Y zeolite supported Pt and Pt,Sn catalysts,” *Appl. Catal. A Gen.*, vol. 274, no. 1–2, pp. 151–157, Mar. 2004.
- [256] Z. I. Önsan, “Microkinetic analysis of heterogeneous catalytic systems,” in *Multiphase Catalytic Reactors*, John Wiley & Sons, Ltd, 2016, pp. 17–52.
- [257] H. S. Fogler, *Pearson - Elements of Chemical Reaction Engineering: Pearson New International Edition, 4/E - H. Scott Fogler*, 4th Editio. Pearson, 2013.



## APPENDICES

### A. Supplementary Information – Fundamentals of Hydrogen Storage Properties over Ru/SiO<sub>2</sub> and Ru/Vulcan

#### A.1. H<sub>2</sub>-Chemisorption Experiment

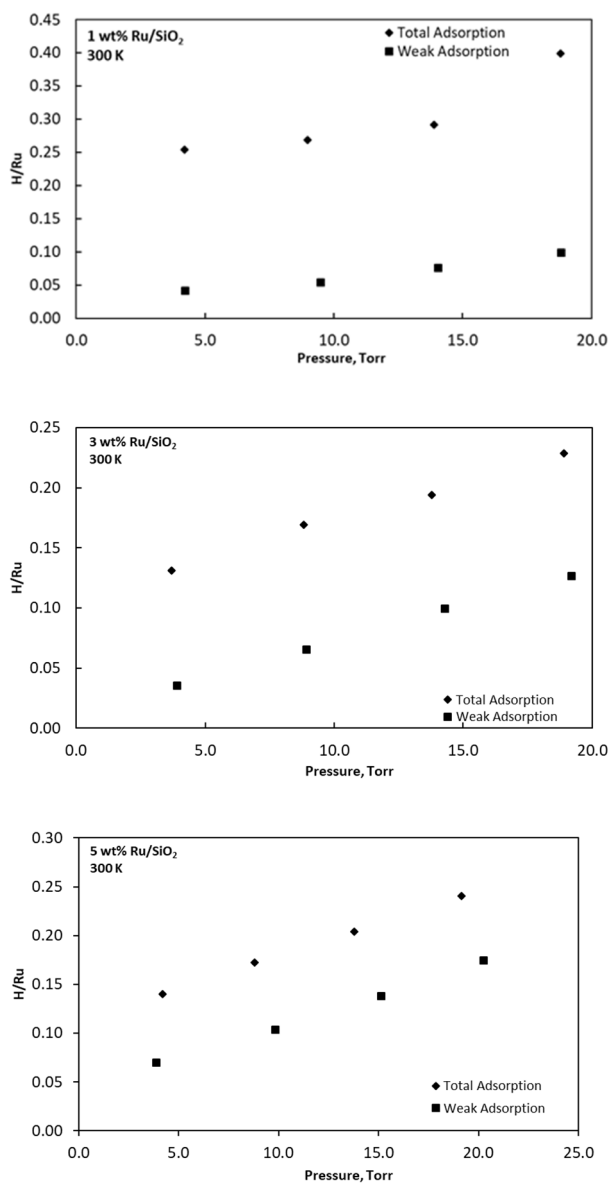


Figure A.1. H<sub>2</sub>-chemisorption results of 1,3, and 5 wt% Ru/SiO<sub>2</sub> at 300 K

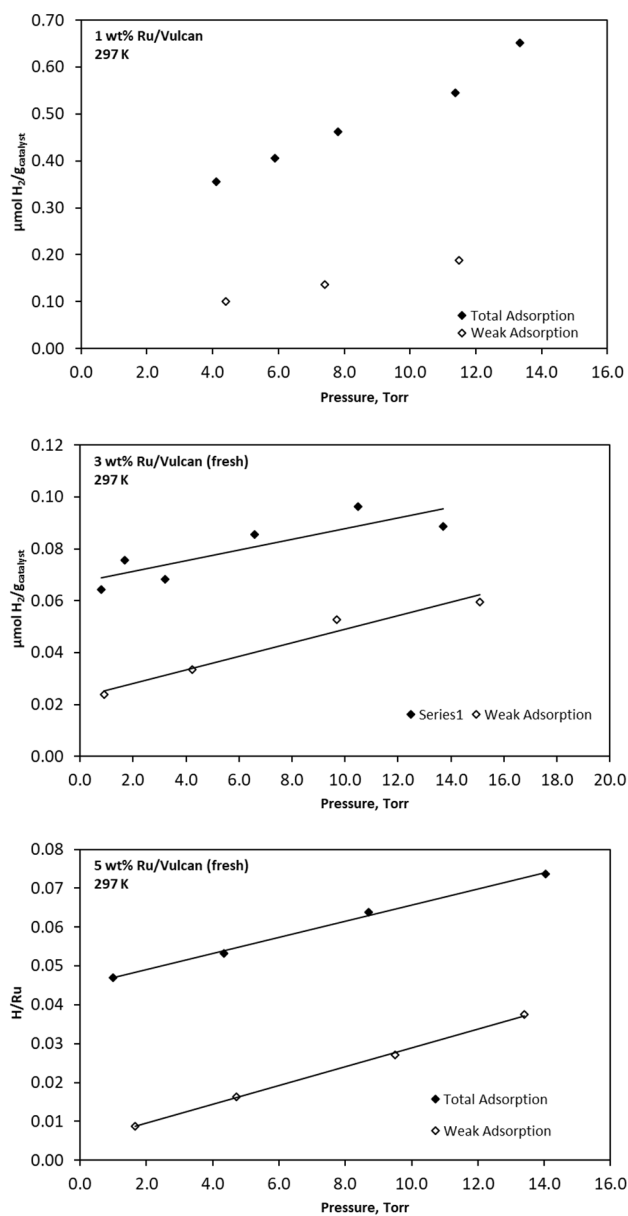


Figure A.2. H<sub>2</sub>-chemisorption results of 1,3, and 5 wt% Ru/Vulcan at 297 K

## A.2. Average Particle Size Distribution of Ru/SiO<sub>2</sub> and Ru/Vulcan

Table A.1. Summary of Results of H<sub>2</sub>-Chemisorption and HR-TEM Analysis of Ru/SiO<sub>2</sub>

	Total H/Ru	Weak H/Ru	Strong H/Ru	d <sub>p</sub> , nm H <sub>2</sub> -Chemisorption	d <sub>p</sub> , nm HR-TEM
1 wt% Ru/SiO <sub>2</sub>	0.25	0.03	0.22	5	1.2
3 wt% Ru/SiO <sub>2</sub>	0.12	0.02	0.10	10	2.1
5 wt% Ru/SiO <sub>2</sub>	0.12	0.05	0.07	14	2.5

Table A.2. Summary of Results of H<sub>2</sub>-Chemisorption and HR-TEM Analysis of Ru/Vulcan

	Total H/Ru	Weak H/Ru	Strong H/Ru	d <sub>p</sub> , nm H <sub>2</sub> -Chemisorption	d <sub>p</sub> , nm HR-TEM
1 wt% Ru/Vulcan	0.29	0.01	0.28	3.6	2.1
3 wt% Ru/Vulcan	0.07	0.02	0.05	20.0	6.3
5 wt% Ru/Vulcan	0.05	0.01	0.04	25.0	9.4

## A.3. Cooling in H<sub>2</sub> Flow

As a part of temperature programmed analysis, the catalysts were cooled down to room temperature in the presence of H<sub>2</sub> flow (%10 H<sub>2</sub> in Ar) and TCD signals were recorded as shown in Figure A.3 and A.4. When Figure A.3 was analyzed, H<sub>2</sub> adsorption started for 1,3, and 5 wt% Ru/SiO<sub>2</sub> catalysts at 408 °C, 317 °C, and 166 °C, respectively. When the cooling down in H<sub>2</sub> flow profiles of 1,3, and 5 wt% Ru/Vulcan materials were examined (Figure A.4), a peak at high temperature (above 500 °C) and a peak at medium temperature (310 °C) were observed. It can be said that the hydrogen uptake continued over Ru/SiO<sub>2</sub> and Ru/Vulcan materials during the cooling process under the flow of H<sub>2</sub> to room temperature.

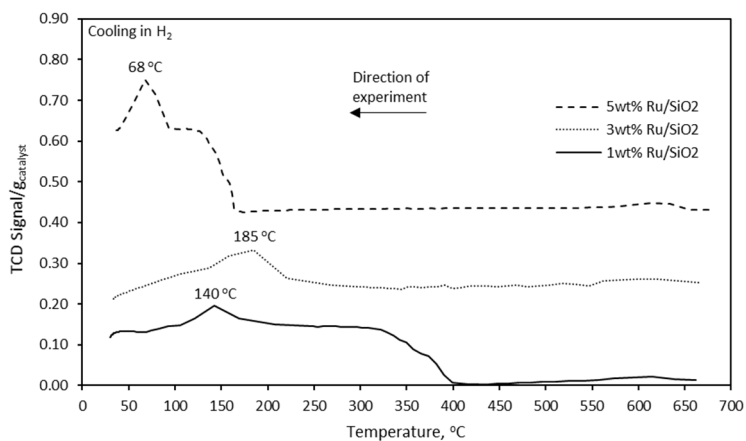


Figure A.3. Cooling profiles of Ru/SiO<sub>2</sub> catalysts under 10% H<sub>2</sub> in Ar flow. The profiles were obtained after TPR analysis

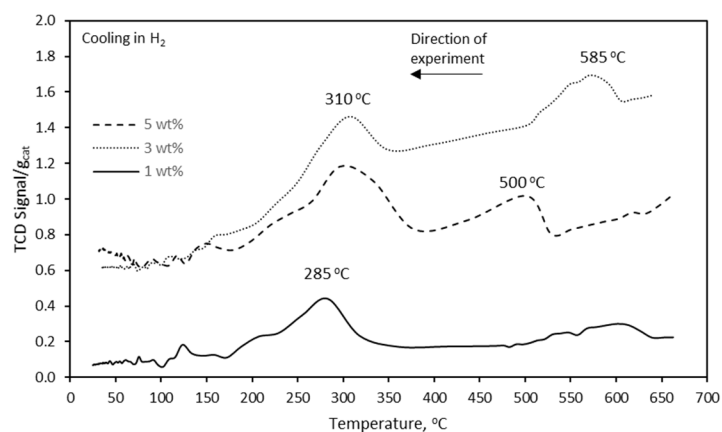


Figure A.4. Cooling profiles of Ru/Vulcan catalysts under 10% H<sub>2</sub> in Ar flow. The profiles were obtained after TPR analysis

## B. Supplementary Information – Support Effects in Ammonia Synthesis

### B.1. Heat of Adsorption of H<sub>2</sub> and CO Measurement

The heat of adsorption of H<sub>2</sub> and CO over 1.37 wt% Ru/Zeolite-Y were determined and shown in Figure B.1. The initial heat of adsorption value of CO and H<sub>2</sub> were measured as 233 kJ mol<sup>-1</sup> and 98 kJ mol<sup>-1</sup>, respectively. Both H<sub>2</sub> and CO adsorbates exhibited a relatively constant heat of adsorption until a saturation coverage of 0.30 adsorbate/Ru stoichiometry, indicating energetically uniform active sites.

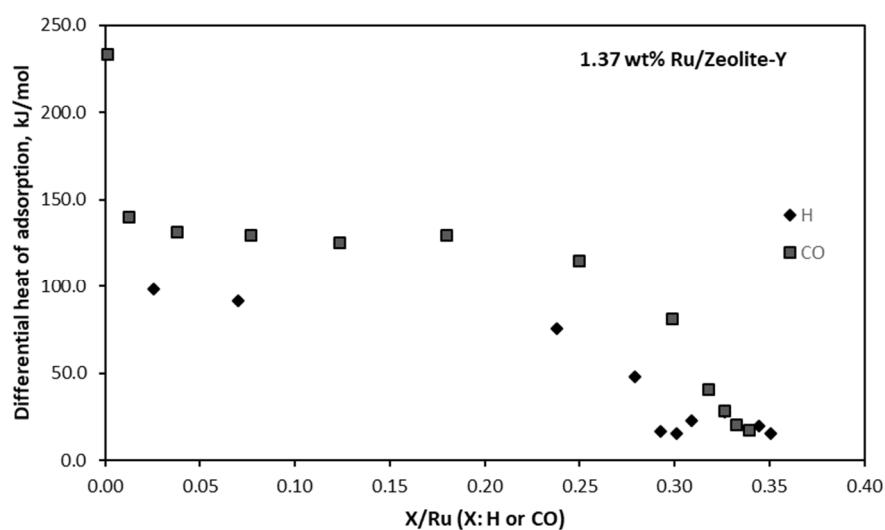


Figure B.1. Differential heats of adsorption of hydrogen and CO over 1.37 wt% Ru/Zeolite-Y.

### B.2. Ru metal dispersions of Ru/HAp catalysts

Table B.1 H<sub>2</sub>-chemisorption results of Ru/HAp catalysts with different Ru metal loadings.

	Metal Loading (ICP-OES), wt %	H <sub>2</sub> Chemisorption, %	Average Particle Diameter, nm (H <sub>2</sub> -chem.)
1 wt% Ru/HAp	1.00	8	12.5
2 wt% Ru/HAp	2.00	12	8.3
3 wt% Ru/HAp	2.93	16	6.2
4 wt% Ru/HAp	3.96	30	3.3

### B.3. Details of Single Point Ammonia Adsorption Calorimetry

#### Ammonia Adsorption

The change of heat flow during the adsorption of ammonia over Zeolite-Y, HAp, and Vulcan are given in Figure B.2. It is obvious that HAp material has a sharp heat flow peak with respect to Zeolite-Y and Vulcan materials. On the contrary, Zeolite-Y and Vulcan have a tail-like behavior with time.

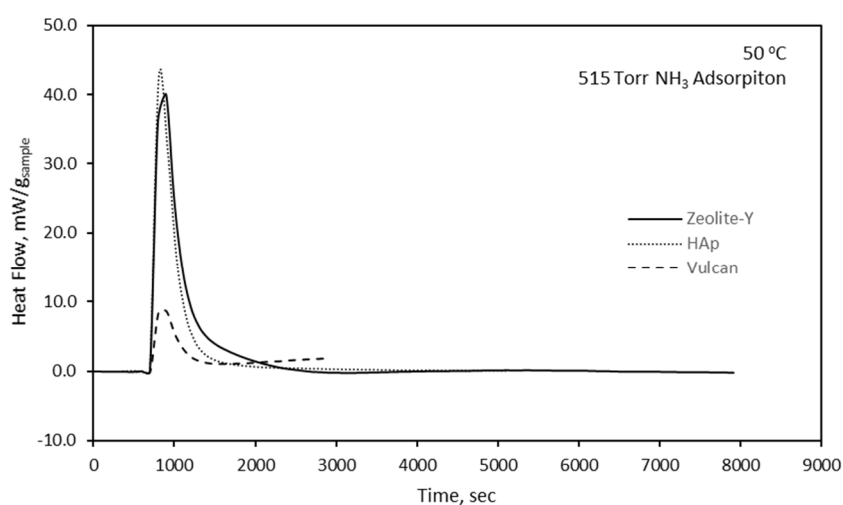


Figure B.2 Heat flow during 515 Torr NH<sub>3</sub> adsorption at 50 °C

The summary of single point integral heat of adsorption of ammonia obtained by adsorption calorimetry on Zeolite-Y, HAp and Vulcan Carbon support materials are given in Table 3. While the lowest ammonia adsorption is measured over HAp, the highest heat release is calculated over HAp.

### Evacuation

Following ammonia adsorption at 50 °C, the heat flow during the evacuation of the manifold at 50 °C is also monitored and given in Figure B.3. Zeolite-Y and Vulcan materials give one negative peak during the evacuation. While, the heat flow over Vulcan material reaches its starting value with time, the heat flow does not turn back to its starting value over Zeolite-Y. On the contrary, two negative peaks are observed in the presence of HAp material. The observed negative peaks during the evacuation of the manifold (Figure B.3.) is due to desorption of adsorbed ammonia from the support materials.

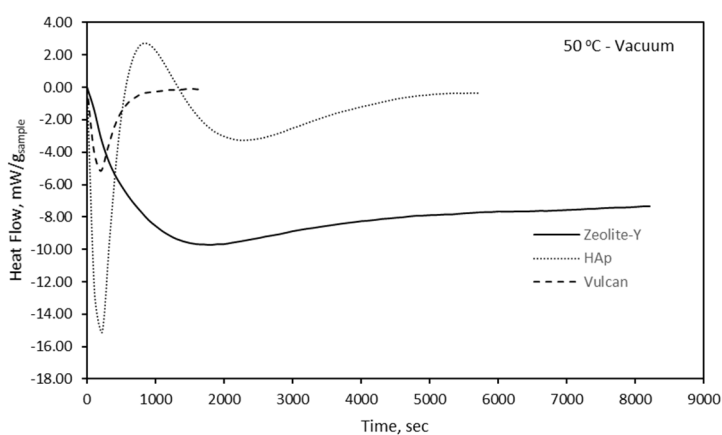


Figure B.3. Heat flow during evacuation at 50 °C after 515 Torr NH<sub>3</sub> adsorption

### **B.4. Effect of reactant pressure on NH<sub>3</sub> synthesis reaction rate**

Table B.1 Ammonia formation rates at various reactant partial pressures at 300 °C

	NH <sub>3</sub> formation rate with Ar flow, $\mu\text{mol NH}_3/\text{g}_{\text{catalyst-h}}$ , H <sub>2</sub> :N <sub>2</sub> :Ar=3:1:2 100 mL/min	NH <sub>3</sub> formation rate without Ar flow, $\mu\text{mol NH}_3/\text{g}_{\text{catalyst-h}}$ , H <sub>2</sub> :N <sub>2</sub> =3:1 100 mL/min
4 wt% Ru/HAp	103	981
1.37 wt% Ru/Zeolite-Y	304	1118
1 wt% Ru/Vulcan	249	518

The results of ammonia formation rate experiments, operated at 300 °C and atmospheric pressure and under flow of 100 mL/min gas mixture, in the presence/absence of Ar flow are given in Table B.1. It can be seen from Table B.1 that initial ammonia synthesis rates are higher in the absence of Ar content in the reactant flow. In both cases, the highest ammonia synthesis reaction rate is observed in the presence of 1.37 wt% Ru/Zeolite-Y catalyst at 300 °C and atmospheric pressures.

The higher ammonia synthesis reaction rates obtained in the absence of Ar flow can be explained with the increase in the partial pressures of N<sub>2</sub> and H<sub>2</sub> over the catalyst surface. In addition to this, A.K. Santra *et al.* showed that increasing the partial pressure of hydrogen promoted the desorption rate of ammonia from the catalyst surface [253].

### B.5. Ammonia synthesis rate with quartz dilution

Table B.2 Initial NH<sub>3</sub> formation rates over Ru catalysts diluted with quartz (1:1, by weight), (H<sub>2</sub>:N<sub>2</sub>:Ar=3:1:2)

	Reaction Rates					
	4 wt% Ru/HAp		1.37 wt% Ru/Zeolite-Y		1 wt% Ru/Carbon	
	μmol NH <sub>3</sub> /g <sub>cat</sub> -h	TOF, s <sup>-1</sup>	μmol NH <sub>3</sub> /g <sub>cat</sub> -h	TOF, s <sup>-1</sup>	μmol NH <sub>3</sub> /g <sub>cat</sub> -h	TOF, s <sup>-1</sup>
300 °C	48.5	0.10x10 <sup>-4</sup>	78.1	0.48x10 <sup>-4</sup>	93.5	0.74x10 <sup>-4</sup>
325 °C	63.0	0.13x10 <sup>-4</sup>	150.4	0.92x10 <sup>-4</sup>	148.0	1.16x10 <sup>-4</sup>
350 °C	161.6	0.34x10 <sup>-4</sup>	307.2	1.88x10 <sup>-4</sup>	184.2	1.45x10 <sup>-4</sup>
375 °C	167.2	0.35x10 <sup>-4</sup>	364.5	2.24x10 <sup>-4</sup>	250.3	1.97x10 <sup>-4</sup>
400 °C	432.5	0.91x10 <sup>-4</sup>			410.1	3.22x10 <sup>-4</sup>

Ammonia synthesis reaction experiments over Ru catalysts diluted with quartz with a weight ratio of 1:1 were also performed at different temperatures under flow of 100 ml/min (H<sub>2</sub>:N<sub>2</sub>:Ar=3:1:2) gas mixture. Initial ammonia formation rates, reported in Table B.2 exhibited an increasing trend with increasing temperature indicating that the reaction is far away from equilibrium. The highest activity, in terms of turnover frequency, is calculated as 3.22 x 10<sup>-4</sup> s<sup>-1</sup> over 1 wt% Ru/Vulcan at 400 °C.

## B.6. Ammonia desorption over Ru catalysts diluted with quartz

Table B.3 Total desorbed amount of NH<sub>3</sub> after the reaction over Ru catalysts diluted with quartz with a weight ratio of 1:1

	Total amount of desorbed NH <sub>3</sub> , μmol/g <sub>catalyst</sub>		
	4 wt% Ru/HAp	1.37 wt% Ru/Zeolite-Y	1 wt% Ru/Vulcan
300 °C	113	55	92
325 °C	108	105	92
350 °C	120	85	88
375 °C	92	90	79
400 °C	84	75	63

The desorbed amount of ammonia decreases with increasing temperature for all catalysts as shown in Table S.4. The studies in the literature reported a low (180 – 200 °C) and a high (370 – 450 °C) desorption temperature of NH<sub>3</sub> over supported noble metal catalysts [254],[255]. It can be said that the amount of ammonia adsorption decreases with increasing temperature due to that at higher temperatures ammonia can desorb easily from the catalyst surface.

## B.7. Conversion vs. Space Time Graph

N<sub>2</sub> conversion is calculated as follows:

$$\text{Conversion} = \left( \frac{F_{N_2(\text{inlet})} - F_{N_2(\text{outlet})}}{F_{N_2(\text{inlet})}} \right)$$

Where  $F_{N_2}$  is the molar flow rate of N<sub>2</sub>. The molar flow rate of N<sub>2</sub> at the inlet of the reactor can be calculated as follows:

$$F_{N_2(\text{inlet})} = 100 \frac{\text{mL of gas mixture}}{\text{min}} \times \frac{1 \text{ mL of } N_2 \text{ gas}}{6 \text{ mL of gas mixture}} \times \frac{1 \text{ min}}{60 \text{ sec}} \\ \times \frac{1 \text{ mol of gas}}{22.4 \text{ L gas at STP}} \times \frac{1 \text{ L of gas}}{1000 \text{ mL of gas}} = 1.24 \times 10^{-5} \frac{\text{mol } N_2}{\text{sec}}$$

In order to calculate molar flow rate of N<sub>2</sub> in the outlet of the reactor, the material balance around the reactor should be set up:

$$F_{N_2(\text{inlet})} - F_{N_2(\text{outlet})} - R_{N_2} \times W_{\text{catalyst}} = \frac{dN_{N_2}}{dt}$$

Where R<sub>N<sub>2</sub></sub> is the consumption rate of N<sub>2</sub> in the reactor and W is the weight of the catalyst. The ammonia formation rate is measured as 49 μmol g<sub>catalyst</sub><sup>-1</sup> h<sup>-1</sup> over 2 wt% Ru/HAp catalyst at 300 °C. The accumulation term equal to zero due to that ammonia synthesis reaction is carried out under steady state conditions.

$$F_{N_2(\text{outlet})} = 1.24 \times 10^{-5} \frac{\text{mol N}_2}{\text{sec}} - \left[ 49 \frac{\mu\text{mol NH}_3}{\text{g}_{\text{cat}} \text{ h}} \times \frac{1 \text{ h}}{3600 \text{ sec}} \times \frac{1 \text{ mol}}{10^6 \mu\text{mol}} \times \frac{1 \text{ mol N}_2 \text{ consumed}}{2 \text{ mol NH}_3 \text{ produced}} \times \frac{1 \text{ g}_{\text{cat}}}{1000 \text{ mg}_{\text{cat}}} \times 70 \text{ mg}_{\text{cat}} \right] = 1.2399 \times 10^{-5} \frac{\text{mol N}_2}{\text{sec}}$$

Finally, conversion can be calculated as

$$\text{Conversion} = \frac{1.24 \times 10^{-5} - 1.2399 \times 10^{-5}}{1.24 \times 10^{-5}} = 8.06 \times 10^{-4}$$

In Figure B.4, the change of conversion with space-time over HAp supported Ru catalysts were given. As it can be seen Figure B.4, the N<sub>2</sub> conversion over Ru/HAp catalyst increased with increasing space-time (decreasing volumetric flow rate). Theoretically, the conversion increases with decreasing flow rate (or increasing space-time), if the reaction is carried out at lower conversions. As a result, theoretical and experimental data are in an agreement.

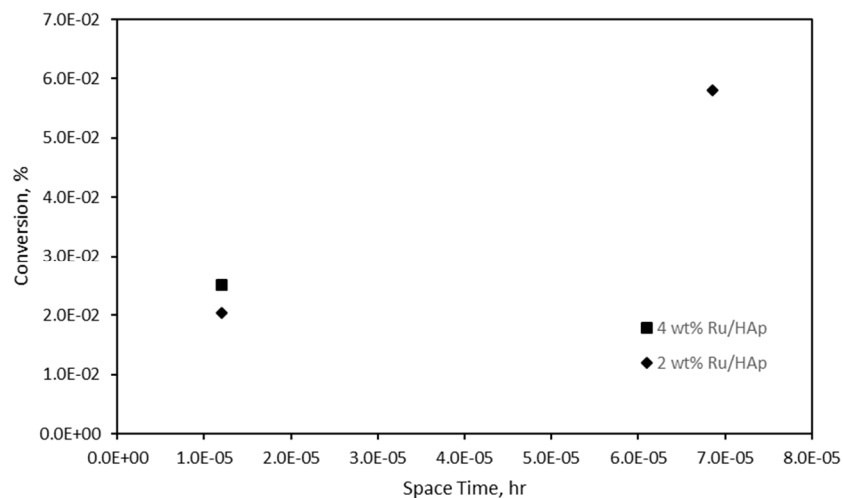


Figure B.4. Conversion vs. space-time plot for ammonia synthesis reaction over Ru/HAp catalysts at 400 °C and atmospheric pressure.

The change of conductivity with time during ammonia synthesis reaction for different volumetric flow rates given in Figure B.5. indicate that the behavior of conductivity change is different in each case which validate the data obtained in the kinetic study.

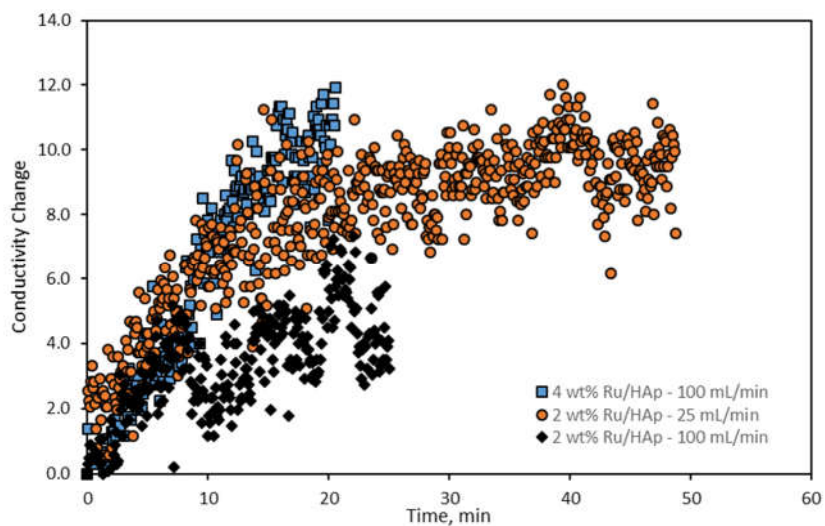


Figure B.5. Change of conductivity with time over HAp supported Ru catalysts at 400 °C and atmospheric pressures

## **C. H<sub>2</sub>-Chemisorption Experiment**

### **C.1. Reduction Procedure**

1. The appropriate amount of supported Ru catalyst is put into sample holder and sample holder is connected to the manifold.
2. Sample holder and manifold are evacuated for approximately 10 min and leak test is performed.
3. If the leak through the inside of the manifold is sufficiently low (for example; leak rate < 0.01 Torr/min), 600-700 Torr of helium gas is taken to the manifold and sample holder is started heating to the 150 °C with a temperature ramp of ca. 2 °C/min.
4. The sample was heated to 150 °C and kept at 150 °C for 30 min, followed by evacuation for 10 min.
5. After that, 100 Torr of hydrogen gas is admitted to the manifold and the temperature of the sample is increased to the 350 °C with a ramp of 5 °C/min.
6. After 30 min treatment under 100 Torr of hydrogen gas, the system is vacuumed for 10 min.
7. The same hydrogen treatment procedure (item 6) was repeated for 3-4 times with 500-600 Torr of hydrogen pressure.
8. After reduction of the catalyst at high temperature, the catalyst is cooled to the room temperature while the manifold is evacuated. The sample is vacuumed for at least 3 hours before chemisorption measurement was started.

### **D.2. Measurement of H<sub>2</sub> Adsorption Isotherms**

1. After the reduction of the catalyst is completed, the dead volume measurement is conducted. Approximately 50 Torr of helium gas is taken to the manifold while the valve of sample chamber is closed. The valve of the sample chamber is opened and waited for ca. 10 min before the pressure is recorded. Finally, the valve of the sample holder is closed and pressure is recorded again.
2. After dead volume measured is done, the manifold is evacuated for 10 min.

3. To obtain total hydrogen adsorption isotherm, a hydrogen gas pressure between 0.1 and 0.5 Torr is admitted to the manifold while valve of sample chamber is closed. The gas pressure in the manifold is recorded as  $P_1$ . Then, the valve of sample holder is opened, waited for 10 min. At the end of 10 min, the pressure of manifold is recorded again as  $P_2$ . After valve of sample chamber is closed, the pressure is recorded for the last time as  $P_3$ .
4. The procedure for hydrogen gas adsorption is repeated with increasing the pressure of hydrogen that taken to the manifold incrementally up to 600 – 700 Torr. The same explained in item 3 was repeated at each pressure.
5. After total adsorption isotherm is obtained, the manifold and sample chamber are evacuated for 10 min at room temperature.
6. After evacuation, weak adsorption isotherm is obtained with the same method that applied to get total adsorption isotherm.

## D. Heat and Mass Transfer Limitations

### D.1. External Mass Transfer Resistance

#### *Experimental Study*

Ammonia synthesis experiments were carried out at two different total flow rates (60 mL/min and 120 mL/min) in order to check if there was observed external mass transfer resistances over 4wt% Ru/HAP catalyst. In Figure D.1, the data corresponding to cumulative ammonia synthesis with respect to time at different flow rates at 375 °C is given.

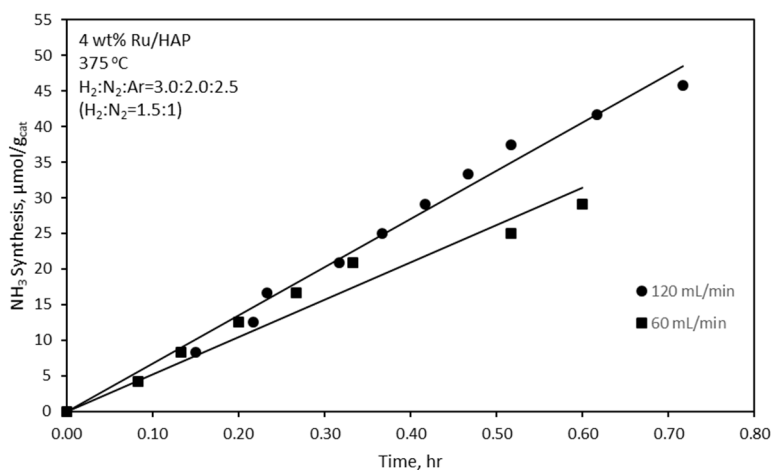


Figure D.1. Cumulative ammonia synthesis with respect to time at different total flow rates at 375 °C and atmospheric pressure. Gas flow mixture is H<sub>2</sub>:N<sub>2</sub>=1.5:1

As it can be seen in Figure D.1, the amount of ammonia synthesis with time is nearly same in the presence of different total flow rates. As a result of experimental study, external mass transfer limitation is not observed.

#### *Theoretical Study*

##### Mears' External Mass Transfer Criterion

The equation for criterion is given below:

$$\left[ \frac{(-R_A)_p \rho_b \left(\frac{d_p}{2}\right)^n}{k_m C_{A,b}} \right] < 0.15$$

$(-R_A)_p$  is measured rate during the experimental study,  $\rho_b$  is the density of the catalyst bed,  $d_p$  is the catalyst particle diameter,  $n$  is the reaction order,  $k_m$  is external mass transfer coefficient and  $C_{A,b}$  is the bulk concentration of reactant A.

The data and/or parameters obtained during the experimental studies are given in tabulated form in below:

Data	Value
$(-R_A)_p$ , kmol/kg-s	$3.0 \times 10^{-4}$
$\rho_b$ , kg/m <sup>3</sup>	3541
$d_p$ , m	$1.0 \times 10^{-4}$
$C_{A,b}$ , kmol/m <sup>3</sup>	$3.03 \times 10^{-3}$
$n$ (assumption)	1

#### Estimation of External Mass Transfer Coefficient

In order to estimate external mass transfer coefficient, Figure 2.7 in [256] and the relationship given in equation 2.43 [256] are used as given in below:

$$j_D = \frac{k_m \rho}{G} \left( \frac{\mu}{\rho D} \right)^{2/3}$$

$$Re = \frac{d_p(u\rho)}{\mu} = \frac{(1.0 \times 10^{-4} \text{ m}) \left( 0.133 \frac{\text{m}}{\text{s}} \right) \left( 0.346 \frac{\text{kg}}{\text{m}^3} \right)}{2.71 \times 10^{-5} \frac{\text{kg}}{\text{m} \cdot \text{s}}} = 0.17$$

From Figure 2.7 in [256] page 35,

$$j_D \cong 4.0$$

Using the relationship given above for  $j_D$  and  $k_m$ , we can estimate  $k_m$  as:

$$4.0 = \frac{k_m \left(0.346 \frac{\text{kg}}{\text{m}^3}\right)}{\left(0.133 \frac{\text{m}}{\text{s}}\right) \left(0.346 \frac{\text{kg}}{\text{m}^3}\right)} \left( \frac{2.71 \times 10^{-5} \frac{\text{kg}}{\text{m} \cdot \text{s}}}{\left(0.346 \frac{\text{kg}}{\text{m}^3}\right) \left(3.57 \times 10^{-4} \frac{\text{m}^2}{\text{s}}\right)} \right)^{2/3} \Rightarrow k_m = 1.46 \frac{\text{m}}{\text{s}}$$

Finally, if the values are used in Mears's criterion for external mass transfer limitation;

$$\left[ \frac{(3.0 \times 10^{-4})(3541) \left(\frac{1.0 \times 10^{-4}}{2}\right) (1)}{(1.46)(3.03 \times 10^{-3})} \right] < 0.15 \Rightarrow 0.012 < 0.15$$

Which means that there is no external mass transfer resistances in experimental study.

## E.2. Heat Transfer Resistance

### *Experimental Study – Intra Particle*

During the ammonia synthesis experiments over supported Ru catalysts (Support: HAp, zeolite-Y, Vulcan Carbon), a bench of experiments were carried out in order to check if there were a heat transfer problem over the catalyst surfaces. Powder quartz was used in order to increase the heat transfer rate over the quartz-catalyst physical mixture. Quartz was added to the catalysts with a weight ratio of 1:1. The results of ammonia synthesis experiments in the presence of supported Ru catalysts with quartz dilution is given in Figure D.2.

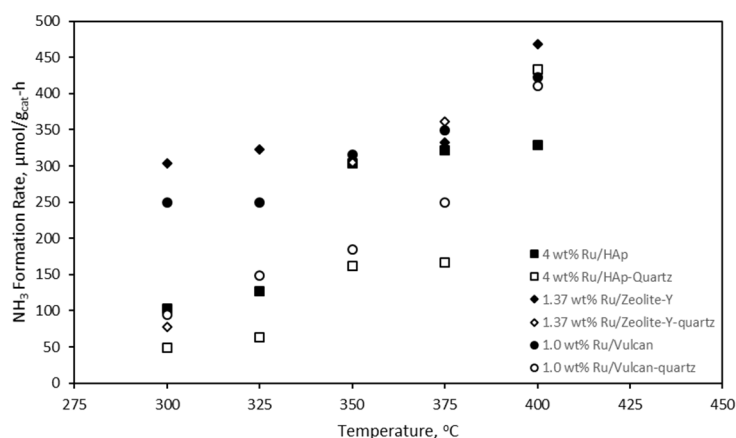


Figure D.2. Comparison of ammonia formation rates over supported Ru catalysts with and/or without quartz dilution between 300-400 °C and atmospheric pressure. 100 ml/min of H<sub>2</sub>:N<sub>2</sub>:Ar (3:1:2) gas flow is fed to the reactor.

As it can be seen in Figure D.2, ammonia synthesis rates measured in the presence of quartz dilution are nearly same with the rates measured in the absence of quartz dilution especially at high temperatures although it was observed some differences at 300 and 325 °C. As a result, it can be said that there is no distinct heat transfer limitation detected over supported Ru catalysts.

## ***Theoretical Study***

### ***Mears' External Heat Transfer Resistance Criterion***

The equation for criterion is given below:

$$\left[ \frac{(-\Delta H_R)(-R_A)_p \rho_b \left(\frac{d_p}{2}\right) (E_A)}{hT^2R} \right] < 0.15$$

$(-R_A)_p$  is measured rate during the experimental study,  $(-\Delta H_R)$  is the heat of reaction,  $\rho_b$  is the density of the catalyst bed,  $d_p$  is the catalyst particle diameter,  $E_A$  is the apparent activation energy,  $h$  is heat transfer coefficient and  $R$  is the ideal gas constant.

The data and/or parameters obtained during the experimental studies are given in tabulated form in below:

Data	Value
$(-R_A)_p$ , kmol/kg-s	$3.0 \times 10^{-4}$
$(-\Delta H_R)$ , kJ/mol	46.0
$\rho_b$ , kg/m <sup>3</sup>	3541
$d_p$ , m	$1.0 \times 10^{-4}$
$E_A$ , kJ/mol	63.7
$R$ , kJ/mol-K	$8.314 \times 10^{-3}$

### ***Estimation of External Heat Transfer Coefficient***

In order to estimate external heattransfer coefficient, Chilton-Colburn analogy is used so that it is assumed that  $j_D \approx j_H$ .

$$j_D = j_H = 4.0 = \frac{h}{C_p G} \left( \frac{C_p \mu}{\lambda} \right)^{2/3}$$

$$Re = \frac{d_p(u\rho)}{\mu} = \frac{(1.0 \times 10^{-4} \text{ m}) \left( 0.133 \frac{\text{m}}{\text{s}} \right) \left( 0.346 \frac{\text{kg}}{\text{m}^3} \right)}{2.71 \times 10^{-5} \frac{\text{kg}}{\text{m} \cdot \text{s}}} = 0.17$$

Using the relationship given above for  $j_H$  and  $h$ , we can estimate  $h$  as:

$$4.0 = \frac{h}{\left(7.63 \frac{\text{kJ}}{\text{kgK}}\right) \left(0.133 \frac{\text{m}}{\text{s}}\right) \left(0.346 \frac{\text{kg}}{\text{m}^3}\right)} \left( \frac{\left(7.63 \frac{\text{kJ}}{\text{kgK}}\right) \left(2.71 \times 10^{-5} \frac{\text{kg}}{\text{m} \cdot \text{s}}\right)}{\left(0.194 \times 10^{-3} \frac{\text{kW}}{\text{mK}}\right)} \right)^{2/3} \Rightarrow h = 1.34 \frac{\text{kW}}{\text{m}^2\text{K}}$$

Finally, if the values are used in Mears's criterion for external mass transfer limitation;

$$\left[ \frac{(46)(3.0 \times 10^{-4})(3541) \left(\frac{1.0 \times 10^{-4}}{2}\right) (63.7)}{(1.34)(673^2)(8.314 \times 10^{-3})} \right] < 0.15 \Rightarrow 3.1 \times 10^{-5} < 0.15$$

Which means that there is no external heat transfer resistances in experimental study.

#### Weisz-Prater Criterion for Internal Transport Resistances

Weisz-Prater criterion is used to show the absence of diffusional limitation during the reaction. The equation is given below as:

$$\eta\phi^2 = \left[ \frac{(-R_A)_p \rho_b \left(\frac{d_p}{2}\right)^2}{D_e C_{A,S}} \right] \ll 1.0$$

#### Estimation of effective diffusion coefficient

An expression is given in [257] to estimate the effective diffusion coefficient using tortuosity,  $\tau=3.0$ , porosity,  $\phi_p=0.4$ , and constriction factor,  $\sigma_c=0.8$  of the catalyst.

$$D_e = \frac{D_{AB} \phi_p \sigma_c}{\tau} = \frac{\left(3.57 \times 10^{-4} \frac{\text{m}^2}{\text{s}}\right) (0.40)(0.8)}{3.0} = 3.81 \times 10^{-5} \frac{\text{m}^2}{\text{s}}$$

If the data and/or parameters are put to the Weisz-Prater criterion;

$$\eta\phi^2 = \left[ \frac{(3.0 \times 10^{-4})(3541) \left(\frac{1.0 \times 10^{-4}}{2}\right)^2}{(3.81 \times 10^{-5})(3.03 \times 10^{-3})} \right] \ll 1.0 \Rightarrow 0.02 \ll 1.0$$

Therefore, it can be said that there is no diffusion limitation in the reaction conditions.

## F. Calculation for Conductivity Measurements

The mean conductivities five different measurement of 0.00108 M H<sub>2</sub>SO<sub>4</sub> solution and corresponding (NH<sub>4</sub>)<sub>2</sub>SO<sub>4</sub> salt are given in Table E.1.

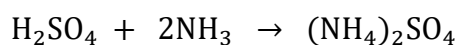
Table E.1. Conductivities of 1.1 mM sulfuric acid and ammonium sulfate solutions

Measurement	Conductivity of 0.00108 M H <sub>2</sub> SO <sub>4</sub>	Conductivity of 0.00108 M (NH <sub>4</sub> ) <sub>2</sub> SO <sub>4</sub>
1	860	344
2	879	355
3	853	334
4	875	360
5	862	348
Mean	866	348

The amount of H<sub>2</sub>SO<sub>4</sub> (in moles) can be calculated as follows:

$$\text{moles of H}_2\text{SO}_4 \text{ in wash bottle} = (0.00108 \text{ M H}_2\text{SO}_4) \times 0.14 \text{ L} = 1.512 \times 10^{-4} \text{ mol H}_2\text{SO}_4$$

The neutralization reaction of H<sub>2</sub>SO<sub>4</sub> with NH<sub>3</sub> is given below:



Therefore, the required amount of NH<sub>3</sub> (in moles) to completely neutralize the H<sub>2</sub>SO<sub>4</sub> solution can be calculated as:

$$\text{moles of NH}_3 = 1.512 \times 10^{-4} \text{ mol H}_2\text{SO}_4 \times \frac{2 \text{ mol NH}_3}{1 \text{ mol H}_2\text{SO}_4} = 3.024 \times 10^{-4} \text{ mol NH}_3$$

During the neutralization reaction of H<sub>2</sub>SO<sub>4</sub>, the total conductivity change is

$$\text{Conductivity change} = \text{conductivity of H}_2\text{SO}_4 - \text{conductivity of (NH}_4)_2\text{SO}_4$$

$$\text{Conductivity change} = 866 - 348 = 518 \mu\text{Scm}^{-1}$$

The corresponding conductivity change with consumption of NH<sub>3</sub> can be calculated as:

$$\frac{\text{\# of moles NH}_3}{\text{total conductivity change}} = \frac{3.024 \times 10^{-4} \text{ mol NH}_3}{518 \mu\text{Scm}^{-1}} = 5.83 \times 10^{-7} \frac{\text{mol NH}_3}{\mu\text{Scm}^{-1}}$$

### G. Calculation of H<sub>2</sub> Consumption in Temperature Programmed Analysis

H<sub>2</sub> consumption and/or desorption during TPR and TPD experiments is calculated using the calibration factor that is obtained from H<sub>2</sub>-TPR experiment of standard Ag<sub>2</sub>O material. In Figure F.1, H<sub>2</sub>-TPR profile of Ag<sub>2</sub>O is given. The peak centered at 122 °C is attributed to the reduction of Ag<sub>2</sub>O to Ag, which is determined by Micromeritics as 119 ± 15 °C.

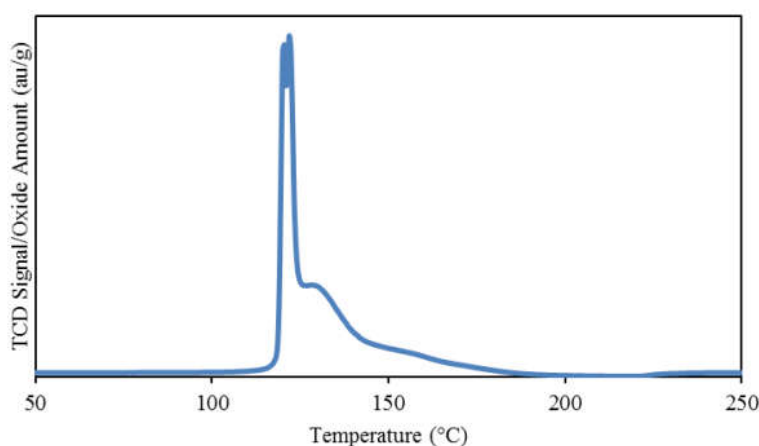


Figure F.1. H<sub>2</sub>-TPR profile of Ag<sub>2</sub>O under 25 mL/min flow of H<sub>2</sub> in Ar (10% H<sub>2</sub> by volume) with a temperature ramp of 10 °C/min [adopted from Deniz Kaya, 2016, The Role of Precious Metal Nanoparticles on the Oxygen Exchange Kinetics from Ceria, M.Sc. Thesis, METU, Ankara]

The area under TCD signal is calculated as 1.4116. The reduction stoichiometry of Ag<sub>2</sub>O to Ag is given in Equation F.1.:



The initial amount of Ag<sub>2</sub>O is weighed as 0.024 g. It is assumed that Ag<sub>2</sub>O is completely reduced to the Ag. According to the reaction stoichiometry given in Equation F.1, 1 mol of H<sub>2</sub> is needed to reduce Ag<sub>2</sub>O. As a result, amount of H<sub>2</sub> consumption per unit area can be calculated as given in below:

$$0.024 \text{ g Ag}_2\text{O} \times \frac{1 \text{ mol Ag}_2\text{O}}{231.74 \text{ Ag}_2\text{O}} \times \frac{1 \text{ mol H}_2}{1 \text{ mol Ag}_2\text{O}} \times \frac{1}{1.4116 \text{ unit area}} = 7.30 \times 10^{-5} \frac{\text{mol H}_2}{\text{unit area}}$$



## CURRICULUM VITAE

### PERSONAL INFORMATION

Surname, Name : Aslan, Mustafa Yasin  
Nationality : Turkish (TC)  
Date and Place of Birth : September 19<sup>th</sup>, 1986, Erzurum  
Phone : +905356049115  
E-mail : mustafa.aslan@usak.edu.tr

### EDUCATION

Degree	Institution	Year of Graduation
MS	METU, Chemical Engineering	2012
BS	Gazi University, Chemical Engineering	2009
High School	Keçiören High School, Ankara	2004

### WORK EXPERIENCE

Year	Place	Enrollment
2019-Present	Usak University	Teaching Assistant
2011-2019	Middle East Technical University	Teaching Assistant

### FOREIGN LANGUAGES

Advanced English, (YOKDIL: 86)

### PUBLICATIONS

1. D. Üner ve M.Y.Aslan, Using spilled over hydrogen in NH<sub>3</sub> synthesis over supported Ru catalysts, *Catalysis Today*, 272 (2016), 49-57
2. E. Erünal, F. Uysal, M.Y. Aslan, B. Güzel, D. Üner, Enhancement of Hydrogen Storage Capacity of Multi-Walled Carbon Nanotubes with Palladium Doping Prepared Through Supercritical CO<sub>2</sub> Deposition Method, *International Journal of Hydrogen Energy*, 43 (2018), 10755-10764
3. M.Y. Aslan ve D. Üner, Fundamentals of hydrogen storage processes over Ru/SiO<sub>2</sub> and Ru/Vulcan, *International Journal of Hydrogen Energy*, 44 (2019), 18903-189014

## **CONFERENCE PRESENTATIONS**

5 proceedings in international and 6 proceedings in national conferences were presented as oral and/or poster presentations

## **HOBBIES**

History of science and technology, documentaries, hiking, anything related to nature